UNIVERSITY OF MODENA AND REGGIO EMILIA

DEPARTMENT OR PHYSICS, COMPUTER SCIENCES AND MATHEMATICS

DOCTORAL THESIS IN PHYSICS AND NANOSCIENCES

Numerical approaches to Quantum Field Theory in curved space

Author:
Maurizio MURATORI

Supervisor:
Prof. Olindo CORRADINI

Director of Doctoral School:
Prof. Stefano FRABBONI

Cycle XXXIV

Abstract

A pillar for the modern study of theoretical physics is certainly quantum field theory (QFT), since an always increasing number of physical problems are formulated and approached according to QFT. Indeed, the quantization of fields allows to study multi-particle phenomena, both involving non-relativistic particles, as in condensed matter, and relativistic particles, as in the study of fundamental interactions. Actually, more than a theory it is thought as a paradigm on top of which different physical theories are proposed and developed. The classic formulation of QFT is given as a "second quantization", *i.e.* quantizing fields which depend, parametrically, on spacetime coordinates. The reason is two-fold. In doing so, one can treat space and time on equal footing, thus circumventing the problem of unifying quantum mechanics and special relativity. On the other hand, as already mentioned, QFT allows to describe multiparticle phenomena. However, the aforementioned unification problem can as well be achieved treating space and time both as dynamical fields and using the proper time as parameter. This leads to a particle quantization, known as worldline formalism, which thus provides a first-quantized approach to QFT. The worldline formulation of QFT is the main subject of the present thesis. The worldline formalism allows to write QFT quantities of interest (propagators, effective actions and scattering amplitudes) in terms of quantum mechanical path integrals which ultimately correlate such observables to the behaviour of different quantum mechanical particles. These particle-models, called sigma-models, have been extensively studied for years from an analytical perspective, providing valid results, particularly when the particle is coupled to external fields, i.e. vector gauge fields, gravity, etc. In the presence of gravitational couplings, i.e. in curved spacetimes, the almost totality of analytic results has involved a perturbative approach. In general, attempts to reach non-perturbative results, in flat and in curved space, have led to the development of numerical interpretations of the worldline formalism. The main candidate of these strategies is the so called Worldline Monte Carlo, for which several numerical algorithms have been developed: the key idea is to approximate the

path integral of a point particle with a discrete set of discretized paths sampled numerically according to Monte Carlo based routines. In this thesis we will see this method in action, providing first a series of analytical calculations of some QFT relevant quantities, and then we will focus on the numerical part, that is computations based on the WLMC approach in flat and curved spaces. In particular, numerical applications of the worldline Monte Carlo theory in curved space represent and absolute novelty and in this thesis we will provide an efficient construction which allows to possibly implement a large number of curved space configurations as backgrounds. The goal is to obtain non-perturbative results which, analytically, can be investigated so far only by means of perturbative techniques.

Un pilastro della fisica teorica moderna è senza dubbio la teoria quantistica dei campi (QFT), poiché un numero sempre maggiore di problemi fisici sono formulati e affrontati in accordo con quest'ultima. Infatti, la quantizzazione dei campi permette di studiare fenomeni riguardanti più particelle, sia non relativistiche, come in materia condensata, sia relativistiche, come nello studio delle interazioni fondamentali. In realtà, più che una teoria, la QFT è pensata come un paradigma in base al quale diverse teorie fisiche sono proposte e sviluppate. La formulazione classica della QFT è data in "seconda quantizzazione", cioè quantizzando campi che dipendono in modo parametrico dalle coordinate spaziotemporali. La ragione è duplice. Così facendo, è possibile trattare spazio e tempo in modo analogo, aggirando quindi il problema di unificare meccanica quantistica e relatività speciale. D'altro canto, come già accennato, la QFT permette di descrivere sistemi multiparticellari. Ad ogni modo, il problema di unificazione menzionato sopra può essere affrontato anche trattando spazio e tempo come campi dinamici e usando il tempo proprio come parametro. Questo porta ad una quantizzazione della particella, conosciuta anche come formalismo a linea di mondo, che quindi fornisce un approccio in prima quantizzazione alla QFT. Il formalismo a linea di mondo della QFT è il soggetto principale di questa tesi. Esso permette di formulare quantità di interesse per la QFT (propagatori, azioni efficaci, ampiezze d'urto) in termini di integrali sui cammini quantomeccanici, che legano tali osservabili al comportamento di diverse particelle quantomeccaniche. Questi modelli particellari, chiamati modelli-sigma, sono stati studiati esaustivamente per anni da un punto di vista

analitico, fornendo ottimi risultati in particolar modo quando la particella è accoppiata a campi esterni, come campi di gauge, gravità, ecc. In presenza di accoppiamenti gravitazionali, come in spaziotempi curvi, la quasi totalità di risultati analitici coinvolge un approccio perturbativo. In generale, alcuni tentativi di ottenere risultati non perturbativi, in spazi piatti e curvi, hanno portato allo sviluppo di interpretazioni numeriche del formalismo a linea di mondo. Il principale candidato di queste tecniche è il cosiddetto formalismo a linea di mondo Monte Carlo (WLMC), rispetto al quale numerosi algoritmi numerici sono stati sviluppati: l'idea centrale è di approssimare l'integrale sui cammini di una particella puntuale con un insieme discreto di cammini discretizzati, campionati numericamente secondo routine che adottano il metodo Monte Carlo. In questa tesi vedremo questo metodo in azione, fornendo prima una serie di risultati analitici su alcune grandezze della QFT, e poi ci concentreremo sulla parte numerica, cioè calcoli basati sul metodo WLMC in spazio piatto e curvo. In particolare, le applicazioni numeriche di questa teoria in spazio curvo rappresentano una novità assoluta a in questa tesi mostreremo come ottenere una costruzione efficiente che permetta di implementare un grande numero di configurazioni di spazio curvo in termini di background. Lo scopo è ottenere risultati non perturbativi che, dal punto di vista analitico, possono essere studiare (fino ad ora) soltanto attraverso tecniche perturbative.

Acknowledgements

I would like to thank my advisor Prof. Olindo Corradini for guiding me through these three intense years of Ph.D. He always proved to be available when I needed help, always gave me good advice and confirmed that he was the best person to turn to for this experience.

I thank my parents and my sister for always supporting me.

I thank Erika, who gave me the strength and the motivation needed to do always my best, always reminding me the importance of the path that I chose.

I thank my friends Aldro, Espo and Je for always being a source of happiness in my life.

I thank my Ph.D. colleagues for all the fruitful discussions (serious or not), in particular Luca Razzoli.

I thank UNIMORE Professors Franchini and Bizzeti for giving me the opportunity to collaborate with them.

I thank Professors Edwards, Huet, Flachi, Vitagliano, Bastianelli spread all around the world for our collaborations, discussions, advice and help.

Contents

Chapter 1

Introduction

Quantum Field Theory (QFT) is probably one of the most successful theories in physics of all time. Its value is not merely factual, as it allows for the most accurate theoretical predictions ever made; the electron g-factor which parameterizes the (anomalous) magnetic dipole moment [1, 2], is considered the most precise prediction in all human history. Rather its value is potential, since it laid the foundations of a large number of theories on which modern physics is based, such as quantum electrodynamics and chromodynamics, renormalization theory, gauge theories, supersymmetry, the Standard Model and string theory. And it's no wonder: QFT is the son of the two most revolutionary and outstanding theories that humans came up with, *i.e.* quantum mechanics and special relativity. Both they not only drastically changed the way of making physics, but, even more important, generated an abyss between science and intuitiveness. Furthermore, as scientists, we learn from quantum mechanics that what we study is not actually what it *is*, but what *appears* to us, how we *feel* it. This is the fundamental problem of the *observation*: anything which is observed changes and this must be taken into account during experiments and calculations. Special relativity, instead, teaches us that space and time are much more connected than we can notice at ordinary (macroscopic) scales. They are not just coordinates to determine when and where an event takes place, rather they are homogeneous quantities whose relation determines whether the event can happen or not. One of the most counter-intuitive consequences of the spacetime homogeneity is certainly the velocity cap: any physical object[1] can travel at a maximum speed limit, that is the speed of light. Close to this limit, the more we push an object, the greater becomes its inertia to be accelerated, *as if nature doesn't want objects to be arbitrary fast*. This last sentence encodes our subliminal mental misconception: more or less consciously, we always gave a great

[1] More precisely, any physical source of information.

importance to intuitiveness for our experiments and theories, hence, we had been led to believe that what we observe at common conditions should happen at all conditions. Hence we feel the limit that nature imposes as a limit to our understanding of the nature itself, and not one of its features.

Quantum mechanics and special relativity told us that when we study a phenomenon, we are part of the experiment as observers, and that we must be ready to be contradicted the more often we deviate from common scales.

This might appear as a scary scenario (and maybe it is), but it also teaches that what actually is now important as never before is to trust the fact that a theory truly describes the world if it agrees with measurements, regardless how far from intuition its ideas are felt.

This is what leads most of the modern theories like string theory and supergravity, to name two: if they bring good agreements with experiments, we can make the effort of thinking that we live in eleven (or more) dimensions.

Quantum Field Theory is actually only one of the two main characters of modern physics. The other is certainly General Relativity (GR), that is the physics at cosmological scales. As we did between quantum mechanics and special relativity, we would like to combine a marriage between QFT and GR. This is felt as the greatest challenge of all history of physics. Basically, we are dealing with two theories which work very well in their regimes of applications, that are totally opposed: QFT describes the world of elementary particle, thus at extremely small scales, whereas GR is the mother theory of gravitation. It is a *geometric* classical theory which describes both gravitational phenomena and the cosmological evolution of the universe. Thus, it naturally applies to effects which occur at very large scales. The main issue is that an intermediate point at which both theories (or at list part of them) may be combined cannot be found since some characteristic features of QFT and GR start to conflict. On the other hand, a consistent quantum theory of gravity is expected to exist. In fact, quantum effects in gravity are expected to occur at the Planck scale, where the Compton wavelength of a particle— which characterizes its quantum properties— and the Schwarzschild radius— which characterizes its gravitational properties, are equal, *i.e.*

$$\frac{2GM}{c^2} = \frac{\hbar}{Mc} \rightarrow \ell_p = \sqrt{\frac{\hbar G}{c^3}}. \tag{1.1}$$

Starting from these difficulties, an increasing number of new theories have been arising

over the past few years. The main goal is to formulate a theory which asymptotically tends to GR for large scales, to QFT for small scales, and provides new predictions at intermediate scales. Yet, the Planck scale, which is the scale where quantum gravitational phenomena are expected to be relevant, is way out of reach of terrestrial experimental devices. On the other hand these effects are certainly relevant in the very early stages of the universe, and may have left their *finger prints* in the observable gravitational waves— see e.g. [3]. The main difficulty met in the construction of a quantum theory of gravity is self consistency. Firstly, the straightforward quantization of Einstein's GR theory, such as a perturbative theory about flat space, leads to a non-renormalizable theory, *i.e.* a theory which, as the perturbative order increases, needs an increasingly higher amount of external input to renormalize away the divergences present in the scattering amplitudes. On the other hand, string theory— which to date is the most promising scenario to quantize gravity— is a finite theory (no renormalization needed), but is consistent only if the spacetime is higher-dimensional. The needed extra-dimensions thus need to be suitably compactified: this process leaves an enormous amount of solutions which are consistent with Standard Model and GR, as low energy effective field theory. Hence, string theory, as a unifying scenario, has so far shown to be a poorly predictive theory. We shall not address such issues in the present thesis.

However, a lot can be said even without a new theory: for instance, it is possible to somehow mitigate or just use some ingredients of a theory in the realm of another theory. This is conceptually what happens when we try to include GR as a background in QFT calculations, as an example. In fact, it turns out that the tools one acquires in the study of QFT in curved spaces, can be applied to various scenarios, such as the classical scattering of black holes [4] and the diffusion of nonrelativistic particles (such as proteins) on curved substrates (such as cells), just to name a few. From a more theoretical (and speculative) viewpoint, they have been used as a tool to compute scattering amplitudes and effective actions involving gravitons, which allegedly are the helicity-two elementary particles that *mediate* gravity.

An important tool for theoretical physics, as already mentioned, is Perturbation Theory (PT). It can be formulated in various ways depending on the specific problem it is applied to. From basic quantum mechanics to advance quantum field theory, it allows to provide approximated solutions to problems which are analytically prohibitive or even unsolved. Typically, the more accurate the solution the greater the effort. In the

realm of QFT, perturbation theory is often applied to the (semi)analytical computation of vacuum scattering amplitudes, whereas non-perturbative methods can treat strong coupling theories, or models with external fields. In recent years, guided also by the technological development and the increasing computer power, a lot of efforts have been made in the formulation of QFT-problems which can be implemented in numerical routines to provide more and more accurate estimate of the result. Even though these numerical implementations can be useful for perturbative problems to count and order an increasingly high number of terms from the pertubative series which represents the result of a calculation, the main gain we can get from computers is probably when we deal with non-perturbative problems: this the case of the Worldline Monte Carlo (WLMC) technique. In fact, it allows to approach non-perturbative problems, including especially those defined in a background curved space, and provides results which reproduce the correct solutions up to a numerical degree of accuracy. The WLMC technique is the core of this thesis and its extension to curved space configurations represents an absolute novelty: we will show how a non-trivial metric can enter the WLMC algorithms and apply this method to a number of models including scalar field propagators in maximally symmetric spaces, for which analytical and perturbative solutions can be used as a benchmark.

This thesis is structured as follows: in chapter 2 we introduce the construction of path integrals in flat space and their use in first quantization, defining then the so called linear σ-models; in chapter 3 we see how such path integrals are defined (and regularized) in curved space backgrounds, leading to non-linear σ-models; a first application of the latter is given in chapter 4 and consists of an analytical computation of the trace anomaly of a scalar field in maximally symmetric curved space using BRST quantization; in chapter 5 we focus on the dynamics of a scalar particle in a D-dimensional curved space and prove the equivalence between two different regularization schemes for path integrals in curved space, that is mode and dimensional regularization; in chapter 6 we introduce the worldline Monte Carlo numerical approach, which is then exploited in chapter 7 where curved space is considered; chapter 8 focuses on further WLMC applications, including Casimir configurations and electromagnetic couplings; chapter 9 is dedicated to a specific numerical algorithm (Creutz's algorithms) which allows to estimate Grassmannian path integrals, *i.e.* path integrals over anticommuting scalar variables; we also suggest a possible application of a combination between WLMC and Creutz's algorithms to study non-linear σ-models, including then both

commuting and anticommuting scalar fields; in chapter 10 we study the particular case of a scalar field rotating on a ring in presence of a punctual defect, and solve numerically the associated equations of motion; finally, in chapter 11 we draw our conclusions and provide possible outlooks.

Chapter 2

Path Integrals and σ-models

As we have anticipated in the previous chapter, Quantum Field Theory is considered the most important framework on which modern particle physics is based, in particular when it is formulated using path integrals. In fact, it is not always stressed enough that non-abelian gauge theories, upon which weak and strong interactions are based, have only been consistently formulated at the full quantum level through field path integrals, which are the natural, second-quantized, extension of particle path integrals. This fundamental tool was introduced by R. P. Feynman [5] in the 1940's after some suggestions by Dirac of considering the action instead of the Hamiltonian as a preferred quantity to encode the information of the dynamics. Actually a primordial version of path integral was introduced previously by Wiener in the 1920's to study the Brownian motion of a particle, even though a complete and accurate formulation of the framework is universally ascribed to Feynman.

This construction actually has constituted a milestone for quantum field theories in the following years: as an alternative to second quantized approaches to QFT for the computation of anomalies [6–10] and for effective actions and Feynman diagrams [11–14] for instance. This method can be straightforwardly extended to curved spacetime, as reviewed in [15], and direct applications involve one-loop effective actions [16–18], the one-loop graviton photon mixing in an electromagnetic field [19], gravitational corrections to Euler-Heisenberg Lagrangians [20], worldline representations of quantum gravity [21, 22], supergravity [23], and higher spin field theories [24, 25] and simplified methods for anomaly computations [26, 27] as we'll see in detail.

Because of their importance in QFT and since they are directly involved in the numerical Worldline Monte Carlo routines, it is worth to provide a quick sketch of how a Feynman particle path integral can be constructed and what it represents for

quantum mechanics and QFT.

The evolution of a quantum mechanical state of a scalar point-particle in n spacial dimensions from an initial point $(x_\mathrm{i}, t_\mathrm{i})$ to a final point $(x_\mathrm{f}, t_\mathrm{f})$ in a time interval T is governed by the so called transition amplitude and can be expressed by

$$K(x_\mathrm{f}, t_\mathrm{f}; x_\mathrm{i}, t_\mathrm{i}) = \langle x_\mathrm{f}| \, e^{\frac{-i(t_\mathrm{f}-t_\mathrm{i})}{\hbar}\mathbf{H}} \, |x_\mathrm{i}\rangle \,, \tag{2.1}$$

where the Hamiltonian reads

$$\mathbf{H}(x) = -\frac{\hbar^2}{2m}\frac{\partial}{\partial x_\mathrm{i}}\frac{\partial}{\partial x^i} + \mathbf{V}(x), \tag{2.2}$$

at any intermediate $x \in [x_\mathrm{i}, x_\mathrm{f}]$. Here and in the following we are using bold letters to denote operators. Performing a Wick-rotation from Minkowskian time t_M to Euclidean time $t_E = it_M$ and defining $\beta = t_{E,f} - t_{E,i}$, we can express the transition amplitude as

$$K(x_\mathrm{f}, x_\mathrm{i}; \beta) = \langle x_\mathrm{f}| \, e^{-\frac{\beta}{\hbar}\mathbf{H}} \, |x_\mathrm{i}\rangle \tag{2.3}$$

satisfying the heat equation

$$-\hbar\frac{\partial}{\partial\beta}K(x_\mathrm{f}, x_\mathrm{i}; \beta) = \mathbf{H}(x_\mathrm{f})K(x_\mathrm{f}, x_\mathrm{i}; \beta) \tag{2.4}$$

which can be regarded as the Wick-rotated version of the Schrödinger equation. So far we have been using operators to express dynamical variables, as prescribed by quantum mechanics. However, in most cases when a time evolution is present, this imposes the need to consider a time ordering for such operators. To get rid of this difficulty, it is useful to set a framework where only functions, instead of operators, are used. This is one the most useful features of path integrals. To do that, let us time-split the transition amplitude as follows,

$$\begin{aligned} K(x_\mathrm{f}, x_\mathrm{i}; \beta) &= \langle x_\mathrm{f}| \left(e^{-\frac{\beta}{\hbar N}\mathbf{H}}\right)^N |x_\mathrm{i}\rangle = \langle x_\mathrm{f}| \, e^{-\frac{\epsilon}{\hbar}\mathbf{H}} \ldots e^{-\frac{\epsilon}{\hbar}\mathbf{H}} \, |x_\mathrm{i}\rangle \\ &= \int \left(\prod_{k=1}^{N-1} d^n x_k\right) \prod_{k=1}^{N} \langle x_k| \, e^{-\frac{\epsilon}{\hbar}\mathbf{H}} \, |x_{k-1}\rangle \,, \end{aligned} \tag{2.5}$$

where we have inserted $N-1$ times the identity operator

$$\int d^n x \, |x\rangle \, \langle x| = \mathbf{1}. \tag{2.6}$$

and have defined the quantities $x_0 = x_\mathrm{i}$, $x_N = x_\mathrm{f}$ and $\epsilon = \frac{\beta}{N}$. If we insert N times the identity in momentum space

$$\int d^n p \, |p\rangle \, \langle p| \,, \tag{2.7}$$

we obtain

$$K(x_\mathrm{f}, x_\mathrm{i}; \beta) = \int \left(\prod_{k=1}^{N-1} d^n x_k \right) \left(\prod_{k=1}^{N} d^n p_k \right) \prod_{k=1}^{N} \langle x_k | p_k \rangle \, \langle p_k | e^{-\frac{\epsilon}{\hbar}\mathbf{H}} | x_{k-1} \rangle \,. \tag{2.8}$$

To be more precise, the second equality in eq. (2.5) is allowed by Trotter's formula in the large N limit. Namely, if we rewrite the exponent of the evolution operator as

$$-\frac{\beta}{\hbar}\mathbf{H} = -\frac{N\epsilon}{\hbar}\mathbf{H} = -\lambda(\mathbf{T} + \mathbf{V}), \tag{2.9}$$

with parameter $\lambda = \frac{N\epsilon}{\hbar}$ and $\mathbf{T}, \mathbf{V}$ being the kinetic and potential contributions to $\mathbf{H}$ respectively, then we have

$$e^{-\frac{\lambda}{N}(\mathbf{T}+\mathbf{V})} = e^{-\frac{\lambda}{N}\mathbf{T}} e^{-\frac{\lambda}{N}\mathbf{V}} + \frac{\lambda^2}{2N^2} [\mathbf{V}, \mathbf{T}] + \ldots = e^{-\frac{\lambda}{N}\mathbf{T}} e^{-\frac{\lambda}{N}\mathbf{V}} + o\left(N^{-1}\right), \tag{2.10}$$

and

$$\left(e^{-\frac{\lambda}{N}\mathbf{T}} e^{-\frac{\lambda}{N}\mathbf{V}} \right)^N - \left(e^{-\frac{\lambda}{N}(\mathbf{T}+\mathbf{V})} \right)^N = o\left(N^{-2}\right), \tag{2.11}$$

producing the limit

$$e^{-\lambda(\mathbf{T}+\mathbf{V})} = \lim_{N\to\infty} \left(e^{-\frac{\lambda}{N}\mathbf{T}} e^{-\frac{\lambda}{N}\mathbf{V}} \right)^N. \tag{2.12}$$

This procedure allows us to break the full exponential into a chain N exponentials (close to unity) whose order is irrelevant of the large N-limit. The last term in eq. (2.8) can be written as

$$\begin{aligned} \langle p | e^{-\frac{\epsilon}{\hbar}\mathbf{H}(\mathbf{x},\mathbf{p})} | x \rangle &= \langle p | 1 - \frac{\epsilon}{\hbar}\mathbf{H}(\mathbf{x},\mathbf{p}) + o(\epsilon^2) | x \rangle \\ &= \langle p | x \rangle - \frac{\epsilon}{\hbar} \langle p | \mathbf{H}(\mathbf{x},\mathbf{p}) | x \rangle + o(\epsilon^2) \\ &= \langle p | x \rangle \left[1 - \frac{\epsilon}{\hbar} H(x,p) + o(\epsilon^2) \right] \\ &= \langle p | x \rangle \, e^{-\frac{\epsilon}{\hbar}H(x,p)}, \end{aligned} \tag{2.13}$$

for Hamiltonians of the kind of eq. (2.2), where x's and p's do not mix. In fact, in curved space this is not the case and a more involved manipulation will be needed.

Now, using plane waves

$$\langle x|p\rangle = \frac{1}{(2\pi\hbar)^{\frac{n}{2}}} e^{\frac{i}{\hbar}p\cdot x}, \tag{2.14}$$

and eq. (2.13), we find

$$\langle x_k|p_k\rangle \, \langle p_k|e^{-\frac{\epsilon}{\hbar}\mathbf{H}}|x_{k-1}\rangle = \frac{1}{(2\pi\hbar)^n} e^{\frac{i}{\hbar}p_k\cdot(x_k-x_{k-1})-\frac{\epsilon}{\hbar}H(x_{k-1},p_k)}, \tag{2.15}$$

which can be inserted into the transition amplitude (2.8) to get

$$\begin{aligned} &K(x_\mathrm{f}, x_\mathrm{i}; \beta) = \\ &= \lim_{N\to\infty} \int \left(\prod_{k=1}^{N-1} d^n x_k\right) \left(\prod_{k=1}^{N} \frac{d^n p_k}{(2\pi\hbar)^n}\right) e^{-\frac{\epsilon}{\hbar}\sum_{k=1}^{N}\left[-\frac{i}{\epsilon}p_k\cdot(x_k-x_{k-1})+H(x_{k-1},p_k)\right]} \\ &= \int \mathcal{D}x\, \mathcal{D}p\, e^{-\frac{1}{\hbar}S[x,p]}. \end{aligned} \tag{2.16}$$

Eq. (2.16) identifies a path integral in phase space for the point-particle subjected to $H(x,p)$ and is governed by the corresponding action

$$\epsilon \sum_{k=1}^{N} \left[-\frac{i}{\epsilon}p_k\cdot(x_k-x_{k-1}) + H(x_{k-1},p_k)\right] \to \int_0^\beta d\tau \left[-ip\cdot\dot{x} + H(x,p)\right] = S[x,p]. \tag{2.17}$$

Furthermore, it is possible to perform the phase-space path integral via Gaussian integration, to get the associated path integral in configuration space

$$\begin{aligned} &K(x_\mathrm{f}, x_\mathrm{i}; \beta) = \\ &= \lim_{N\to\infty} \int \left(\prod_{k=1}^{N-1} d^n x_k\right) \left(\frac{m}{2\pi\hbar\epsilon}\right)^{\frac{nN}{2}} e^{-\frac{\epsilon}{\hbar}\sum_{k=1}^{N}\left[\frac{m}{2}\left(\frac{x_k-x_{k-1}}{\epsilon}\right)^2+V(x_{k-1})\right]} \\ &= \int \mathcal{D}x\, e^{-\frac{1}{\hbar}S[x]}, \end{aligned} \tag{2.18}$$

with action

$$\epsilon \sum_{k=1}^{N} \left[\frac{m}{2}\left(\frac{x_k-x_{k-1}}{\epsilon}\right)^2 + V(x_{k-1})\right] \to \int_0^\beta d\tau \left[\frac{m}{2}\dot{x}^2 + V(x)\right] = S[x]. \tag{2.19}$$

At this point we can also Wick-rotate back to Minkowski time, to get the quantum mechanical transition amplitude

$$K(x_\mathrm{f}, x_\mathrm{i}\ T) = \int \mathcal{D}x\, e^{\frac{i}{\hbar}S[x]}, \tag{2.20}$$

with

$$S[x] = \int_0^T d\tau \left[\frac{m}{2}\dot{x}^2 - V(x)\right]. \tag{2.21}$$

The x-representation (2.21) actually encodes the theoretical recipe that one should follow to compute the transition amplitude $K(x_\mathrm{f}, x_\mathrm{i}; T)$: in principle, one should construct all the possible (an infinite number) n-dimensional trajectories which join the endpoints x_i and x_f in a propagation time T; to each path (here comes the name path integral), one assigns a weight given by $e^{\frac{i}{\hbar}S[x]}$ and then sums over all the paths to get the final estimation of T.

A few comments are in order. Each path that contributes to K is weighted by $e^{\frac{i}{\hbar}S}$, which is a unit-norm complex number, which can be obviously represented as a unit-length arrow in a $2D$ plane. Hence, heuristically, it is easy to convince oneself that the most important paths are those for which the action is stationary, *i.e.* the classical trajectory: neighboring paths to it give rise to constructive interference. Thus, in the limit when $|S[x_{cl}]| \gg \hbar$ only the classical path counts. Moreover, by writing K as

$$K(x_\mathrm{f}, x_\mathrm{i}; T) = e^{\frac{i}{\hbar}S[x_{cl}]} N(x_\mathrm{f}, x_\mathrm{i}; T) = e^{\frac{i}{\hbar}\Gamma(x_\mathrm{f}, x_\mathrm{i}; T)} \tag{2.22}$$

it is easy to show that Γ satisfies a Hamilton-Jacobi like equation, which reduces to the classical one when $|S[x_{cl}]| \gg \hbar$.

The problem of computing a quantum mechanical transition amplitude has turned into the computation of the propagation of a scalar point-particle through all possible trajectories in flat spacetime. The particle action involved in the flat space path integral will be referred to as linear σ-model[1]. The idea that, at quantum scales, a point-particle which is born at an initial point x_i and dies at x_f has to travel *simultaneously* all the possible trajectories between such points, has bothered physicists for a long time. Actually, the complication comes when we try to use too much intuition into our formulas: the interpretation process which we insert at each step of our theoretical derivation would ask us to introduce a bunch of stereotypes coming from our macroscopic experience that unfortunately do not apply in the quantum world. Anyway, where common sense fails, experiments come into play, and now more than ever they must be the guiding lights to prove or disprove a theory, however absurd it may seem. One of the most remarkable experiments which ultimately confirm the validity of Feynman's path integral construction is the double-slit experiment. Originally, the

[1] In the case of a curved space, we use to call the model nonlinear.

double-slit experiment was first performed by Young in 1801 to demonstrate the wave behaviour of light, which produces an interference pattern when it shines a double slit. Later, in 1927, Davisson and Gerner showed that electrons produce the same type of pattern if they are made to scatter a crystal surface. Young's double-slit experiment was thus re-proposed, for the case of quantum particle beams (electrons), as a *gedanken* experiment, by Feynman, and it dubbed "Young-Feynman experiment". Interestingly, a true double-slit experiment for electron was realized only quite recently—see e.g. [28] The Young-Feynman gedanken experiment can *a posteriori* also be seen as a guiding principle for the construction of the Feynman path integral. His idea was to produce

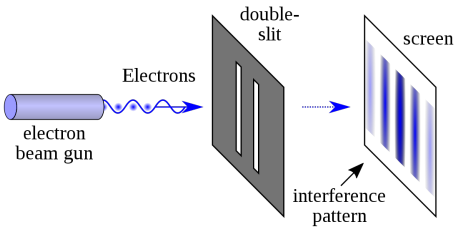

FIGURE 2.1: Stylization of the Young-Feynman experiment: an electron beam generator emits electrons which propagate across two slits on a plate and form a pattern on a screen. Image from Wikipedia.

a beam of electron from an electron beam gun, to be sent to a screen crossing a plate with two parallel slits, as sketch in Fig. 2.1. Intuitively, one would have expected electrons to arrive to only two separated portions of the screen, corresponding to the two intermediate slits. Contrary, the experiment showed a pattern of interference producing multiple bands, just like if those electrons behaved like waves. And so they did. And maybe a more astonishing version of the experiment was proposed after that some questions arose: were some electrons favoured to be found in the middle of the screen, with respect to those at the edges? What happens if a single electron is shot? Fortunately, the technological means where sufficient to repeat the experiment with ultra low intensity beams, that is one electron at a time. What was observed was that each electron reached the screen at a position which seemed to be randomic. But, repeating the single-electron experiment for a sufficient number of times, it was realized that the same interference patterns emerged. If we want to look at the experiment in terms of trajectories, each electron selects a particular path $x(\tau)$ joining the gun and a point on the screen according to a probability which is essentially proportional to $\left|e^{\frac{i}{\hbar}S[x(\tau)]}\right|^2$. The total probability to reach the screen is obtained summing the probability amplitudes of all the trajectories and squaring, and the path integral calculation for the final

pattern confirms what was observed in the experiment. Thus, from a quantum mechanical point of view, we conclude that the electron beam shows its wave nature, whereas from a path integral perspective, each electron reaches the screen choosing a path but interfering with the other, *a priori* possible, paths. Near to the maxima of interference on the screen, there is a constructive interference as opposed to the points which are closer to the minima.

Going back to eq. (2.18), only in some easier cases it is possible to compute the path integral in closed form: in most interesting situations we can only approximate the solution using perturbation theory. This technique is a powerful tool of quantum mechanics and Quantum Field Theories, as it allows to express the solution for any perturbative problem, in principles, with any order of precision. The downside is that the greater the accuracy, the longest the calculation. This is the reason why an increasing interest towards nonperturbative methods has been arising through recent years, in particular for numerical techniques. Before introducing the numerical techniques on which this thesis is based, let us see once how perturbation theory is used in theoretical physics, in particular in σ-models.

First of all, it is convenient to split the path $x^i(\tau)$ into background + quantum fluctuation parts,

$$x^i(\tau) = x^i_{\rm bg}(\tau) + q^i(\tau) \tag{2.23}$$

where $x^i_{\rm bg}$ solves the classical equation of motion for the free theory with endpoints $x^i_{\rm bg}(0) = x^i_{\rm i}$, $x^i_{\rm bg}(\beta) = x^i_{\rm f}$, namely (for convenience here we consider the Euclidean version)

$$x^i_{\rm bg}(\tau) = x^i_{\rm i} + (x^i_{\rm f} - x^i_{\rm i})\frac{\tau}{\beta} \tag{2.24}$$

and $q^i(\tau)$ satisfies Dirichlet boundary conditions. With this construction, it is possible to rewrite the transition amplitude (2.18) as

$$K(x_{\rm f}, x_{\rm i}; \beta) = K_{\rm free}(x_{\rm f}, x_{\rm i}; \beta)\frac{\int_{q(0)=0}^{q(1)=0} \mathcal{D}q\; e^{-\int_0^1 d\tau\left(\frac{m}{2\beta}\dot{q}^2 + \beta V(x_{\rm bg}+q)\right)}}{\int_{q(0)=0}^{q(1)=0} \mathcal{D}q\; e^{-\frac{m}{2\beta}\int_0^1 d\tau \dot{q}^2}} \tag{2.25}$$

where the time has been rescaled, $\tau \to \frac{\tau}{\beta}$, we have set $\hbar = 1$ and multiplied and divided by the free path integral, that is

$$K_{\rm free}(x_{\rm f}, x_{\rm i}; \beta) = \int \mathcal{D}x_{\rm bg} \int_{q(0)=0}^{q(1)=0} \mathcal{D}q\; e^{-\frac{m}{2\beta}\int_0^1 d\tau \dot{q}^2}. \tag{2.26}$$

Now, the idea behind perturbation theory is to Taylor-expand the potential $V(x_{\rm bg}+q)$ about $V(x_{\rm bg})$ assuming that perturbations are "small" compared to the kinetic term,

$$S_{\rm int} = \beta \int_0^1 d\tau \left[V(x_{\rm bg}(\tau)) + V^{(1)}(x_{\rm bg}(\tau))q(\tau) + \frac{1}{2!}V^{(2)}(x_{\rm bg}(\tau))q^2(\tau) + \dots \right]. \tag{2.27}$$

At this point we can expand the exponential in the numerator of (2.25) and get terms proportional to

$$\frac{\int_{q(0)=0}^{q(1)=0} \mathcal{D}q\; e^{-\frac{m}{2\beta}\int_0^1 d\tau\, \dot{q}^2} q(\tau_1)\dots q(\tau_k)}{\int_{q(0)=0}^{q(1)=0} \mathcal{D}q\; e^{-\frac{m}{2\beta}\int_0^1 d\tau\, \dot{q}^2}} = \langle q(\tau_1)\dots q(\tau_k)\rangle \tag{2.28}$$

called *correlation functions* of the quantum fields $q(\tau)$. Hence the transition amplitude (2.25) is written has

$$K(x_{\rm f}, x_{\rm i}; \beta) = K_{\rm free}(x_{\rm f}, x_{\rm i}; \beta) \left\langle e^{-\beta \int_0^1 d\tau\, V(x_{\rm bg}(\tau)+q(\tau))} \right\rangle. \tag{2.29}$$

An efficient way to compute perturbatively eq. (2.29) is by means of the so called generating functional $Z[j]$, where $j(\tau)$ are source fields to be attached to $q(\tau)$ as follows

$$Z[j] = \int_{q(0)=0}^{q(1)=0} \mathcal{D}q\; e^{-\frac{m}{2\beta}\int_0^1 d\tau\, \dot{q}^2(\tau) - \int_0^1 d\tau\, q(\tau)j(\tau)}. \tag{2.30}$$

The correlation function is then obtained as

$$\langle q(\tau_1)\dots q(\tau_k)\rangle = (-1)^k \frac{1}{Z(0)} \frac{\delta^k}{\delta j(\tau_1)\dots j(\tau_k)} Z[j]|_{j=0}. \tag{2.31}$$

Partially integrating the square of fluctuations and completing the square leads to

$$Z[j] = e^{-\frac{1}{2}\int_0^1 d\tau \int_0^1 d\tau' j(\tau) D^{-1}(\tau,\tau') j(\tau')} \int_{q(0)=0}^{q(1)=0} \mathcal{D}q'\; e^{-\frac{m}{2\beta}\int_0^1 d\tau\, \dot{q}'^2} \tag{2.32}$$

with $D^{-1}(\tau,\tau')$ being the inverse of the kinetic term $D(\tau,\tau') = \frac{m}{\beta}\partial_\tau^2 \delta(\tau-\tau')$ or propagator. It is associated to the rescaled fields $q'(\tau) = q(\tau) - \int_0^1 d\tau'\; j(\tau')D(\tau',\tau)$ and gives

$$D^{-1}(\tau,\tau') = \frac{\beta}{m}\Delta(\tau,\tau') \tag{2.33}$$

satisfying $^{\bullet\bullet}\Delta(\tau,\tau') = \delta(\tau,\tau')$[2]. According also to the properties $\Delta(\tau,\tau') = \Delta(\tau',\tau)$ and $\Delta(\tau,0) = \Delta(0,\tau') = 0$, one realizes that the Green's function has the form

$$\Delta(\tau,\tau') = \frac{|\tau-\tau'|}{2} - \frac{\tau+\tau'}{2} + \tau\tau'. \tag{2.34}$$

At this point, the generating functional (2.32) contains a path integral which is source-independent and can be performed obtaining exactly $Z(0)$,

$$Z[j] = Z(0)e^{-\frac{\beta}{2m}\int_0^1 d\tau \int_0^1 d\tau' j(\tau)\Delta(\tau,\tau')j(\tau')}. \tag{2.35}$$

Now, eq. (2.35) can be inserted into eq. (2.31) to compute correlation functions. Doing that, we notice that:

1. correlations functions of an odd number of fields are null;

2. the 2-point correlation function is just proportional to the known propagator,

$$\langle q(\tau)q(\tau')\rangle = -\frac{\beta}{m}\Delta(\tau,\tau'); \tag{2.36}$$

3. non-null correlation functions are built up from 2-point ones, for instance

$$\begin{aligned}\langle q(\tau_1)q(\tau_2)q(\tau_3)q(\tau_4)\rangle &= \langle q(\tau_1)q(\tau_2)\rangle\langle q(\tau_3)q(\tau_4)\rangle + \\ &+ \langle q(\tau_1)q(\tau_3)\rangle\langle q(\tau_2)q(\tau_4)\rangle + \langle q(\tau_1)q(\tau_4)\rangle\langle q(\tau_2)q(\tau_3)\rangle\,;\end{aligned} \tag{2.37}$$

This last property is known as Wick's theorem and can be applied to any even number of quantum fields. The prescription is then to build all possible couples between the involved fields and to sum all contributions. In this way, it is possible to compute the transition amplitude (2.29) at any perturbation order, just by expanding the exponent and computing correlation functions of fields $q(\tau)$. This is the basic machinery that one exploits to compute perturbatively transition amplitudes in flat space. In the following we will see what changes when we embed our theory in a curved space background.

[2]Dots on the left (right) mean derivatives taken with respect to the first (second) variable.

Chapter 3

Curved space in σ-models

3.1 Generalities

An easy way to include curved space in our theory is to introduce a minimal coupling with gravity by means of the metric tensor $g_{\mu\nu}(x)$ which models the free dynamics of the point-particle. For a $m = 1$ particle, the associated Lagrangian in Euclidean notation then reads

$$L(x) = \frac{1}{2} g_{\mu\nu}(x) \frac{\partial x^\mu}{\partial \tau} \frac{\partial x^\nu}{\partial \tau} + V(x) \tag{3.1}$$

when a scalar potential $V(x)$ can be included. If the point-particle, usually identified directly with its coordinates $x(\tau)$, lives for a time-interval β that we call propagation time, then its associated action reads

$$S[x] = \int_0^\beta d\tau \; L(x) \tag{3.2}$$

and identifies a nonlinear σ-model where the nonlinearity stems from the fact that the free particle ($V = 0$) obeys a nonlinear equation of motion. Furthermore, this model in particular is called one dimensional because the point-particle has only one parameter, that is the proper time τ. The particle is then seen as moving on a line parametrized by τ, whose shape follows the curved space where it lives. Such line is named worldline[1]. The study of $1D$ nonlinear σ-models is *per se* non trivial even though the only kinetic term is considered: from eq. (3.1) we see that is has double derivatives coupled to a non flat metric which, in a perturbation expansion, imply derivative interactions that lead to ultraviolet divergences. One then finds Feynman diagrams which are separately divergent. However, once summed together, the final

[1] Actually it is possible to introduce further degrees of freedom: if another affine parameter σ is included, then the particle $x(\tau, \sigma)$ lives on a sheet, called worldsheet. In such way strings may be described, for instance.

result must be finite, due to divergence cancellations. Thus, it is particularly important in the perturbative derivation to define a technique to perform the emerging worldline integrals, which usually include distributions. An example is

$$I = \int_{-1}^{0} d\tau_1 \int_{-1}^{0} d\tau_2 \; \delta(\tau_1 - \tau_2)\theta^2(\tau_1 - \tau_2). \tag{3.3}$$

These integrals are definitely non trivial, as the result may change according to how one treats the distributions. Historically there are three procedures to study the perturbation theory of worldline models in curved space, which are called regularization schemes. They are time-slicing (TS), mode regularization (MR) and dimensional regularization (DR). TS essentially breaks the whole propagation time β into a large number of shorter intervals, for which a discretized definition of the propagators is guaranteed; MR achieves discretization by mode-expanding the fields in terms of convenient functions and limiting its number with a cut-off; DR, finally, introduces a number of extra-dimensions. Each of them provides different recipes to perform integrals like (3.3). However, as one expects, the final result at each perturbative order is scheme independent [15].

In the following, we briefly review these schemes, pointing out the main differences and features. In fact depending on the type of calculation that one performs, some schemes turn out to be more convenient than others. As an example, for a pure analytical perturbative computation, one may prefer DR or MR, whereas in the case of numerical WLMC, the choice is TS.

3.2 Time-slicing

Let us start from the quantum Hamiltonian of a free scalar point-particle minimally coupled to gravity and satisfying Einstein invariance[2], *i.e.*

$$\mathbf{H}(\mathbf{x},\mathbf{p}) = \frac{1}{2} g^{-\frac{1}{4}}(\mathbf{x})\mathbf{p}_\mu g^{\mu\nu}(\mathbf{x}) g^{\frac{1}{2}}(\mathbf{x})\mathbf{p}_\nu g^{-\frac{1}{4}}(\mathbf{x}), \tag{3.4}$$

with $g(\mathbf{x}) = \det g_{\mu\nu}(\mathbf{x})$. As done in flat space, we can define the transition amplitude as

$$K(x_\mathrm{f}, x_\mathrm{i}; \beta) = \langle x_\mathrm{f} | \, e^{-\frac{\beta}{\hbar}\mathbf{H}} \, | x_\mathrm{i} \rangle \tag{3.5}$$

[2]The requirement of Einstein inavriance allows us to study the dynamics in any coordinate system.

with identity operators

$$\begin{aligned} \int |x\rangle \sqrt{g(x)} \langle x| \, d^n x = \mathbf{1} \\ \int |p\rangle \langle p| \, d^n p = \mathbf{1} \end{aligned} \tag{3.6}$$

and

$$\begin{aligned} \langle x|x'\rangle = \frac{\delta^n(x-x')}{\sqrt{g(x)}} \\ \langle p|p'\rangle = \delta^n(p-p') \end{aligned} \tag{3.7}$$

guaranteeing K to be a bi-scalar under Einstein transformations. A plane wave then reads

$$\langle x|p\rangle = \frac{e^{\frac{i}{\hbar}p\cdot x}}{(2\pi\hbar)^{\frac{n}{2}} g^{\frac{1}{4}}(x)}. \tag{3.8}$$

Following what we did in flat space, we insert N p-space identities and $N-1$ x-space identities from (3.6) into the transition amplitude,

$$\begin{aligned} &K(x_\mathrm{f}, x_\mathrm{i}; \beta) = \langle x_\mathrm{f}| \left(e^{-\frac{\epsilon}{\hbar}\mathbf{H}}\right)^N |x_\mathrm{i}\rangle = \\ &= \int d^n p_N \int d^n p_{N-1} \ldots \int d^n p_1 \, \langle x_\mathrm{f}| \, e^{-\frac{\epsilon}{\hbar}\mathbf{H}} \, |p_N\rangle \, \langle p_N|x_{N-1}\rangle \int \sqrt{g(x_{N-1})} d^n x_{N-1} \times \\ &\times \langle x_{N-1}| \, e^{-\frac{\epsilon}{\hbar}\mathbf{H}} \, |p_{N-1}\rangle \, \langle p_{N-1}|x_{N-2}\rangle \int \sqrt{g(x_{N-2})} d^n x_{N-2} \times \\ &\times \ldots \times \langle x_1| \, e^{-\frac{\epsilon}{\hbar}\mathbf{H}} \, |p_1\rangle \, \langle p_1|x_\mathrm{i}\rangle \,, \end{aligned} \tag{3.9}$$

with $x_N = x_\mathrm{f}$, $x_0 = x_\mathrm{i}$, $\epsilon = \frac{\beta}{N}$. Now, a key observation is that the infinitesimal evolution operator $e^{-\frac{\epsilon}{\hbar}\mathbf{H}(\mathbf{x},\mathbf{p})}$ mixes the configuration space and momentum space operators $\mathbf{x}$, $\mathbf{p}$ as prescribed by eq. (3.4) in a non trivial way. For it to be applied within the contractions of (3.9) in an easy way, such operators have to be Weyl-ordered, that is symmetrized with respect to all $\mathbf{x}$'s and $\mathbf{p}$'s. To provide an example, we symmetrize the operator $\mathbf{xp}$ as follows

$$\mathbf{xp} = \frac{1}{2}\{\mathbf{x},\mathbf{p}\} + \frac{1}{2}[\mathbf{x},\mathbf{p}] = \frac{1}{2}\{\mathbf{x},\mathbf{p}\} + \frac{1}{2}i\hbar. \tag{3.10}$$

For a Weyl-ordered operator $\mathbf{O}_W(\mathbf{x},\mathbf{p})$ one then has

$$\begin{aligned}
&\int \langle x_k|\,\mathbf{O}_W(\mathbf{x},\mathbf{p})\,|p_k\rangle\,\langle p_k|x_{k-1}\rangle\,d^n p_k = \\
&= \frac{1}{2}\int \langle x_k|\,\mathbf{O}_W(\mathbf{x},\mathbf{p})\,|p_k\rangle\,\langle p_k|x_{k-1}\rangle\,d^n p_k + \frac{1}{2}\int \langle x_k|p_k\rangle\,\times \\
&\times \langle p_k|\,\mathbf{O}_W(\mathbf{x},\mathbf{p})\,|x_{k-1}\rangle\,d^n p_k \\
&= \int \langle x_k|p_k\rangle\,O_W\left(\frac{x_k+x_{k-1}}{2},p_k\right)\langle p_k|x_{k-1}\rangle\,d^n p_k,
\end{aligned} \tag{3.11}$$

implying that for symmetrized operators, we can replace operators with numbers

$$\mathbf{O}_W(\mathbf{x},\mathbf{p}) \to O_W\left(\frac{x_k+x_{k-1}}{2},p_k\right) \tag{3.12}$$

using the so called midpoint rule. Hence in (3.9) we apply[3]

$$\begin{aligned}
&\int \langle x_k|\left(e^{-\frac{\epsilon}{\hbar}\mathbf{H}}\right)_W|p_k\rangle\,\langle p_k|x_{k-1}\rangle\,d^n p_k \\
&= \int \langle x_k|p_k\rangle\left(e^{-\frac{\epsilon}{\hbar}H\left(\frac{x_k-x_{k-1}}{2},p_k\right)}\right)_W\langle p_k|x_{k-1}\rangle\,d^n p_k.
\end{aligned} \tag{3.13}$$

Now, the Weyl-ordered Hamiltonian reads

$$\mathbf{H}_W(\mathbf{x},\mathbf{p}) = \left(\frac{1}{2}g^{\mu\nu}(\mathbf{x})\mathbf{p}_\mu\mathbf{p}_\nu\right)_S + \frac{\hbar^2}{8}\left[R(x) + g^{\mu\nu}(x)\Gamma^\rho{}_{\mu\sigma}(x)\Gamma^\sigma{}_{\nu\rho}(x)\right] \tag{3.14}$$

with $(\ldots)_S$ being the symmetrized part of $(\ldots)$, $R(x)$ being the curvature scalar and $\Gamma^\mu{}_{\nu\rho}(x)$ being the torsionless Christoffel's symbol. In our case, we have explicitly

$$\left(\frac{1}{2}g^{\mu\nu}(\mathbf{x})\mathbf{p}_\mu\mathbf{p}_\nu\right)_S = \frac{1}{8}g^{\mu\nu}(\mathbf{x})\mathbf{p}_\mu\mathbf{p}_\nu + \frac{1}{4}\mathbf{p}_\mu g^{\mu\nu}(\mathbf{x})\mathbf{p}_\nu + \frac{1}{8}\mathbf{p}_\mu\mathbf{p}_\nu g^{\mu\nu}(\mathbf{x}). \tag{3.15}$$

Using (3.13) inside (3.9), we get

$$\begin{aligned}
K(x_\mathrm{f},x_\mathrm{i};\beta) &= \lim_{N\to\infty}\left[g(x_\mathrm{f})g(x_\mathrm{i})\right]^{-\frac{1}{4}}\int\left(\prod_{k=1}^{N}\frac{d^n p_k}{(2\pi\hbar)^n}\prod_{l=1}^{N-1}d^n x_l\right)\times \\
&\times\exp\left[\sum_{k=1}^{N}\left\{\frac{i}{\hbar}p_k\cdot(x_k-x_{k-1}) - \frac{\epsilon}{\hbar}H_W(\bar{x}_{k-\frac{1}{2}},p_k)\right\}\right]
\end{aligned} \tag{3.16}$$

where $\bar{x}_{k-\frac{1}{2}} = \frac{1}{2}(x_k + x_{k-1})$ and

$$H_W\left(\bar{x}_{k-\frac{1}{2}},p_k\right) = \frac{1}{2}g^{\mu\nu}\left(\bar{x}_{k-\frac{1}{2}}\right)p_{k,\mu}p_{k,\nu} + V_{TS}\left(\bar{x}_{k-\frac{1}{2}}\right) \tag{3.17}$$

[3] We actually can exploit the replacement $\left(e^{-\frac{\epsilon}{\hbar}\mathbf{H}}\right)_W \to e^{-\frac{\epsilon}{\hbar}\mathbf{H}_W}$.

$$V_{TS} = \frac{\hbar^2}{8}\left(R + g^{\mu\nu}\Gamma^{\rho}{}_{\mu\sigma}\Gamma^{\sigma}{}_{\nu\rho}\right). \tag{3.18}$$

V_{TS} is the time-slicing counterterm which emerges from the specific previous treatment of slicing the time interval to regularize the path integral, and constitutes a contribution to the potential which encodes spacetime curvature information. However, the most striking feature of V_{TS} is the presence of noncovariant $\Gamma\Gamma$ terms. This is due to the fact that H_s, needed to obtain the time-sliced path integral, is not Einstein-invariant.

If we now integrate (3.16) over momenta after completing the square in the exponent, we obtain N determinants

$$\left[\det g^{\mu\nu}\left(\bar{x}_{k-\frac{1}{2}}\right)\right]^{-\frac{1}{2}} = \left[\det g_{\mu\nu}\left(\bar{x}_{k-\frac{1}{2}}\right)\right]^{\frac{1}{2}} \tag{3.19}$$

which are usually represented as ghost fields path integrals. These fields are called ghosts as they are nonphysical, hence do not emerge as asymptotic states, rather are mathematical tools which reproduce the path integral measure, and that we can exploit at the perturbative level to produce those Feynman diagrams which cancel ultraviolet divergences and make the final result finite. Ghost fields are denoted as a (commuting) and b, c (anticommuting) [9], specifically,

$$\begin{aligned}\left[\det g_{\mu\nu}\left(\bar{x}_{k-\frac{1}{2}}\right)\right]^{\frac{1}{2}} \sim \int \left(\prod_{j=1}^{N} da^{\nu}_{k-\frac{1}{2}} db^{\nu}_{k-\frac{1}{2}} dc^{\nu}_{k-\frac{1}{2}}\right) \times \\ \times \exp\left[-\frac{\epsilon}{2\beta^2\hbar} g_{\mu\nu}\left(\bar{x}_{k-\frac{1}{2}}\right)\left(b^{\mu}_{k-\frac{1}{2}} c^{\nu}_{k-\frac{1}{2}} + a^{\mu}_{k-\frac{1}{2}} a^{\nu}_{k-\frac{1}{2}}\right)\right].\end{aligned} \tag{3.20}$$

The standard procedure at this point is to split the fields x_k into background fields $x_{bg,k}$ plus quantum fluctuations q_k and decompose the action S into a part $S^{(0)}$ quadratic in q and an interaction part $S^{(\text{int})}$. $S^{(0)}$ is used to build up propagators, whereas $S^{(\text{int})}$ provides interaction vertices. External sources F and G are then coupled to the combinations $\frac{1}{2}(q_k + q_{k-1})$ and $q_k - q_{k-1}$, whereas for the ghost sector we use the sources A, B and C,

$$\begin{aligned}-\frac{1}{\hbar} S_{(\text{sources, no-ghost})} &= \sum_{k=1}^{N}\left(F_{k-\frac{1}{2},\mu}\frac{q^{\mu}_k - q^{\mu}_{k-1}}{\epsilon/\beta} + G_{k-\frac{1}{2},\mu} q^{\mu}_{k-\frac{1}{2}}\right) \\ -\frac{1}{\hbar} S_{(\text{sources, ghost})} &= \sum_{k=0}^{N-1}\left(A_{k+\frac{1}{2},\mu} a^{\mu}_{k+\frac{1}{2}} + b^{\mu}_{k+\frac{1}{2}} B_{k+\frac{1}{2},\mu} + C_{k+\frac{1}{2},\mu} c^{\mu}_{k+\frac{1}{2}}\right).\end{aligned} \tag{3.21}$$

After diagonalizing $S^{(0)} + S_{(\text{sources, no-ghost})} + S_{(\text{sources, ghost})}$ with a convenient orthogonal variable transformation, one defines the generating functional $Z_N^{(0)}$as the path integral with the quadratic parts of the action and the external sources. Replacing the quantum fields in $S^{(\text{int})}$ with the corresponding (derivatives with respect to the) sources, one reconstructs the full generating functional by applying $S^{(\text{int})}$ onto $Z_N^{(0)}$,

$$Z_N(x_\text{f}, x_\text{i}; \beta) = \left[\frac{g(x_\text{f})}{g(x_\text{i})}\right]^{\frac{1}{4}} \frac{1}{(2\pi\hbar\beta)^{\frac{n}{2}}} \left(e^{-\frac{1}{\hbar}S^{(\text{int})}} e^{-\frac{1}{\hbar}S[F,G,A,B,C]}\right)|_0 \tag{3.22}$$

where $S[F, G, A, B, C]$ contains the terms bilinear in sources. Propagators are extracted by taking derivatives of $e^{-\frac{1}{\hbar}S[F,G,A,B,C]}$ and then setting sources to zero. As an example, the $\dot{q}\dot{q}$ propagator is given by

$$\left\langle \dot{q}^\mu_{k+\frac{1}{2}} \dot{q}^\nu_{k'+\frac{1}{2}} \right\rangle = \frac{\partial}{\partial F_{k+\frac{1}{2},\mu}} \frac{\partial}{\partial F_{k'+\frac{1}{2},\nu}} e^{-\frac{1}{\hbar}S[F,G,A,B,C]}|_0 \,, \tag{3.23}$$

where the discretized time-derivative of the coordinate is given by (for later convenience we consider the derivative w.r.t. the rescaled time $\tau = t/\beta$)

$$\dot{q}^\mu_{k+\frac{1}{2}} := \frac{\beta}{\epsilon}(q^\mu_{k+1} - q^\mu_k) \,. \tag{3.24}$$

In this way we can find the discretized expressions for the propagators, that is

$$\begin{aligned}
\left\langle q^\mu_{k+\frac{1}{2}} q^\nu_{k'+\frac{1}{2}} \right\rangle &= \epsilon\hbar g^{\mu\nu}(x_\text{f})\Big[- \frac{(k+1/2)(k'+1/2)}{N} + (k'+1/2)\theta_{k,k'} + \\
&\qquad + (k+1/2)\theta_{k,k'} - \frac{1}{4}\delta_{k,k'}\Big] \\
\left\langle q^\mu_{k+\frac{1}{2}} \dot{q}^\nu_{k'+\frac{1}{2}} \right\rangle &= \beta\hbar g^{\mu\nu}(x_\text{f}) \left(-\frac{k+1/2}{N} + \theta_{k,k'}\right) \\
\left\langle \dot{q}^\mu_{k+\frac{1}{2}} \dot{q}^\nu_{k'+\frac{1}{2}} \right\rangle &= \beta\hbar g^{\mu\nu}(x_\text{f})(-1 + N\delta_{k,k'}) \\
\left\langle a^\mu_{k+\frac{1}{2}} a^\nu_{k'+\frac{1}{2}} \right\rangle &= \frac{\hbar}{\epsilon} g^{\mu\nu}(x_\text{f})\delta_{k,k'} \\
\left\langle b^\mu_{k+\frac{1}{2}} c^\nu_{k'+\frac{1}{2}} \right\rangle &= -2\frac{\hbar}{\epsilon} g^{\mu\nu}(x_\text{f})\delta_{k,k'},
\end{aligned} \tag{3.25}$$

where we used the discrete functions

$$\theta_{k,k'} = \begin{cases} 1, & k > k' \\ 0, & k < k' \\ \frac{1}{2}, & k = k' \end{cases}$$

$$\delta_{k,k'} = \begin{cases} 1, & k = k' \\ 0, & k \neq k' \end{cases}, \tag{3.26}$$

and the (rescaled) time discretization

$$\tau_k = -1 + \frac{k\epsilon}{\beta} = -1 + \frac{k}{N}, \quad k = 1, \dots, N, \tag{3.27}$$

so that $\tau_1 = -1 + \frac{1}{N} \to -1$ and $\tau_N = 0$.

In the continuum limit the propagators for the coordinates q^μ (and derivatives thereof), can be obtained from (2.36) by setting $m = 1$, whereas the ghost propagators are simply (proportional to) the Dirac's delta function, i.e.

$$\begin{aligned} \langle q^\mu(\tau_1) q^\nu(\tau_2) \rangle &= -\beta\hbar g^{\mu\nu}(x_{\mathrm{f}}) \Delta(\tau_1, \tau_2) \\ \langle q^\mu(\tau_1) \dot{q}^\nu(\tau_2) \rangle &= -\beta\hbar g^{\mu\nu}(x_{\mathrm{f}}) \left(\tau_1 + \theta(\tau_2 - \tau_1)\right) \\ \langle \dot{q}^\mu(\tau_1) \dot{q}^\nu(\tau_2) \rangle &= -\beta\hbar g^{\mu\nu}(x_{\mathrm{f}}) \left(1 - \delta(\tau_2 - \tau_1)\right) \\ \langle a^\mu(\tau_1) a^\nu(\tau_2) \rangle &= \beta\hbar g^{\mu\nu}(x_{\mathrm{f}}) \delta(\tau_1 - \tau_2) \\ \langle b^\mu(\tau_1) c^\nu(\tau_2) \rangle &= -2\beta\hbar g^{\mu\nu}(x_{\mathrm{f}}) \delta(\tau_1 - \tau_2) \end{aligned} \tag{3.28}$$

with

$$\Delta(\tau_1, \tau_2) = \tau_1(\tau_2 + 1)\theta(\tau_1 - \tau_2) + \tau_2(\tau_1 + 1)\theta(\tau_2 - \tau_1) . \tag{3.29}$$

In the perturbative calculation of the transitions amplitude, whenever ambiguous products of distributions occur, time slicing regularization can be used at the discretized level. Basically, the discretized version of the propagators yield the "rules of thumb" to unambiguously compute the integrals. Indeed, by comparing the propagators in the continuum (3.28) to their discretized counterparts, we have that

$$N\delta_{k,k'} = \beta\epsilon\delta_{k,k'} \longleftrightarrow \beta\delta(t - t') = \delta(\tau - \tau') \tag{3.30}$$

$$\theta_{k,k'} \longleftrightarrow \theta(\tau - \tau') \tag{3.31}$$

$$\tfrac{k}{N} \longleftrightarrow \tau + 1 . \tag{3.32}$$

For example it is easy at this point to compute the integral (3.3). Namely,

$$I \longrightarrow \sum_{k,k'} \frac{1}{N^2} N\delta_{k,k'}\theta^2_{k,k'} = \frac{1}{N}\sum_k \theta^2_{k,k} = \frac{1}{4} , \tag{3.33}$$

i.e. one can treat the $\theta(\tau)$ as a regular function with $\theta(0) = \frac{1}{2}$, as the Dirac delta function gets discretized as a Kronecker delta.

Such propagators can now be used when $S^{(\mathrm{int})}$ is expanded and Wick contractions are applied to the fields of the interaction vertices.

As we have seen, the time-slicing regularization scheme is constructed from first principles: indeed it is a generalization to curved space of the ideas that let Feynman to introduce path integrals themselves. The approaches that we will sketch in the following, that is mode and dimensional regularization, are not genuinely coming from first principles, hence renormalization conditions have to be applied to the relative counterterms.

3.3 Mode regularization

Let us here summarize how Mode Regularization works. Let us start from a generic classical action in Euclidean time for a scalar point-particle (we set $\hbar = 1$),

$$S = \int_{t_\mathrm{i}}^{t_\mathrm{f}} d\tau \left[\frac{1}{2} g_{\mu\nu}(x) \frac{\partial x^\mu}{\partial \tau} \frac{\partial x^\nu}{\partial \tau} + V(x)\right], \tag{3.34}$$

which is used to define directly the transition amplitude as the path integral

$$\langle x^k_\mathrm{f}, t_\mathrm{f} | x^k_\mathrm{i}, t_\mathrm{i} \rangle = \int_{\mathrm{DBC}} \mathcal{D}x \; e^{-S} \tag{3.35}$$

with Dirichlet boundary conditions $x^k(t_\mathrm{i}) = x^k_\mathrm{i}$, $x^k(t_\mathrm{f}) = x^k_\mathrm{f}$. The path integral measure itself includes curved space information and is given by

$$\mathcal{D}x = \prod_{\tau \in (t_\mathrm{i}, t_\mathrm{f})} \sqrt{\det g_{\mu\nu}(x(\tau))}\, d^n x(\tau). \tag{3.36}$$

As the measure is general coordinate invariant but not translationally invariant under $x^\mu(\tau) \to x^\mu(\tau) + \epsilon^\mu$, ones prefers to use ghost fields as previously done in time-slicing,

$$\prod_{\tau \in (t_\mathrm{i}, t_\mathrm{f})} \sqrt{\det g_{\mu\nu}(x(\tau))} = \int DaDbDc \; e^{-S_{\mathrm{gh}}} \tag{3.37}$$

with

$$S_{\mathrm{gh}} = \int_{t\mathrm{i}}^{t\mathrm{f}} d\tau \frac{1}{2} g_{\mu\nu}(x) \left(a^\mu a^\nu + b^\mu c^\nu\right), \tag{3.38}$$

$$Da = \prod_{\tau\in(t_\mathrm{i},t_\mathrm{f})} d^n a(\tau), \quad Db = \prod_{\tau\in(t_\mathrm{i},t_\mathrm{f})} d^n b(\tau), \quad Dc = \prod_{\tau\in(t_\mathrm{i},t_\mathrm{f})} d^n c(\tau). \tag{3.39}$$

Again using rescaled times $\beta = t_\mathrm{f} - t_\mathrm{i}$ and $\tau \to \frac{\tau - t_\mathrm{f}}{\beta}$, and writing the action as $S = \frac{1}{\beta} S'$, we find

$$S' = \int_{-1}^{0} d\tau \ \left[\frac{1}{2} g_{\mu\nu}(x)\dot{x}^\mu \dot{x}^\nu + \beta^2 \left(V(x) + V_\mathrm{MR}(x)\right)\right] , \tag{3.40}$$

with $\dot{x}^k = \frac{\partial x^k}{\partial \tau}$. Upon these rescalings, we can identify β as the loop-counting parameter, the role that is usually played by $\hbar$. Thus, one solves the path integral perturbatively in β and in the displacements $\xi^\mu = x^\mu_\mathrm{i} - x^\mu_\mathrm{f}$, helped by the usual quantum - background splitting

$$x^\mu(\tau) = x^\mu_\mathrm{bg}(\tau) + q^\mu(\tau) \, . \tag{3.41}$$

Now, the key point is to expand the fluctuations, which vanish at the boundaries of the τ-line, in Fourier modes. Generalizing the fields as $\phi^\mu(\tau) = (q^\mu(\tau), a^\mu(\tau), b^\mu(\tau), c^\mu(\tau))$, we write their mode expansion as

$$\phi^\mu(\tau) = \sum_{m=1}^{\infty} \phi^\mu_m \sin(\pi m \tau), \tag{3.42}$$

$$\phi^\mu_m = (q^\mu_m, a^\mu_m, b^\mu_m, c^\mu_m) \, , \tag{3.43}$$

and for the measure, we set

$$\mathcal{D}x = \prod_{\tau\in(-1,0)} \sqrt{\det g_{\mu\nu}(x(\tau))} Dx = Dq \int DaDbDc \ e^{-\frac{1}{\beta} S_\mathrm{gh}} \, . \tag{3.44}$$

In terms of the Fourier modes, we thus have

$$DqDaDbDc = \lim_{M\to\infty} A \prod_{m=1}^{M} \prod_{\mu=1}^{n} m dq^\mu_m da^\mu_m db^\mu_m dc^\mu_m \tag{3.45}$$

where the normalization constant A is fixed later. The factor of m is nothing but the square root of the inverse of kinetic term for mode q_m, and it serves to suitably normalize the q measure, leaving the overall β-dependent part of the normalization inside A. As we can see, the regularization is actually achieved by limiting the number M of expansion mode and, at the end, sending it to infinity. However, as sketched below, practically this yields some specific rules of integration by parts, which allow

to cast the integrand in an unambiguous form, that can be safely computed using the continuum version of the propagators. At this point, in order to perform perturbative calculations, one extracts the quadratic piece of action, S_2 and the interacting part $S_{\rm int}$: the first defines propagators whereas the second produces vertices. Expressing the $x^\mu(\tau)$ field as

$$x^\mu(\tau) = x^\mu_{\rm f} - \xi^\mu \tau + q^\mu(\tau) \tag{3.46}$$

with $q^\mu(\tau)$ vanishing at the boundaries, we can use eq. (3.40) at the level of S_2 where $g_{\mu\nu}$ is evaluated at $\tau_{\rm f}$, so to get

$$S_2 = \frac{1}{2} g_{\mu\nu}(x_{\rm f})\xi^\mu\xi^\nu + \frac{1}{4} g_{\mu\nu}(x_{\rm f}) \sum_{m=1}^{M} \left(\pi^2 m^2 q^\mu_m q^\nu_m + a^\mu_m a^\nu_m + b^\mu_m c^\nu_m\right). \tag{3.47}$$

Eq. (3.47) is used within the path integral with sources and completing squares the extract propagators, as previously done. As an example, the discretized version of the qq propagator will read

$$\langle q^\mu(\tau_1) q^\nu(\tau_2)\rangle = \beta g^{\mu\nu}(x_{\rm f}) \sum_{m=1}^{M} \frac{2}{\pi^2 m^2} \sin(\pi m \tau_1)\sin(\pi m \tau_2), \tag{3.48}$$

where $\frac{2}{\pi^2 m^2}$ is just the inverse kinetic *operator* for the m-th mode. So, one has

$$\begin{aligned}
\langle q^\mu(\tau_1) q^\nu(\tau_2)\rangle &= -\beta g^{\mu\nu}(x_{\rm f})\Delta(\tau_1,\tau_2) \\
\langle a^\mu(\tau_1) a^\nu(\tau_2)\rangle &= \beta g^{\mu\nu}(x_{\rm f})\Delta_{\rm gh}(\tau_1,\tau_2) \\
\langle b^\mu(\tau_1) c^\nu(\tau_2)\rangle &= -2\beta g^{\mu\nu}(x_{\rm f})\Delta_{\rm gh}(\tau_1,\tau_2)
\end{aligned} \tag{3.49}$$

where, in the continuum limit,

$$\begin{aligned}
\Delta(\tau_1,\tau_2) &= \sum_{m=1}^{M} \left[-\frac{2}{\pi^2 m^2}\sin(\pi m\tau_1)\sin(\pi m\tau_2)\right] \\
&\xrightarrow[M\to\infty]{} \tau_1(\tau_2+1)\theta(\tau_1-\tau_2) + (\tau_1 \leftrightarrow \tau_2) \\
\Delta_{\rm gh}(\tau_1,\tau_2) &= \sum_{m=1}^{M} 2\sin(\pi m\tau_1)\sin(\pi m\tau_2) \xrightarrow[M\to\infty]{} \delta(\tau_1-\tau_2).
\end{aligned} \tag{3.50}$$

We emphasize that the dotted propagators

$$\begin{aligned}
{}^\bullet\Delta(\tau_1,\tau_2) &= \partial_{\tau_1}\Delta(\tau_1,\tau_2) \\
\Delta^\bullet(\tau_1,\tau_2) &= \partial_{\tau_2}\Delta(\tau_1,\tau_2) \\
{}^\bullet\Delta^\bullet(\tau_1,\tau_2) &= \partial_{\tau_1}\partial_{\tau_2}\Delta(\tau_1,\tau_2)
\end{aligned} \tag{3.51}$$

are obtained sending $M \to \infty$ after taking derivatives at the discretized level.

Actually, the formal expression of the propagators are the same as those of time-slicing, but for finite M, their properties change. In particular there are different rules for the computation of worldline integrals like

$$I = \int_{-1}^{0}\int_{-1}^{0} d\tau_1 d\tau_2 \, {}^{\bullet}\Delta(\tau_1,\tau_2){}^{\bullet}\Delta^{\bullet}(\tau_1,\tau_2)\Delta^{\bullet}(\tau_1,\tau_2). \tag{3.52}$$

In the time-slicing scheme, $\delta(\tau_1-\tau_2)$ is used as a Kronecker's delta function in the sense that, also in presence of distributions θ's, it sets $\tau_1=\tau_2$. Hence, this ultimately leads to

$$I(\mathrm{TS}) = -\frac{1}{6}. \tag{3.53}$$

In the mode regularization scheme, a direct inspection of the discretized propagators suggests the following treatment,

$$\begin{aligned} I(\mathrm{MR}) &= \int_{-1}^{0}\int_{-1}^{0} d\tau_1 d\tau_2 \, ({}^{\bullet}\Delta)({}^{\bullet}\Delta^{\bullet})(\Delta^{\bullet}) \\ &= \int_{-1}^{0}\int_{-1}^{0} d\tau_1 d\tau_2 \, \frac{1}{2}\left[({}^{\bullet}\Delta)^2\right]^{\bullet}(\Delta^{\bullet}) \\ &= -\frac{1}{2}\int_{-1}^{0}\int_{-1}^{0} d\tau_1 d\tau_2 \, ({}^{\bullet}\Delta)^2(\Delta^{\bullet\bullet}) \\ &= -\frac{1}{2}\int_{-1}^{0}\int_{-1}^{0} d\tau_1 d\tau_2 \, ({}^{\bullet}\Delta)^2({}^{\bullet\bullet}\Delta) \\ &= -\frac{1}{6}\int_{-1}^{0}\int_{-1}^{0} d\tau_1 d\tau_2 \, {}^{\bullet}\left[({}^{\bullet}\Delta)^3\right] \\ &= -\frac{1}{12}. \end{aligned} \tag{3.54}$$

In the first pass we have used that, at finite M, $\Delta^{\bullet\bullet}\Delta^{\bullet} = \frac{1}{2}\left[({}^{\bullet}\Delta)^2\right]^{\bullet}$; in the second pass we have integrated by parts in τ_2, and picked up no boundary terms given that, at finite M, $({}^{\bullet}\Delta)^2$ vanishes at the endpoints of τ_2; in the third step we have used that ${}^{\bullet\bullet}\Delta = \Delta^{\bullet\bullet}$ and have used again integration by parts. In the last pass we are left with the boundary term $-\frac{1}{6}\int_{-1}^{0} d\tau_2 \, \left[{}^{\bullet}\Delta^3(0,\tau_2) - {}^{\bullet}\Delta^3(-1,\tau_2)\right]$ which can be safely computed in the continuum limit.

In this way, one can compute all the worldline integrals which are involved at each perturbative level of the β-expansion of the transition amplitude. However, as anticipated, also the counterterm results to be scheme - dependent. We see now how to obtain an expression for V_{MR} from renormalization conditions rather than first principles as done for time-slicing. One possible strategy is to use the Schrödinger equation

for the transition amplitude. The wavefunction evolves as

$$\Psi(x_{\rm f},t_{\rm f})=\int d^n x_{\rm i}\sqrt{g(x_{\rm i})}\,\langle x^\mu_{\rm f},t_{\rm f}|x^\mu_{\rm i},t_{\rm i}\rangle\,\Psi(x_{\rm i},t_{\rm i}) \tag{3.55}$$

and one imposes that $\Psi(x_{\rm f},t_{\rm f})$ satisfies the Schrödinger equation with Hamiltonian

$$H=-\frac{1}{2}\nabla^2+V \tag{3.56}$$

with $\nabla^2=g^{\mu\nu}(\nabla_\mu)(\partial_\nu)$ being the Einstein covariant laplacian. Expanding $\Psi(x_{\rm i},t_{\rm i})$ and $\sqrt{g(x_{\rm i})}$ around $x_{\rm f}$ produces the normalization $A=(2\pi\beta)^{\frac{n}{2}}$ for the order β^0. For the order β, one gets

$$\partial_t\Psi+\frac{1}{2}\nabla^2\Psi-\left(V+V_{\rm MR}-\frac{1}{8}R+\frac{1}{24}g^{\mu\nu}g^{\rho\sigma}g_{\alpha\beta}\Gamma^\alpha{}_{\mu\rho}\Gamma^\beta{}_{\nu\sigma}\right)\Psi=0, \tag{3.57}$$

which satisfies the Schrödinger equation, provided that

$$V_{\rm MR}=\frac{1}{8}R-\frac{1}{24}g^{\mu\nu}g^{\rho\sigma}g_{\alpha\beta}\Gamma^\alpha{}_{\mu\rho}\Gamma^\beta{}_{\nu\sigma}, \tag{3.58}$$

constitutes the mode regularization counterterm. Once again, the striking feature of V_{MR} is the presence of a noncovariant $\Gamma\Gamma$ term (different than the one present in V_{TS}). The noncovariance of V_{MR} can be ascribed to the fact that the mode expansion, at finite M, breaks Einstein invariance. Mode regularization counterterm was originally found in [29].

3.4 Dimensional regularization

This scheme is probably the most preferable one for analytical perturbative computations because the associated counterterm $V_{\rm DR}$ is particularly simple: as we will show it is covariant. The name itself suggests the idea: one produces an analytical continuation in the number of dimensions of the critical worldline integrals (namely, those exhibiting divergences) and, once divergences are removed, extra-dimensions are suppressed. Practically, once again, the method yields (new) integration by parts rules, which can be employed to cast the integrands in an unambiguous form, which can be safely computed at the unregularized level (extra dimensions removed). Hence, let us consider a number D of extra-dimensions for the particle proper time, defining $\mathbf{t}=(t^1,\ldots,t^D)$. The full time interval is then given by $t^\mu=(\tau,\mathbf{t})$, with $\mu=0,1,\ldots,D$

and $d^{D+1}t = d\tau\, d\mathbf{t}$, so that the extended action now reads

$$S = \int_\Omega d^{D+1}t \left[\frac{1}{2} g_{\alpha\beta}(\partial_\mu x^\alpha \partial_\mu x^\beta + a^\alpha a^\beta + b^\alpha c^\beta) + \beta^2 (V + V_{\rm DR})\right] \tag{3.59}$$

where Ω is a $(D+1)$-dimensional interval obtained by $[-1,0]$ and D infinitely extended intervals. In this way, derivatives are extended to $\partial_\tau \xrightarrow[1\to D+1]{} \partial_\mu$, with $\mu = (0,\ldots,D)$, and $\partial_0 = \partial_\tau$. The propagators in this case read

$$\begin{aligned}
\Delta(t_1,t_2) &= \int \frac{d^D\mathbf{k}}{(2\pi)^D} \sum_{m=1}^{\infty} \frac{-2}{(\pi m)^2 + \mathbf{k}^2} \sin(\pi m \tau_1)\sin(\pi m \tau_2) e^{i\mathbf{k}\cdot(\mathbf{t}_1-\mathbf{t}_2)} \\
\Delta_{\rm gh}(t_1,t_2) &= \int \frac{d^D\mathbf{k}}{(2\pi)^D} \sum_{m=1}^{\infty} 2\sin(\pi m \tau_1)\sin(\pi m \tau_2) e^{i\mathbf{k}\cdot(\mathbf{t}_1-\mathbf{t}_2)} \\
&= \delta(\tau_1-\tau_2)\delta^D(\mathbf{t}_1-\mathbf{t}_2) = \delta^{D+1}(t_1-t_2).
\end{aligned} \tag{3.60}$$

and, for $D \to 0$, they become the continuum limit propagators treated in the previous sections, *i.e.*

$$\begin{aligned}
\Delta(\tau_1,\tau_2) &= \tau_1(\tau_2+1)\theta(\tau_1-\tau_2) + (\tau_1 \leftrightarrow \tau_2) \\
\Delta_{\rm gh}(\tau_1,\tau_2) &= {}^{\bullet\bullet}\Delta(\tau_1,\tau_2) = \delta(\tau_1-\tau_2).
\end{aligned} \tag{3.61}$$

The key advantage here is to use dimensionally-continued propagators to compute worldline integrals using integrations by parts and neglecting all boundary terms, due to momentum conservation in the D added dimensions and by direct vanishing of the involved propagators at the endpoints of the compact direction. Once ambiguities and divergences are removed, the initial compact time interval $[-1,0]$ can finally be restored. Let us see this procedure in action with the integral already computed in MR in (3.54),

$$\begin{aligned}
I({\rm DR}) &= \int_{-1}^{0}\int_{-1}^{0} d\tau_1 d\tau_2\ ({}^\bullet\Delta)({}^\bullet\Delta^\bullet)(\Delta^\bullet) \\
&\to \int d^{D+1}t_1 \int d^{D+1}t_2\ ({}_\mu\Delta)(\Delta_\nu)({}_\mu\Delta_\nu) \\
&= \frac{1}{2}\int d^{D+1}t_1 \int d^{D+1}t_2\ ({}_\mu\Delta)\left[{}_\mu\left(\Delta_\nu^2\right)\right] \\
&= -\frac{1}{2}\int d^{D+1}t_1 \int d^{D+1}t_2\ ({}_{\mu\mu}\Delta)\Delta_\nu^2 \\
&= -\frac{1}{2}\int d^{D+1}t_1 \int d^{D+1}t_2\ \delta^{D+1}(t_1,t_2)\Delta_\nu^2 \\
&= -\frac{1}{2}\int d^{D+1}t_1\ \Delta_\nu^2|_{t_2=t_1} \\
&\to -\frac{1}{2}\int_{-1}^{0} d\tau_1\ \Delta^{\bullet 2}|_{\tau_2=\tau_1} = -\frac{1}{24},
\end{aligned} \tag{3.62}$$

where we adopted the notation ${}_{\mu}(\ldots) = \partial_{\mu}(\ldots)$ in analogy with the dot-notation of the one dimensional case. The method is thus similar to MR. However, having promoted ∂_{τ} to ∂_{μ} does not allow to replace ${}_{\mu\mu}\Delta$ with $\Delta_{\nu\nu}$. Rather, here the Green's function ${}_{\mu\mu}\Delta = \delta^{(D+1)}(t,s)$ is used— the validity of such step was shown in [30]. The above integral hence exhibits different values depending on the scheme,

$$I(\mathrm{TS}) = -\frac{1}{6}, \quad I(\mathrm{MR}) = -\frac{1}{12}, \quad I(\mathrm{DR}) = -\frac{1}{24}, \tag{3.63}$$

but this does not have to compromise the agreement in the final result at each perturbative order once all contributions are summed up. To evaluate the counterterm V_{DR}, we can exploit the work done for mode regularization and realize that what changes is the value of some worldline integrals. The difference between the two schemes is written as

$$\Delta \langle x^k_{\mathrm{f}}, t_{\mathrm{f}} | x^k_{\mathrm{i}}, t_{\mathrm{i}} \rangle = \langle x^k_{\mathrm{f}}, t_{\mathrm{f}} | x^k_{\mathrm{i}}, t_{\mathrm{i}} \rangle_{\mathrm{DR}} - \langle x^k_{\mathrm{f}}, t_{\mathrm{f}} | x^k_{\mathrm{i}}, t_{\mathrm{i}} \rangle_{\mathrm{MR}} \tag{3.64}$$

and must cancel when counterterms are taken into account. This provides a relation between V_{DR} and V_{MR}, namely

$$V_{\mathrm{DR}} - V_{\mathrm{MR}} = \frac{1}{24} g^{\mu\nu} g^{\rho\sigma} g_{\alpha\beta} \Gamma^{\alpha}{}_{\mu\rho} \Gamma^{\beta}{}_{\nu\sigma}, \tag{3.65}$$

which, using eq. (3.58), gives

$$V_{\mathrm{DR}} = \frac{1}{8} R. \tag{3.66}$$

As anticipated, the counterterm from dimensional regularization is covariant and this allows DR to preserve general covariance at intermediate steps of the computation.

Chapter 4

A string-inspired method for trace anomaly calculations

Without doubt, the first important application of quantum mechanical path integrals in curved spaces, invented by Alvarez-Gaumé and Witten in Ref. [7], was the computation of gravitational anomalies, both chiral and trace anomalies. It is well known that the structure of trace anomalies becomes rapidly harder as the number of space dimensions increases (see e.g. Ref. [31] for a detailed study of trace anomalies in six dimensions), since the number of curvature invariants with the correct mass dimensions fastly increases with the space dimension. Hence, it is helpful to find methods to uncover (parts of) such anomalies.

In this section, we will precisely see a simplified method based on path integrals in curved space to compute the trace anomaly of a scalar field theory, which is the part of the anomaly proportional to the Euler density. To single out such term we consider maximally symmetric (MS) spaces, since in such case the remaining part vanishes, as it is made out of Weyl invariants (and trivial anomalies, *i.e.* total derivatives), which are null in MS spaces. The calculation is performed using a Riemann normal coordinate representation and BRST techniques to properly handle the zero modes on the 1d circle path integrals, needed for the trace anomaly computation. The main point, in fact, is that the trace anomaly can be expressed in terms of path integral consisting in a non linear σ-model for a scalar point particle, which can then be computed perturbatively exploiting the machinery which has been presented previously.

Let us start introducing the trace anomaly for a scalar quantum field theory in a D-dimensional curved space, by considering an infinitesimal local scale transformation

of the metric $g_{\mu\nu}(x)$ and the field $\phi(x)$

$$\begin{aligned} \delta g_{\mu\nu}(x) &= \sigma(x) g_{\mu\nu}(x), \\ \delta\phi(x) &= \frac{k}{2}\sigma(x)\phi(x) \end{aligned} \tag{4.1}$$

where $k = 1 - \frac{D}{2}$ is (minus) the mass dimension of the scalar field. Here we are assuming an Euclidean signature obtained by Wick-rotating the time coordinate $ix_0 \to x^D$ and defining the Euclidean action $S_E = -iS_M$. Then $\sqrt{-g} \to \sqrt{g}$.

With these changes, a Weyl-invariant classical action can be written as

$$S = \frac{1}{2}\int d^D x\ \sqrt{g}\left(g^{\mu\nu}\partial_\mu\phi\partial_\nu\phi - \xi R\phi^2\right) \tag{4.2}$$

with $\xi = \frac{D-2}{4(D-1)}$ being the so-called conformal coupling. Now we can define the path integral functional

$$Z[g_{\mu\nu}] = \int \mathcal{D}\phi\ e^{-S[\phi, g_{\mu\nu}]} \tag{4.3}$$

and then rescale the field $\phi(x) \to \tilde{\phi}(x) = g^{\frac{1}{4}}(x)\phi(x)$ to make the infinitesimally transformed field D-independent,

$$\begin{aligned} \delta\tilde{\phi} &= \delta\left(g^{\frac{1}{4}}\phi\right) = \delta g^{\frac{1}{4}}\phi + g^{\frac{1}{4}}\delta\phi = \frac{1}{4}g^{-\frac{3}{4}}g g^{\mu\nu}\delta g_{\mu\nu}\phi + g^{\frac{1}{4}}\delta\phi \\ &= \frac{1}{4}g^{\frac{1}{4}}g^{\mu\nu}\sigma g_{\mu\nu}\phi + g^{\frac{1}{4}}\frac{k}{2}\sigma\phi = \frac{1}{2}\sigma\tilde{\phi}. \end{aligned} \tag{4.4}$$

The new functional

$$Z[g_{\mu\nu}] = \int \mathcal{D}\tilde{\phi}\ e^{-S[\tilde{\phi}, g_{\mu\nu}]} = e^{W[g_{\mu\nu}]} \tag{4.5}$$

can now be used to extract the Fujikawa's anomaly from the path integral measure. Above, W is (minus) the gravitational effective action. The jacobian for the infinitesimal transformation $\tilde{\phi}'(x) = \tilde{\phi}(x) + \delta\tilde{\phi}(x)$ reads

$$J = \det\frac{\partial\tilde{\phi}'(x)}{\partial\tilde{\phi}(y)} = 1 + \mathrm{tr}\frac{\partial\delta\tilde{\phi}'(x)}{\partial\tilde{\phi}(y)} \tag{4.6}$$

and the Weyl anomaly can formally be expressed by

$$\mathrm{An_W} = \mathrm{tr}\frac{\partial\delta\tilde{\phi}'(x)}{\partial\tilde{\phi}(y)} = \mathrm{tr}\left[\frac{1}{2}\sigma\delta^D(x-y)\right] = \delta_\sigma J. \tag{4.7}$$

On the other hand, the anomaly can be identified with the functional variation of the effective action $W[g_{\mu\nu}] = \ln Z[g_{\mu\nu}]$,

$$\begin{aligned} \mathrm{An_W} = \delta_\sigma W &= \int d^D x \, \frac{\sqrt{g}}{2} \delta_\sigma g^{\mu\nu} \frac{2}{\sqrt{g}} \frac{\delta_\sigma W}{\delta g^{\mu\nu}} \\ &= \frac{1}{2} \int d^D x \, \sqrt{g} \sigma g^{\mu\nu} \left\langle T_{\mu\nu} \right\rangle \end{aligned} \tag{4.8}$$

where we defined

$$\left\langle T_{\mu\nu}(x) \right\rangle = \frac{\int \mathcal{D}\tilde{\phi} \, e^{-S} \frac{2}{\sqrt{g}} \frac{\delta S}{\delta g^{\mu\nu}}}{\int \mathcal{D}\tilde{\phi} \, e^{-S}} \tag{4.9}$$

vacuum expectation value of the stress tensor, computed from the effective action. Hence, up to an x-integration, the trace anomaly is proportional to $g^{\mu\nu}(x) \left\langle T_{\mu\nu}(x) \right\rangle = \left\langle T^{\mu}{}_{\mu}(x) \right\rangle$, *i.e.* the averaged trace of the stress tensor. Classically such object is zero on shell. In fact, for Weyl invariance, we have that

$$S[g_{\mu\nu}, \tilde{\phi}] = S[g_{\mu\nu} + \delta g_{\mu\nu}, \tilde{\phi} + \delta\tilde{\phi}] \simeq S[g_{\mu\nu}, \tilde{\phi}] + \delta g^{\mu\nu} \frac{\delta S}{\delta g^{\mu\nu}} + \delta\tilde{\phi} \frac{\delta S}{\delta \tilde{\phi}} \tag{4.10}$$

where the last bit is zero, then

$$0 = \delta g^{\mu\nu}(x) \frac{\delta S}{\delta g^{\mu\nu}}(x) = -\sigma(x) g^{\mu\nu}(x) \frac{1}{2} \sqrt{g(x)} T_{\mu\nu}(x) \propto T^{\mu}{}_{\mu}(x). \tag{4.11}$$

Hence, the trace anomaly it due to the non-vanishing of the traced path integral average of the stress tensor associated to Weyl invariance. Now, to compute actually the anomaly (4.7), the trace has to be regulated since it is a trace over an infinite dimensional (Hilbert) space. One can then write it as

$$\mathrm{An_W} = \lim_{\beta \to 0} \mathrm{tr} \left[\frac{1}{2} \sigma(x) e^{-\beta \mathcal{R}} \right] \tag{4.12}$$

with β being a positive real parameter and $\mathcal{R}$ being the so-called consistent regulator[1]

$$\mathcal{R} = \mathbf{H} = \frac{1}{2} g^{-\frac{1}{4}} \mathbf{p}_\mu g^{\frac{1}{2}} g^{\mu\nu} \mathbf{p}_\nu g^{-\frac{1}{4}} - \frac{1}{2} \xi R. \tag{4.13}$$

Eq. (4.13) is in fact the field operator of $\tilde{\phi}$ coming from the classical action (4.2). The limit $\beta \to 0$ in eq. (4.12) ensures the removal of the regulator once the trace is taken and divergences are removed with local QFT counterterms. This construction

[1] Due to aesthetic reasons, we actually omitted bold notation for metric tensors and determinants even though, here, they act as operators, being dependent on the operator $\mathbf{x}$.

in some way is the bridge from quantum field theory and the worldline formalism: the quantum mechanical worldline particle $x^\mu(\tau)$ lives in a curved space preserving Einstein invariance and corresponds to the coordinates x^μ of the original quantum field theory. With this identification in mind, we interpret the trace as a trace over quantum mechanical ket states, as if the particles moves in closed loops for a proper time interval β, *i.e.*

$$\mathrm{An_W} = \lim_{\beta\to 0} \mathrm{tr}\left[\sigma' e^{-\beta \mathbf{H}}\right] = \lim_{\beta\to 0} \int_{\mathrm{PBC}} \mathcal{D}x\ \sigma'(x) e^{-S[x]} \tag{4.14}$$

with $\sigma' = \frac{1}{2}\sigma$ and action

$$S[x] = \frac{1}{\beta}\int_{-1}^{0} d\tau \left[\frac{1}{2} g_{\mu\nu}(x)\dot{x}^\mu \dot{x}^\nu + \beta^2 (V(x) + V_{\mathrm{DR}}(x)),\right] \tag{4.15}$$

where $V = -\frac{\xi R}{2}$ is a scalar potential and V_{DR} is the counterterm for dimensional regularization, as this scheme will be adopted in the following computation. A comparison between equations (4.8) and (4.14) leads to the trace

$$\left\langle T^\mu{}_\mu(x)\right\rangle = \lim_{\substack{\beta\to 0 \\ x(-1)=x(0)=x}} \int \mathcal{D}x\ e^{-S[x]}. \tag{4.16}$$

Defining the partition function density (an integral over x is factored out)

$$\mathcal{Z}(\beta) = \int_{x(-1)=x(0)=x} \mathcal{D}x\ e^{-S[x]}, \tag{4.17}$$

we have

$$\left\langle T^\mu{}_\mu(x)\right\rangle = \lim_{\beta\to 0} \mathcal{Z}(\beta). \tag{4.18}$$

Multiplying and dividing eq. (4.17) by the free path integral, we get

$$\mathcal{Z}(\beta) = \frac{1}{(2\pi\beta)^{\frac{D}{2}}} \left\langle e^{-S_{\mathrm{int}}}\right\rangle \tag{4.19}$$

where S_{int} is the whole action except the kinetic term. This quantity was already computed using Dirichlet boundary condition propagators for a maximally space and

reads [26]

$$\mathcal{Z}(\beta) = \frac{1}{(2\pi\beta)^{\frac{D}{2}}} \exp\Big[\frac{\beta}{12}(6\xi-1)R - \frac{\beta^2}{6!}\frac{(D-3)}{D(D-1)}R^2 + \\ + \frac{\beta^3}{8!}\frac{16(D+2)(D-3)}{9D^2(D-1)^2}R^3 + o(\beta^4)\Big]. \tag{4.20}$$

We would like to show the same result using another method based on a string-inspired worldline approach, that we are going to describe. First of all, we notice that setting $g_{\mu\nu}(x) = \delta_{\mu\nu}$ and $V + V_{\rm DR} = 0$ in the action (4.15), it is invariant under translations $\delta x^\mu(\tau) = \epsilon^\mu$. This produces zero modes, that are constant eigenvectors of the kinetic operator. They can be extracted from the path integral and produce a volume factor of the manifold in which the theory is embedded. For nontrivial metric and potential, the constant shift symmetry is in general broken. However it can be fictitious introduced and then, via BRST technique, it can be fixed, and it corresponds to setting some specific worldline propagators. Here we will choose the so-called string inspired propagators, which are linked to fixing the zero modes as centers of mass of the closed path, hence the name.

BRTS (after Becchi, Rouet, Stora and Tyutin) quantization was born in the context of gauge theory as an alternative approach to represent the relic of gauge invariance left by path integral quantization. We will apply this idea directly to our worldline theory for the computation of the partition function $\mathcal{Z}(\beta)$. Let us split the worldline closed path $x^\mu(\tau)$ into a constant path x_0^μ (the would be zero mode) plus a deviation $y^\mu(\tau)$,

$$x^\mu(\tau) = x_0^\mu + y^\mu(\tau). \tag{4.21}$$

A symmetry for the action is then the shift symmetry

$$\begin{aligned} \delta x_0^\mu &= \epsilon^\mu \\ \delta y^\mu(\tau) &= -\epsilon^\mu. \end{aligned} \tag{4.22}$$

If both variables x_0^μ and $y^\mu(\tau)$ are considered to be dynamical fields, one then promotes the shift symmetry to a gauge symmetry, and then the associated path integral has to be gauge-fixed by removing from the integration all those configurations that are physically equivalent upon the gauge symmetry. In the BRST context, this is realized by means of anticommuting ghost field η^μ and parameter Λ, entering the shift

symmetry as

$$\begin{aligned} \delta x_0^\mu &= \eta^\mu \Lambda \\ \delta y^\mu(\tau) &= -\eta^\mu \Lambda \\ \delta \eta^\mu &= 0, \end{aligned} \tag{4.23}$$

and constant fields $\bar{\eta}_\mu$, π_μ such that

$$\begin{aligned} \delta \bar{\eta}_\mu &= i\pi_\mu \Lambda \\ \delta \pi_\mu &= 0. \end{aligned} \tag{4.24}$$

To fix the gauge, *i.e.* set a specific propagator for $y^\mu(\tau)$, we consider the "gauge fixing fermion"

$$\Psi = \bar{\eta}_\mu \int_{-1}^{0} d\tau \; \rho(\tau) y^\mu(\tau) \tag{4.25}$$

depending on an arbitrary distribution $\rho(\tau)$ normalized to 1, $\int_{-1}^{0} d\tau \;\; \rho(\tau) = 1$. In particular, if $\rho(\tau) = \delta(\tau)$ then DBC propagators are set, if $\rho(\tau) = 1$ then string-inspired (SI) propagators come into play. Keeping a generic $\rho(\tau)$, the generic gauge fixed action is given by[2]

$$S_{\rm gf}[x_0, y, \eta, \bar{\eta}, \pi] = S[x_0 + y] + \frac{\delta}{\delta \Lambda} \Psi = S[x_0 + y] + i\pi_\mu \int_{-1}^{0} d\tau \; \rho(\tau) y^\mu(\tau) - \bar{\eta}_\mu \eta^\mu. \tag{4.26}$$

Using that

$$\begin{aligned} \int d\bar{\eta} d\eta \; e^{-\bar{\eta}_\mu \eta^\mu} &= \int d\bar{\eta} d\eta \; (1 - \bar{\eta}_\mu \eta^\mu) \\ \int d\pi \; e^{i\pi_\mu \int_{-1}^{0} d\tau \; \rho(\tau) y^\mu(\tau)} &= \delta \left(\int_{-1}^{0} d\tau \; \rho(\tau) y^\mu(\tau) \right) \end{aligned} \tag{4.27}$$

we get the constraint

$$\int_{-1}^{0} d\tau \; \rho(\tau) y^\mu(\tau) = 0 \tag{4.28}$$

which explains why the choice $\rho(\tau) = 1$ determines SI propagators: in this case

[2] The derivative $\frac{\delta}{\delta \Lambda}$ with respect to the fermionic field Λ is here taken on the left.

$\int_{-1}^{0} d\tau\ y^\mu(\tau) = 0$ imposes that the field $y^\mu(\tau)$ center of mass is fixed to zero as often done for the center of mass of strings in string theory. Now, the partition function is written as

$$Z(\beta) = \int d^D x_0\ \sqrt{g(x_0)}\mathcal{Z}(x_0,\beta) \tag{4.29}$$

with $\mathcal{Z}(x_0,\beta)$ expressed as a power law in β. At this point let us specialize in a convenient coordinate system, that is Riemann normal coordinates (RNC) $\xi^\mu(\tau)$ centered in x_0^μ. Fluctuations $y^\mu(\tau)$ are then given by

$$y^\mu = \xi^\mu - \sum_{n=2}^{\infty} \frac{1}{n!}\Gamma^\mu{}_{(\mu_1\mu_2;\mu_3\ldots\mu_n)}(x_0)\xi^{\mu_1}\ldots\xi^{\mu_n}, \tag{4.30}$$

where round brackets mean symmetrization and the semicolon stands for covariantization. It is relevant to notice that a trivial shift symmetry for fluctuations $y^\mu(\tau)$ implies a non trivial one for $\xi^\mu(\tau)$,

$$\delta\xi^\mu(\tau) = -Q^\mu{}_\nu(x_0,\xi(\tau))\epsilon^\nu. \tag{4.31}$$

The specific form of the above Q-matrix is due to Friedan [32]. This non linear infinitesimal transformation stems from the fact that, by definition, x_0^μ is the origin of the RNC coordinates, which are vectors on the tangent space T_{x_0}: such vectors are tangent to the geodesics which link x_0^μ to generic points x^μ on the manifold. Hence, if x_0^μ gets shifted, so does the tangent space, and in turns this means that $\xi'^\mu = \xi^\mu + \delta\xi^\mu$ is a vector on the shifted tangent space. Thus, if the manifold is curved, the transformation of the RNC coordinates is a non linear combination of the former RNC coordinates ξ^μ. On the other hand, if the manifold is flat, the different tangent spaces coincide and $Q^\mu{}_\nu(x_0,0) = \delta^\mu_\nu$. A compact and manageable formula for the Q-matrix has been derived for the specific case of a MS space [27] and will be used for the calculation of the partition function. Adopting a more friendly matrix notation

$$\mathcal{Q} = Q^\mu{}_\nu, \tag{4.32}$$

Friedan showed that

$$\mathcal{Q} = 1 + \partial\log\mathcal{V} \tag{4.33}$$

where

$$\partial = \xi^\mu \left(\frac{\partial}{\partial \xi^\mu} - \nabla_\mu \right) \tag{4.34}$$

with ∇_μ is covariant derivative satisfying $\nabla_\mu \xi^\mu = 0$ and

$$\mathcal{V} = \sum_{n=0}^{\infty} \frac{1}{(n+1)!} \mathcal{V}^{(n)}. \tag{4.35}$$

The matrices $\mathcal{V}^{(n)}$ are such that $\mathcal{V}^{(0)} = 1$, $\mathcal{V}^{(1)} = 0$, $\mathcal{V}^{(n)} \propto \xi^n$. In the case of a space with no torsion, the matrices $\mathcal{V}^{(n)}$ satisfy

$$\mathcal{V}^{(n)} = 2\nabla \mathcal{V}^{(n-1)} - \nabla^2 \mathcal{V}^{(n-2)} + \mathcal{V}^{(n-2)} \mathcal{R}, \tag{4.36}$$

with $\mathcal{R} = R^\mu{}_{\rho\sigma\nu} \xi^\rho \xi^\sigma$. Since for MS spaces the curvature tensor reads

$$R_{\mu\nu\rho\sigma} \propto (g_{\mu\rho} g_{\nu\sigma} - g_{\mu\sigma} g_{\nu\rho}) \tag{4.37}$$

and $\nabla_\rho g_{\mu\nu} = 0$, then $\nabla_\alpha R_{\mu\nu\rho\sigma} = 0$, which makes eq. (4.35) much easier. In fact, it can be written as

$$\mathcal{V} = \sum_{n=0,2,4,\ldots}^{\infty} \frac{1}{(n+1)!} \mathcal{R}^{\frac{n}{2}} = \sum_{n=0}^{\infty} \frac{1}{(2n+1)!} \mathcal{R}^n \tag{4.38}$$

where

$$\begin{aligned} \mathcal{R}^n &= R^\mu{}_{\alpha_1\beta_1\mu_1} R^{\mu_1}{}_{\alpha_2\beta_2\mu_2} \cdots R^{\mu_{n-1}}{}_{\alpha_n\beta_n\nu} \xi^{\alpha_1} \xi^{\beta_1} \cdots \xi^{\alpha_n} \xi^{\beta_n} \\ \mathcal{R}^0 &= 1. \end{aligned} \tag{4.39}$$

Eq. (4.38) can be easily proved by induction using eq. (4.36) and $\nabla R^n = 0$. With a closer look at (4.38), one realizes that

$$\mathcal{V} = \frac{\sinh \sqrt{\mathcal{R}}}{\sqrt{\mathcal{R}}} \tag{4.40}$$

from which

$$\partial \log \mathcal{V} = \left(\frac{\coth \sqrt{\mathcal{R}}}{2\sqrt{\mathcal{R}}} - \frac{1}{2\mathcal{R}} \right) \partial \mathcal{R}. \tag{4.41}$$

Since both the curvature tensor and the Riemann normal coordinates are covariantly constant,

$$\partial \mathcal{R} = 2\mathcal{R}, \tag{4.42}$$

so that

$$\partial \log \mathcal{V} = \sqrt{\mathcal{R}} \coth \sqrt{\mathcal{R}} - 1. \tag{4.43}$$

The final form of the Q-matrix for MS spaces is then

$$\mathcal{Q} = \sqrt{\mathcal{R}} \coth \sqrt{\mathcal{R}}. \tag{4.44}$$

An expansion of the hyperbolic cotangent allows to find the first terms of the series, giving

$$\mathcal{Q} = 1 + \frac{1}{3}\mathcal{R} - \frac{1}{45}\mathcal{R}^2 + \frac{2}{945}\mathcal{R}^3 + \dots. \tag{4.45}$$

Eq. (4.45) can now be used in (4.31) to get the transformation for the RNC's in MS spaces.

Coming back to the BRST treatment, the gauge fixing fermion and the gauge fixed action associated to RNC reads respectively

$$\Psi = \bar{\eta}_\mu \int_{-1}^{0} d\tau \; \xi^\mu(\tau) \tag{4.46}$$

and

$$S_{\rm gf}[x_0, \xi, \eta, \bar{\eta}, \pi] = S[x_0, \xi] + i\pi_\mu \int_{-1}^{0} d\tau \; \xi^\mu(\tau) - \bar{\eta}_\mu \int_{-1}^{0} d\tau \; Q^\mu{}_\nu(x_0, \xi(\tau))\eta^\nu. \tag{4.47}$$

As seen in the previous chapters, the $\sqrt{g}$-factor at the level of the path integral measure can be exponentiated using ghost fields a, b and c and the relative ghost action $S_{\rm gh}$,

$$S_{\rm gh}[\xi, a, b, c] = \frac{1}{\beta} \int_{-1}^{0} d\tau \; \left[\frac{1}{2} g_{\mu\nu}(x_0, \xi)(a^\mu a^\nu + b^\mu c^\nu)\right]. \tag{4.48}$$

Finally, we can define the transition amplitude as

$$Z(\beta) = \int dx_0 \, d\bar{\eta} \, d\eta \, d\pi \int \mathcal{D}\xi \, \mathcal{D}a \, \mathcal{D}b \, \mathcal{D}c \; e^{-S_{\rm q}} \tag{4.49}$$

in terms of the quantum action $S_{\rm q} = S_{\rm gf} + S_{\rm gh}$. Propagators are calculated using the quadratic form of the above action by setting $g_{\mu\nu}(x_0, \xi) \to g_{\mu\nu}(x_0)$ and $Q^\mu{}_\nu(x_0, \xi) \to \delta^\mu{}_\nu$, *i.e.*

$$S_2 = \frac{1}{\beta} \int_{-1}^{0} d\tau \; \left[\frac{1}{2} g_{\mu\nu}(x_0)(\dot{\xi}^\mu \dot{\xi}^\nu + a^\mu a^\nu + b^\mu c^\nu)\right]. \tag{4.50}$$

We thus have

$$\begin{aligned}
\langle \xi^\mu(\tau_1)\xi^\nu(\tau_2)\rangle &= -\beta g^{\mu\nu}(x_0)\mathcal{B}(\tau_1,\tau_2)\\
\langle a^\mu(\tau_1)a^\nu(\tau_2)\rangle &= \beta g^{\mu\nu}(x_0)\Delta_{\rm gh}(\tau_1,\tau_2)\\
\langle b^\mu(\tau_1)c^\nu(\tau_2)\rangle &= -2\beta g^{\mu\nu}(x_0)\Delta_{\rm gh}(\tau_1,\tau_2)\\
\langle \bar\eta^\mu\eta_\nu\rangle &= \delta^\mu{}_\nu
\end{aligned} \tag{4.51}$$

with

$$\begin{aligned}
\mathcal{B}(\tau_1,\tau_2) &= \frac{|\tau_1-\tau_2|}{2} - \frac{(\tau_1-\tau_2)^2}{2} - \frac{1}{12}\\
\Delta_{\rm gh}(\tau_1,\tau_2) &= \delta(\tau_1-\tau_2).
\end{aligned} \tag{4.52}$$

Feynman vertices emerge from the interacting part of the action $S_{\rm q}^{(\rm int)}$, which is given by

$$S_{\rm q}^{(\rm int)} = S_{\rm q}[g_{\mu\nu}(x_0,\xi)\to g_{\mu\nu}(x_0,\xi)-g_{\mu\nu}(x_0); Q^\mu{}_\nu(x_0,\xi)\to Q^\mu{}_\nu(x_0,\xi)-\delta^\mu{}_\nu] \tag{4.53}$$

and the partition function reads

$$Z(\beta) = \int d^D x_0\, \frac{\sqrt{g(x_0)}}{(2\pi\beta)^{\frac{D}{2}}} \left\langle e^{-S_{\rm q}^{(\rm int)}}\right\rangle, \tag{4.54}$$

which is computed perturbatively expanding the exponent. Useful properties for the $\mathcal{B}$ propagator are

$$\begin{aligned}
\mathcal{B}(\tau_1,\tau_2) &= \mathcal{B}(\tau_2,\tau_1)\\
{}^\bullet\mathcal{B}(\tau_1,\tau_2) &= \frac{\mathrm{sgn}(\tau_1-\tau_2)}{2} - \tau_1 + \tau_2 = -\mathcal{B}^\bullet(\tau_1,\tau_2)\\
{}^{\bullet\bullet}\mathcal{B}(\tau_1,\tau_2) &= \delta(\tau_1-\tau_2) - 1 = \mathcal{B}^{\bullet\bullet}(\tau_1,\tau_2)\\
\int_{-1}^{0} d\tau\ \mathcal{B}(\tau_1,\tau_2) &= 0\\
({}^\bullet\mathcal{B}(\tau_1,\tau_2))|_{\tau_1=\tau_2} &= 0\\
({}^{\bullet\bullet}\mathcal{B}(\tau_1,\tau_2))|_{\tau_1=\tau_2} &= \delta(0) - 1.
\end{aligned} \tag{4.55}$$

In the last line of (4.55), $\delta(0)$ is a singularity that is perturbatively removed by the ghost sector. Another delicate object is ${}^\bullet\mathcal{B}^\bullet(\tau_1,\tau_2) = 1-\delta(\tau_1-\tau_2)$: it cannot be directly implemented, rather it has to be partially integrated using the rules provided

by the regularization to get regular forms like those in (4.55). The integral constraint comes from setting $\rho(\tau) = 1\text{m}$ which in turn fixes the propagator to be that given in (4.52).

From the partition function (4.54), we can extract the related density

$$\mathcal{Z}(\beta) = \frac{\left\langle e^{-S_{\text{q}}^{(\text{int})}} \right\rangle}{(2\pi\beta)^{\frac{D}{2}}}. \tag{4.56}$$

Adopting dimensional regularization and extracting $-\beta(V + V_{\text{DR}})$ from the quantum action, we have

$$\mathcal{Z}(\beta) = \frac{e^{-\beta(1-4\xi)\frac{R}{8}}}{(2\pi\beta)^{\frac{D}{2}}} \left\langle e^{-\tilde{S}_{\text{q}}^{(\text{int})}} \right\rangle. \tag{4.57}$$

Calling b the curvature constant defined as[3]

$$\begin{aligned} R_{\mu\nu\rho\sigma} &= b(g_{\mu\rho}g_{\nu\sigma} - g_{\mu\sigma}g_{\nu\rho}) \\ b &= \frac{R}{D(1-D)}, \end{aligned} \tag{4.58}$$

the RNC-MS expansion of the metric around the origin reads [26]

$$g_{\mu\nu}(\xi) = \delta_{\mu\nu} + 2(\xi_\mu\xi_\nu - \delta_{\mu\nu}\xi_\alpha\xi^\alpha)\left[\frac{b}{6} - \frac{16}{6!}b^2(\xi_\alpha\xi^\alpha)^2 + \frac{8}{7!}b^3(\xi_\alpha\xi^\alpha)^4 + \dots\right] \tag{4.59}$$

and it can be inserted in the interacting quantum action to give

$$\begin{aligned} \tilde{S}_{\text{q}}^{(\text{int})} = \frac{1}{\beta}\int_{-1}^{0} d\tau \ &\left[\frac{b}{6} - \frac{16}{6!}b^2(\xi_\alpha\xi^\alpha)^2 + \frac{8}{7!}b^3(\xi_\alpha\xi^\alpha)^4 + \dots\right] \times \\ &\times [\xi_\mu(\tau)\xi_\nu(\tau) - \delta_{\mu\nu}\xi_\alpha(\tau)\xi^\alpha(\tau)]\Big[\dot{\xi}^\mu(\tau)\dot{\xi}^\nu(\tau) + a^\mu(\tau)a^\nu(\tau) + \\ &+ b^\mu(\tau)c^\nu(\tau)\Big] - \bar{\eta}_\mu\int_{-1}^{0} d\tau \ (Q^\mu{}_\nu - \delta^\mu{}_\nu)\,\eta^\nu. \end{aligned} \tag{4.60}$$

The expression of the matrix $Q^\mu{}_\nu$ is obtained from eqs. (4.45) and (4.39) and explicitly reads

$$\begin{aligned} Q^\mu{}_\nu = \delta^\mu{}_\nu + \frac{1}{3}R^\mu{}_{\rho\sigma\nu}(0)\xi^\rho\xi^\sigma - \frac{1}{45}R^\mu{}_{\rho\sigma\alpha}R^\alpha{}_{\gamma\delta\nu}\xi^\rho\xi^\sigma\xi^\gamma\xi^\delta + \\ + \frac{2}{945}R^\mu{}_{\alpha\beta\gamma}R^\gamma{}_{\rho\sigma\theta}R^\theta{}_{\eta\epsilon\nu}(0)\xi^\alpha\xi^\beta\xi^\rho\xi^\sigma\xi^\eta\xi^\epsilon + \dots. \end{aligned} \tag{4.61}$$

Since the curvature is given by

$$R^\mu{}_{\rho\sigma\nu}(0) = b(\delta^\mu{}_\sigma\delta_{\rho\nu} - \delta^\mu{}_\nu\delta_{\rho\sigma}), \tag{4.62}$$

[3] Here we adopt the convention introduced in Appendix A.

eqs. (4.39) become

$$\begin{aligned}\mathcal{R}^n &= (-1)^{n+1} b^n [\xi^\mu \xi_\nu - \delta^\mu{}_\nu \xi_\alpha \xi^\alpha](\xi_\alpha \xi^\alpha)^{n-1} \\ \mathcal{R}^0 &= \delta^\mu{}_\nu\end{aligned} \tag{4.63}$$

and, as a consequence eq. (4.61), is rewritten as

$$\begin{aligned}Q^\mu{}_\nu - \delta^\mu{}_\nu = \left[\frac{b}{3} + \frac{b^2}{45}\xi_\alpha \xi^\alpha + \frac{2}{945} b^3 (\xi_\alpha \xi^\alpha)^2 + \dots\right] \times \\ \times (\xi^\mu \xi_\nu - \delta^\mu{}_\nu \xi_\alpha \xi^\alpha),\end{aligned} \tag{4.64}$$

obtaining

$$\begin{aligned}\tilde{S}_{\rm q}^{(\rm int)} = \frac{1}{\beta}\int_{-1}^{0} d\tau \left[\frac{b}{6} - \frac{16}{6!} b^2 (\xi_\alpha \xi^\alpha)^2 + \frac{8}{7!} b^3 (\xi_\alpha \xi^\alpha)^4 + \dots\right] \times \\ \times [\xi_\mu(\tau)\xi_\nu(\tau) - \delta_{\mu\nu}\xi_\alpha(\tau)\xi^\alpha(\tau)]\Big[\dot{\xi}^\mu(\tau)\dot{\xi}^\nu(\tau) + a^\mu(\tau)a^\nu(\tau) + \\ + b^\mu(\tau)c^\nu(\tau)\Big] - \bar{\eta}_\mu \int_{-1}^{0} d\tau \left[\frac{b}{3} + \frac{b^2}{45}\xi_\alpha(\tau)\xi^\alpha(\tau) + \right. \\ \left. + \frac{2}{945} b^3 (\xi_\alpha(\tau)\xi^\alpha(\tau))^2 + \dots\right] \left[\xi^\mu(\tau)\xi_\nu(\tau) - \delta^\mu{}_\nu \xi_\alpha(\tau)\xi^\alpha(\tau)\right] \eta^\nu.\end{aligned} \tag{4.65}$$

Finally eq. (4.65) can be used in eq. (4.57), which is computed perturbatively in β. The interacting quantum action is then split up as[4]

$$\tilde{S}_{\rm q}^{(\rm int)} = \underbrace{S_2'}_{\beta} + \underbrace{S_4}_{\beta} + \underbrace{S_4'}_{\beta^2} + \underbrace{S_6}_{\beta^2} + \underbrace{S_6'}_{\beta^3} + \underbrace{S_8}_{\beta^3} + \dots, \tag{4.66}$$

[4] Under each term we report its overall β-power.

with

$$
\begin{aligned}
S_4 &= \frac{b}{6\beta}\int_{-1}^{0} d\tau\ \left[\xi_\mu(\tau)\xi_\nu(\tau) - \delta_{\mu\nu}\xi_\alpha(\tau)\xi^\alpha(\tau)\right]\left[\dot\xi^\mu(\tau)\dot\xi^\nu(\tau) + a^\mu(\tau)a^\nu(\tau) + \right.\\
&\left. + b^\mu(\tau)c^\nu(\tau)\right]\\
S_6 &= \frac{-16b^2}{6!\beta}\int_{-1}^{0} d\tau\ \xi_\alpha(\tau)\xi^\alpha(\tau)\left[\xi_\mu(\tau)\xi_\nu(\tau) - \delta_{\mu\nu}\xi_\alpha(\tau)\xi^\alpha(\tau)\right]\times\\
&\times\left[\dot\xi^\mu(\tau)\dot\xi^\nu(\tau) + a^\mu(\tau)a^\nu(\tau) + b^\mu(\tau)c^\nu(\tau)\right]\\
S_8 &= \frac{8b^3}{7!\beta}\int_{-1}^{0} d\tau\ \xi_\alpha(\tau)\xi^\alpha(\tau)\xi_\beta(\tau)\xi^\beta(\tau)\left[\xi_\mu(\tau)\xi_\nu(\tau) - \delta_{\mu\nu}\xi_\alpha(\tau)\xi^\alpha(\tau)\right]\times\\
&\times\left[\dot\xi^\mu(\tau)\dot\xi^\nu(\tau) + a^\mu(\tau)a^\nu(\tau) + b^\mu(\tau)c^\nu(\tau)\right]\\
S_2' &= \bar\eta_\mu\frac{b}{3}\int_{-1}^{0} d\tau\ \left[\xi^\mu(\tau)\xi_\nu(\tau) - \delta^\mu{}_\nu\xi_\alpha(\tau)\xi^\alpha(\tau)\right]\eta^\nu\\
S_4' &= -\bar\eta_\mu\frac{b^2}{45}\int_{-1}^{0} d\tau\ \xi_\alpha(\tau)\xi^\alpha(\tau)\left[\xi^\mu(\tau)\xi_\nu(\tau) - \delta^\mu{}_\nu\xi_\alpha(\tau)\xi^\alpha(\tau)\right]\eta^\nu\\
S_6' &= -\bar\eta_\mu\frac{2b^3}{945}\int_{-1}^{0} d\tau\ \xi_\alpha(\tau)\xi^\alpha(\tau)\xi_\beta(\tau)\xi^\beta(\tau)\left[\xi^\mu(\tau)\xi_\nu(\tau) - \delta^\mu{}_\nu\xi_\alpha(\tau)\xi^\alpha(\tau)\right]\eta^\nu.
\end{aligned}
\tag{4.67}
$$

To compute efficiently the quantity $\left\langle e^{-\tilde S_{\rm q}^{(\rm int)}}\right\rangle$, we bring the contraction inside the exponentiation paying attention to select only irreducible connected diagrams,

$$
\begin{aligned}
\left\langle e^{-\tilde S_{\rm q}^{(\rm int)}}\right\rangle = \exp\Big(&-\underbrace{\langle S_4\rangle}_{\beta} - \underbrace{\langle S_2'\rangle}_{\beta} - \underbrace{\langle S_6\rangle}_{\beta^2} - \underbrace{\langle S_4'\rangle}_{\beta^2} + \frac{1}{2}\underbrace{\langle S_2'\rangle_{\rm C}}_{\beta^2} + \frac{1}{2}\underbrace{\langle S_2'^2\rangle_{\rm C}}_{\beta^2} +\\
&+\underbrace{\langle S_2' S_4\rangle_{\rm C}}_{\beta^2} - \underbrace{\langle S_8\rangle}_{\beta^3} - \underbrace{\langle S_6'\rangle}_{\beta^3} + \underbrace{\langle S_4 S_6\rangle_{\rm C}}_{\beta^3} - \frac{1}{3!}\underbrace{\langle S_4{}^3\rangle_{\rm C}}_{\beta^3} - \frac{1}{3!}\underbrace{\langle S_2'^3\rangle_{\rm C}}_{\beta^3} +\\
&+\underbrace{\langle S_2' S_6\rangle_{\rm C}}_{\beta^3} + \underbrace{\langle S_2' S_4'\rangle_{\rm C}}_{\beta^3} + \underbrace{\langle S_4' S_4\rangle_{\rm C}}_{\beta^3} - \frac{1}{2}\underbrace{\langle S_2'^2 S_4\rangle_{\rm C}}_{\beta^3} - \frac{1}{2}\underbrace{\langle S_2' S_4{}^2\rangle_{\rm C}}_{\beta^3}\Big).
\end{aligned}
\tag{4.68}
$$

For simplicity, here we report again the known result for the MS approximated transition amplitude density [26]

$$
\begin{aligned}
\mathcal{Z}(\beta) = \frac{1}{(2\pi\beta)^{\frac{D}{2}}}\exp\Big[&\frac{\beta}{4!}(12\xi - 2)R - \frac{\beta^2}{6!}\frac{(D-3)}{D(D-1)}R^2 +\\
&+\frac{\beta^3}{8!}\frac{16(D+2)(D-3)}{9D^2(D-1)^2}R^3 + o(\beta^4)\Big].
\end{aligned}
\tag{4.69}
$$

computed with DBC. The contractions here involved are

$$\begin{aligned}
\langle S_4\rangle_{\rm DBC} &= -\frac{\beta}{4!}R \\
\langle S_6\rangle_{\rm DBC} &= -\frac{\beta^2}{5!}\frac{D+2}{9D(D-1)}R^2 \\
\langle S_8\rangle_{\rm DBC} &= -\frac{\beta^3}{7!}\frac{(D+2)(D+4)}{15D^2(D-1)^2}R^3 \\
\left\langle {S_4}^2\right\rangle_{\rm C,DBC} &= -\frac{\beta^2}{4!}\frac{1}{9D}R^2 \\
\langle S_4 S_6\rangle_{\rm C,DBC} &= -\frac{\beta^3}{6!}\frac{4(D+2)}{45D^2(D-1)}R^3 \\
\left\langle {S_4}^3\right\rangle_{\rm C,DBC} &= -\frac{\beta^3}{6!}\frac{2(D^2-4)}{3D^2(D-1)^2}R^3
\end{aligned} \tag{4.70}$$

and will be used, order by order, to check the validity of the calculation performed using SI propagators (for which the SI subscript is omitted). To order β, the only DBC contribution comes from

$$\langle S_4\rangle_{\rm DBC} = -\frac{1}{24}\beta R, \tag{4.71}$$

whereas the SI integrals are

$$\begin{aligned}
\langle S_4\rangle =& \frac{b}{6\beta}\int\left\langle\left(\xi_\mu\xi_\nu-\delta_{\mu\nu}\xi_\alpha\xi^\alpha\right)\left(\dot\xi^\mu\dot\xi^\nu+a^\mu a^\nu+b^\mu c^\nu\right)\right\rangle = \\
&= \frac{b\beta}{6}\left[D(1-D)\mathcal{M}_1+(D^2-D)\mathcal{M}_2\right] = -\frac{1}{72}\beta R \\
\langle S_2'\rangle =& \frac{b}{3}\int\langle\bar\eta_\mu\eta^\nu\rangle\langle\xi^\mu\xi_\nu-\delta^\mu{}_\nu\xi_\alpha\xi^\alpha\rangle = \frac{\beta R}{3}\mathcal{M}_1 = -\frac{1}{36}\beta R,
\end{aligned} \tag{4.72}$$

in terms of $\mathcal{M}$-wordline integrals reported at the end of this chapter. We notice that $\langle S_4\rangle + \langle S_2'\rangle = \langle S_4\rangle_{\rm DBC}$.

To order β^2 the DBC contributions are

$$\begin{aligned}
\langle S_6\rangle_{\rm DBC} &= -\frac{D+2}{5!\cdot 9D(D-1)}\beta^2R^2 \\
\left\langle {S_4}^2\right\rangle_{\rm C,DBC} &= -\frac{1}{4!\cdot 9D}\beta^2R^2
\end{aligned} \tag{4.73}$$

and SI ones are

$$\begin{aligned}
\langle S_6\rangle &= -\frac{16R^2}{6!\cdot\beta D^2(1-D)^2}\int\left\langle\xi_\alpha\xi^\alpha[\xi_\mu\xi_\nu-\delta_{\mu\nu}\xi_\alpha\xi^\alpha]\times\left[\dot\xi^\mu\dot\xi^\nu+a^\mu a^\nu+b^\mu c^\nu\right]\right\rangle = \\
&= \frac{16\beta^2R^2}{6!D^2(1-D)^2}(-D^3-D^2+2D)\mathcal{M}_4 = \\
&= -\frac{1}{6480}\frac{D+2}{D(D-1)}\beta^2R^2 \\
\langle S_4'\rangle &= -\frac{R^2}{45D^2(1-D)^2}\int\langle\bar\eta_\mu\eta^\nu\rangle\left\langle\xi_\alpha\xi^\alpha\left[\xi^\mu\xi_\nu-\delta^\mu{}_\nu\xi_\alpha\xi^\alpha\right]\right\rangle = \\
&= -\frac{\beta^2R^2}{45D^2(1-D)^2}(-D^3-D^2+2D)\mathcal{M}_5 = \\
&= \frac{1}{6480}\frac{D+2}{D(D-1)}\beta^2R^2 \\
\left\langle {S_4}^2\right\rangle_{\rm C} &= \frac{R^2}{36\beta^2D^2(1-D)^2}\int_{-1}^0 d\tau\int_{-1}^0 d\sigma\Big\langle[\xi_\mu(\tau)\xi_\nu(\tau)-\delta_{\mu\nu}\xi_\alpha(\tau)\xi^\alpha(\tau)]\times \\
&\times\left[\dot\xi^\mu(\tau)\dot\xi^\nu(\tau)+a^\mu(\tau)a^\nu(\tau)+b^\mu(\tau)c^\nu(\tau)\right][\xi_\rho(\sigma)\xi_\sigma(\sigma)-\delta_{\rho\sigma}\xi_\alpha(\sigma)\xi^\alpha(\sigma)]\times \\
&\times\left[\dot\xi^\rho(\sigma)\dot\xi^\sigma(\sigma)+a^\rho(\sigma)a^\sigma(\sigma)+b^\rho(\sigma)c^\sigma(\sigma)\right]\Big\rangle_{\rm C} = \\
&= \frac{\beta^2R^2}{36D^2(1-D)^2}\Big[(4D^3-8D^2+4D)\mathcal{M}_6+(2D^3-4D^2+2D)\mathcal{M}_7+ \\
&+(2D^3-4D^2-2D)\mathcal{M}_8+(6D^2-6D)\mathcal{M}_9+(-12D^2+12D)\mathcal{M}_{10}+ \\
&=(6D^2-6D)\mathcal{M}_{11}\Big] = \\
&= -\frac{1}{6480}\frac{7D^2-53D+46}{D(D-1)^2}\beta^2R^2 \\
\left\langle {S_2'}^2\right\rangle_{\rm C} &= \frac{R^2}{9D^2(1-D)^2}\int_{-1}^0 d\tau\int_{-1}^0 d\sigma\left\langle\bar\eta_\mu^{(\tau)}\eta^{(\tau)\nu}\bar\eta_\rho^{(\sigma)}\eta^{(\sigma)\sigma}\right\rangle\Big\langle\Big[\xi^\mu(\tau)\xi_\nu(\tau)+ \\
&-\delta^\mu{}_\nu\xi_\alpha(\tau)\xi^\alpha(\tau)\Big][\xi^\rho(\sigma)\xi_\sigma(\sigma)-\delta^\rho{}_\sigma\xi_\alpha(\sigma)\xi^\alpha(\sigma)]\Big\rangle_{\rm C} = \\
&= -\frac{\beta^2R^2}{45D^2(1-D)^2}(3D^3-3D^2)\mathcal{M}_5 = \\
&= -\frac{1}{2160}\frac{1}{D-1}\beta^2R^2
\end{aligned}$$

$$\begin{aligned}
\langle S_2'S_4\rangle_{\rm C} &= -\frac{R^2}{18\beta D^2(1-D)^2}\int_{-1}^0 d\tau\int_{-1}^0 d\sigma\,\langle\bar\eta_\mu\eta^\nu\rangle\Big\langle\Big[\xi^\mu(\tau)\xi_\nu(\tau)+ \\
&-\delta^\mu{}_\nu\xi_\alpha(\tau)\xi^\alpha(\tau)\Big][\xi_\rho(\sigma)\xi_\sigma(\sigma)-\delta_{\rho\sigma}\xi_\alpha(\sigma)\xi^\alpha(\sigma)]\Big[\dot\xi^\rho(\sigma)\dot\xi^\sigma(\sigma)+ \\
&+a^\rho(\sigma)a^\sigma(\sigma)+b^\rho(\sigma)c^\sigma(\sigma)\Big]\Big\rangle_{\rm C} = \\
&= \frac{(D-1)\beta^2R^2}{18D^2(1-D)^2}[(2D^2-2D)\mathcal{M}_{12}+(2D^2-2D)\mathcal{M}_{13}] = \\
&= -\frac{1}{1620}\frac{1}{D}\beta^2R^2.
\end{aligned}\tag{4.74}$$

Summing up all together, the result gives precisely

$$-\langle S_6\rangle-\langle S_4'\rangle+\frac{1}{2}\left\langle {S_2'}^2\right\rangle_{\rm C}+\frac{1}{2}\left\langle {S_4}^2\right\rangle_{\rm C}+\langle S_2'S_4\rangle_{\rm C}=-\langle S_6\rangle_{\rm DBC}+\frac{1}{2}\left\langle {S_4}^2\right\rangle_{\rm C,DBC}. \tag{4.75}$$

The order β^3 is the most complicated one as it involves a large number of fields. The DBC terms are

$$\begin{aligned}\langle S_8\rangle_{\rm DBC}&=-\frac{(D+2)(D+4)}{7!\cdot 15D^2(D-1)^2}\beta^3R^3\\ \langle S_4S_6\rangle_{\rm C,DBC}&=-\frac{4(D+2)}{6!\cdot 45D^2(D-1)}\beta^3R^3\\ \left\langle {S_4}^3\right\rangle_{\rm C,DBC}&=-\frac{2(D+2)(D-2)}{6!\cdot 3D^2(D-1)^2}\beta^3R^3\end{aligned} \tag{4.76}$$

to be compared with the SI ones

$$\begin{aligned}\langle S_8\rangle =&\frac{8R^3}{7!\beta D^3(1-D)^3}\int_{-1}^{0}\mathrm{d}\tau\,\Big\langle\xi_\beta(\tau)\xi^\beta(\tau)\xi_\alpha(\tau)\xi^\alpha(\tau)\big[\xi_\mu(\tau)\xi_\nu(\tau)+\\ &-\delta_{\mu\nu}\xi_\alpha(\tau)\xi^\alpha(\tau)\big]\left[\dot\xi^\mu(\tau)\dot\xi^\nu(\tau)+a^\mu(\tau)a^\nu(\tau)+b^\mu(\tau)c^\nu(\tau)\right]\Big\rangle=\\ =&-\frac{8\beta^3R^3}{7!D^3(1-D)^3}\left(D^4+5D^3+2D^2-8D\right)\mathcal{M}_{14}=\\ =&\frac{8}{7!\cdot 1728}\frac{D^4+5D^3+2D^2-8D}{D^3(1-D)^3}\beta^3R^3\\ \langle S_6'\rangle =&-\frac{2}{945}\frac{R^3}{D^3(1-D)^3}\int_{-1}^{0}\mathrm{d}\tau\,\left\langle\bar\eta_\mu\eta^\nu\right\rangle\Big\langle\xi_\beta(\tau)\xi^\beta(\tau)\xi_\alpha(\tau)\xi^\alpha(\tau)\times\\ &\times\left[\xi^\mu(\tau)\xi_\nu(\tau)-\delta^\mu{}_\nu\xi_\beta(\tau)\xi^\beta(\tau)\right]\Big\rangle=\\ =&\frac{2}{945}\frac{\beta^3R^3}{D^3(1-D)^2}\left(D^3+6D^2+8D\right)\mathcal{M}_{15}=\\ =&-\frac{2}{945\cdot 1728}\frac{D^3+6D^2+8D}{D^3(1-D)^2}\beta^3R^3\\ \langle S_4S_6\rangle_{\rm C}=&-\frac{16R^3}{6\cdot 6!\beta^2D^3(1-D)^3}\int_{-1}^{0}\mathrm{d}\tau\int_{-1}^{0}\mathrm{d}\sigma\,\Big\langle\left[\xi_\mu(\tau)\xi_\nu(\tau)-\delta_{\mu\nu}\xi_\beta(\tau)\xi^\beta(\tau)\right]\times\\ &\times\left[\dot\xi^\mu(\tau)\dot\xi^\nu(\tau)+a^\mu(\tau)a^\nu(\tau)+b^\mu(\tau)c^\nu(\tau)\right]\xi_\alpha(\sigma)\xi^\alpha(\sigma)\times\\ &\times\left[\xi_\rho(\sigma)\xi_\sigma(\sigma)-\delta_{\rho\sigma}\xi_\beta(\sigma)\xi^\beta(\sigma)\right]\left[\dot\xi^\rho(\sigma)\dot\xi^\sigma(\sigma)+a^\rho(\sigma)a^\sigma(\sigma)+\right.\\ &\left.+b^\rho(\sigma)c^\sigma(\sigma)\right]\Big\rangle_{\rm C}=\\ =&-\frac{16\beta^3R^3}{6\cdot 6!D^3(1-D)^3}\Big[\left(-4D^4+12D^2-8D\right)\mathcal{M}_{16}+\\ &+\left(-2D^4+6D^2-4D\right)\mathcal{M}_{17}+\left(-10D^3-10D^2+20D\right)\mathcal{M}_{18}+\\ &+\left(-4D^4+12D^2-8D\right)\mathcal{M}_{19}+\left(20D^3+20D^2-40D\right)\mathcal{M}_{20}+\\ &+\left(-2D^4+6D^2-4D\right)\mathcal{M}_{21}+\left(-10D^3-10D^2+20D\right)\mathcal{M}_{22}\Big]=\end{aligned}$$

$$
\begin{aligned}
&= \frac{16}{6\cdot 6!\cdot 2160}\frac{9D^4-65D^3-92D^2+148D}{D^3(1-D)^3}\beta^3R^3\\
\left\langle {S_4}^3\right\rangle_{\mathrm{C}} &= \frac{R^3}{6^3\beta^3D^3(1-D)^3}\int_{-1}^{0}\mathrm{d}\tau\int_{-1}^{0}\mathrm{d}\sigma\int_{-1}^{0}\mathrm{d}\rho\\
&\quad\Big\langle\left[\xi_\mu(\tau)\xi_\nu(\tau)-\delta_{\mu\nu}\xi_\beta(\tau)\xi^\beta(\tau)\right]\left[\dot\xi^\mu(\tau)\dot\xi^\nu(\tau)+a^\mu(\tau)a^\nu(\tau)+\right.\\
&\quad\left.+b^\mu(\tau)c^\nu(\tau)\right]\left[\xi_\rho(\sigma)\xi_\sigma(\sigma)-\delta_{\rho\sigma}\xi_\alpha(\sigma)\xi^\alpha(\sigma)\right]\left[\dot\xi^\rho(\sigma)\dot\xi^\sigma(\sigma)+\right.\\
&\quad\left.+a^\rho(\sigma)a^\sigma(\sigma)+b^\rho(\sigma)c^\sigma(\sigma)\right]\left[\xi_\mu(\rho)\xi_\nu(\rho)-\delta_{\mu\nu}\xi_\alpha(\rho)\xi^\alpha(\rho)\right]\times\\
&\quad\times\left[\dot\xi^\mu(\rho)\dot\xi^\nu(\rho)+a^\mu(\rho)a^\nu(\rho)+b^\mu(\rho)c^\nu(\rho)\right]\Big\rangle_{\mathrm{C}} =\\
&= \frac{R^3}{6^3\beta^3D^3(1-D)^3}\Big[\left(24D-72D^2+72D^3-24D^4\right)\mathcal{M}_{23}+\\
&\quad+\left(24D-72D^2+72D^3-24D^4\right)\mathcal{M}_{24}+\\
&\quad+\left(-48D+144D^2-144D^3+48D^4\right)\mathcal{M}_{25}+\\
&\quad+\left(24D-72D^2+72D^3-24D^4\right)\mathcal{M}_{26}+\\
&\quad+\left(-72D+144D^2-72D^3\right)\mathcal{M}_{27}+\\
&\quad+\left(24D-72D^2+72D^3-24D^4\right)\mathcal{M}_{28}+\\
&\quad+\left(24D-72D^2+72D^3-24D^4\right)\mathcal{M}_{29}+\\
&\quad+\left(8D-24D^2+24D^3-8D^4\right)\mathcal{M}_{30}+\\
&\quad+\left(-72D+144D^2-72D^3\right)\mathcal{M}_{31}+\\
&\quad+\left(24D-72D^2+72D^3-24D^4\right)\mathcal{M}_{32}+\\
&\quad+\left(-72D+144D^2-72D^3\right)\mathcal{M}_{33}+\\
&\quad+\left(-120D+168D^2-48D^3\right)\mathrm{M}_{34}+\\
&\quad+\left(-24D+72D^2-72D^3+24D^4\right)\mathrm{M}_{35}+\\
&\quad+\left(72D-144D^2+72D^3\right)\mathcal{M}_{36}+\\
&\quad+\left(144D-288D^2+144D^3\right)\mathcal{M}_{37}+\\
&\quad+\left(120D-168D^2+48D^3\right)\mathcal{M}_{38}+\\
&\quad+\left(8D-24D^2+24D^3-8D^4\right)\mathcal{M}_{39}+\\
&\quad+\left(-72D+144D^2-72D^3\right)\mathcal{M}_{40}+\\
&\quad+\left(72D-144D^2+72D^3\right)\mathcal{M}_{41}+\\
&\quad+\left(128D-136D^2+8D^3\right)\mathcal{M}_{42}+\\
&\quad+\left(-144D+288D^2-144D^3\right)\mathcal{M}_{43}+\\
&\quad+\left(-24D+72D^2-72D^3+24D^4\right)\mathcal{M}_{44}+
\end{aligned}
$$

$$
\begin{aligned}
&+\left(72D-144D^2+72D^3\right)\mathcal{M}_{45}+\\
&+\left(144D-288D^2+144D^3\right)\mathcal{M}_{46}+\\
&+\left(-144D+288D^2-144D^3\right)\mathcal{M}_{47}+\\
&+\left(72D-144D^2+72D^3\right)\mathcal{M}_{48}+\\
&+\left(120D-168D^2+48D^3\right)\mathcal{M}_{49}+\\
&+\left(240D-336D^2+96D^3\right)\mathcal{M}_{50}+\\
&+\left(-240D+336D^2-96D^3\right)\mathcal{M}_{51}+\\
&+\left(-240D+336D^2-96D^3\right)\mathcal{M}_{52}+\\
&+\left(-264D+240D^2+24D^3\right)\mathcal{M}_{53}+\\
&+\left(384D-408D^2+24D^3\right)\mathcal{M}_{54}+\\
&+\left(-40D+56D^2-16D^3\right)\mathcal{M}_{55}+\\
&+\left(-88D+80D^2+8D^3\right)\mathcal{M}_{56}\Big]=\\
=&\frac{1}{6^3\cdot 7560}\frac{4068D-1604D^2-2753D^3+289D^4}{D^3(1-D)^3}\beta^3R^3
\end{aligned}
$$

$$
\begin{aligned}
\left\langle {S_2'}^3\right\rangle_{\mathrm{C}} =&-\frac{R^3}{3^3D^3(1-D)^3}\int_{-1}^{0}\mathrm{d}\tau\int_{-1}^{0}\mathrm{d}\sigma\int_{-1}^{0}\mathrm{d}\rho\ \left\langle\bar\eta_\mu^{(\tau)}\eta^{(\tau)\nu}\bar\eta_\rho^{(\sigma)}\eta^{(\sigma)\sigma}\bar\eta_\alpha^{(\rho)}\eta^{(\rho)\beta}\right\rangle\times\\
&\times\Big\langle\left[\xi^\mu(\tau)\xi_\nu(\tau)-\delta^\mu{}_\nu\xi_\beta(\tau)\xi^\beta(\tau)\right]\left[\xi^\rho(\sigma)\xi_\sigma(\sigma)-\delta^\rho{}_l\xi_\alpha(\sigma)\xi^\alpha(\sigma)\right]\times\\
&\times\left[\xi^\alpha(\rho)\xi_\beta(\rho)-\delta^\alpha{}_\beta\xi_\alpha(\rho)\xi^\alpha(\rho)\right]\Big\rangle\Big|_{\mathrm{C}}=\\
=&\frac{\beta^3R^3}{3^3D^3(1-D)^3}\Big[\left(2D-6D^2+6D^3-2D^4\right)\mathcal{M}_{57}+\\
&+3\left(-10D+24D^2-18D^3+4D^4\right)\mathcal{M}_{58}+\\
&+\left(76D-130D^2+62D^3-8D^4\right)\mathcal{M}_{59}\Big]=\\
=&\frac{1}{3^3\cdot 30240}\frac{-6D-17D^2+22D^3+D^4}{D^3(1-D)^3}\beta^3R^3
\end{aligned}
$$

$$
\begin{aligned}
\left\langle S_2'S_6\right\rangle_{\mathrm{C}} =&\frac{16R^3}{3\cdot 6!\beta D^3(1-D)^3}\int_{-1}^{0}\mathrm{d}\tau\int_{-1}^{0}\mathrm{d}\sigma\ \left\langle\bar\eta_\mu\eta^\nu\right\rangle\Big\langle\left[\xi^\mu(\tau)\xi_\nu(\tau)-\delta^\mu{}_\nu\xi_\beta(\tau)\xi^\beta(\tau)\right]\times\\
&\times\xi_q(\sigma)\xi^q(\sigma)\left[\xi_\rho(\sigma)\xi_\sigma(\sigma)-\delta_{\rho\sigma}\xi_\beta(\sigma)\xi^\beta(\sigma)\right]\times\\
&\times\left[\dot\xi^\rho(\sigma)\dot\xi^\sigma(\sigma)+a^\rho(\sigma)a^\sigma(\sigma)+b^\rho(\sigma)c^\sigma(\sigma)\right]\Big\rangle_{\mathrm{C}}=\\
=&\frac{16\beta^3R^3}{3\cdot 6!D^3(1-D)^2}\Big[\left(8D-4D^2-4D^3\right)\mathcal{M}_{60}+\\
&+\left(4D-2D^2-2D^3\right)\mathcal{M}_{61}\Big]=\\
=&-\frac{16}{3\cdot 6!\cdot 1440}\frac{-2D+D^2+D^3}{D^3(1-D)^2}\beta^3R^3
\end{aligned}
$$

$$
\left\langle S_2'S_4'\right\rangle_{\mathrm{C}} =\frac{R^3}{3\cdot 45D^3(1-D)^3}\int_{-1}^{0}\mathrm{d}\tau\int_{-1}^{0}\mathrm{d}\sigma\ \left\langle\bar\eta_\mu^{(\tau)}\eta^{(\tau)\nu}\bar\eta_\rho^{(\sigma)}\eta^{(\sigma)\sigma}\right\rangle\Big\langle\left[\xi^\mu(\tau)\xi_\nu(\tau)+\right.
$$

$$
\begin{aligned}
&- \delta^{\mu}{}_{\nu}\xi_{\beta}(\tau)\xi^{\beta}(\tau)\big]\xi_{\alpha}(\sigma)\xi^{\alpha}(\sigma)\left[\xi^{\rho}(\sigma)\xi_{\sigma}(\sigma) - \delta^{\rho}{}_{l}\xi_{\beta}(\sigma)\xi^{\beta}(\sigma)\right]\rangle\Big|_{\mathrm{C}} = \\
&= -\frac{\beta^3 R^3}{3\cdot 45 D^3(1-D)^3}\big[(1-D)^2\left(8D+4D^2\right)\mathcal{M}_{62} - \left(2D+D^2\right)\mathcal{M}_{63} + \\
&- \left(6D+5D^2+D^3\right)\mathcal{M}_{62} + (2-D)\left(2D^2+D^3\right)\mathcal{M}_{63} + \\
&+ (2-D)\left(8D+4D^2\right)\mathcal{M}_{62}\big] = \\
&= -\frac{1}{3\cdot 45\cdot 8640}\frac{-8D+2D^2+5D^3+D^4}{D^3(1-D)^3}\beta^3 R^3 \\
\langle S_4' S_4\rangle_{\mathrm{C}} &= -\frac{R^3}{6\cdot 45\beta D^3(1-D)^3}\int_{-1}^{0}\mathrm{d}\tau\int_{-1}^{0}\mathrm{d}\sigma\ \langle\bar{\eta}_{\mu}\eta^{\nu}\rangle\Big\langle\left[\xi_{\mu}(\tau)\xi_{\nu}(\tau) - \delta_{\mu\nu}\xi_{\beta}(\tau)\xi^{\beta}(\tau)\right]\times \\
&\times\left[\dot{\xi}^{\mu}(\tau)\dot{\xi}^{\nu}(\tau) + a^{\mu}(\tau)a^{\nu}(\tau) + b^{\mu}(\tau)c^{\nu}(\tau)\right]\left[\xi^{\rho}(\sigma)\xi_{\sigma}(\sigma) - \delta^{\rho}{}_{\sigma}\xi_{\alpha}(\sigma)\xi^{\alpha}(\sigma)\right]\times \\
&\times\xi_{\beta}(\sigma)\xi^{\beta}(\sigma)\Big\rangle_{\mathrm{C}} = \\
&= -\frac{\beta^3 R^3}{6\cdot 45 D^3(1-D)^2}\big[\left(8D+4D^2\right)\mathcal{M}_{64} + \left(8D+4D^2\right)\mathcal{M}_{65} + \\
&+ \left(16D+8D^2\right)\mathcal{M}_{66} - \left(8D^2+4D^3\right)\mathcal{M}_{64} - \left(8D^2+4D^3\right)\mathcal{M}_{65} + \\
&- \left(16D+8D^2\right)\mathcal{M}_{66}\big] = \\
&= -\frac{1}{6\cdot 45\cdot 60480}\frac{224D-112D^2-112D^3}{D^3(1-D)^2}\beta^3 R^3 \\
\left\langle S_2'^{\,2} S_4\right\rangle_{\mathrm{C}} &= \frac{R^3}{6\cdot 3^2\beta D^3(1-D)^3}\int_{-1}^{0}\mathrm{d}\tau\int_{-1}^{0}\mathrm{d}\sigma\int_{-1}^{0}\mathrm{d}\rho\ \left\langle\bar{\eta}_{\mu}^{(\sigma)}\eta^{(\sigma)\nu}\bar{\eta}_{\rho}^{(\rho)}\eta^{(\rho)\sigma}\right\rangle\times \\
&\times\Big\langle\left[\xi_{\alpha}(\tau)\xi_{\beta}(\tau) - \delta_{\alpha\beta}\xi_{\beta}(\tau)\xi^{\beta}(\tau)\right]\left[\dot{\xi}^{\alpha}(\tau)\dot{\xi}^{\beta}(\tau) + a^{\alpha}(\tau)a^{\beta}(\tau) + \right. \\
&+ \left. b^{\alpha}(\tau)c^{\beta}(\tau)\right]\left[\xi^{\mu}(\sigma)\xi_{\nu}(\sigma) - \delta^{\mu}{}_{\nu}\xi_{\alpha}(\sigma)\xi^{\alpha}(\sigma)\right]\left[\xi^{\rho}(\rho)\xi_{\sigma}(\rho) + \right. \\
&- \left.\delta^{\rho}{}_{\sigma}\xi_{\alpha}(\rho)\xi^{\alpha}(\rho)\right]\Big\rangle\Big|_{\mathrm{C}} = \\
&= \frac{\beta^3 R^3}{6\cdot 3^2 D^3(1-D)^3}\big[8D(D-1)^2\mathcal{M}_{67} + 4D(D-1)^2\mathcal{M}_{68} + \\
&+ 8D(D-1)^2\mathcal{M}_{69} + \left(8D+8D^2\right)(D-1)^2\mathcal{M}_{70} + \\
&+ 4D(D-1)^2\mathcal{M}_{71} - 8D^2(D-1)^2\mathcal{M}_{67} - 4D^2(D-1)^2\mathcal{M}_{68} + \\
&- 8D^2(D-1)^2\mathcal{M}_{69} - 16D(D-1)^2\mathcal{M}_{70} + \\
&- 4D^2(D-1)^2\mathcal{M}_{71} - 4D\mathcal{M}_{72} - \left(4D+4D^2\right)\mathcal{M}_{67} + \\
&- 2D\mathcal{M}_{73} - \left(2D+2D^2\right)\mathcal{M}_{68} - \left(4D+4D^2\right)\mathcal{M}_{69} + \\
&- \left(12D+4D^2\right)\mathcal{M}_{70} - 2D\mathcal{M}_{73} - \left(2D+2D^2\right)\mathcal{M}_{71} + \\
&+ 2D^2(2-D)\mathcal{M}_{72} + 8D(2-D)\mathcal{M}_{67} + 2D^2(2-D)\mathcal{M}_{72} + \\
&+ 2D^2(2-D)\mathcal{M}_{73} + 4D(2-D)\mathcal{M}_{71} + 8D(2-D)\mathcal{M}_{69} + \\
&+ (2-D)\left(8D+8D^2\right)\mathcal{M}_{70} + 2D^2(2-D)\mathcal{M}_{73} + 4D(2-D)\mathcal{M}_{68} + \\
&+ 2D^2\mathcal{M}_{72} + \left(4D^2+4D^3\right)\mathcal{M}_{67} + 2D^2\mathcal{M}_{72} +
\end{aligned}
$$

$$
\begin{aligned}
&+2D^2\mathcal{M}_{73}+4D\mathcal{M}_{71}+\left(4D^2+4D^3\right)\mathcal{M}_{69}+\\
&+\left(8D+8D^2\right)\mathcal{M}_{70}+2D^2\mathcal{M}_{73}+4D\mathcal{M}_{68}+\\
&+2D^3(D-2)\mathcal{M}_{72}+8D^2(D-2)\mathcal{M}_{67}+2D^3(D-2)\mathcal{M}_{72}+\\
&+2D^3(D-2)\mathcal{M}_{73}4D^2(D-2)\mathcal{M}_{68}+8D^2(D-2)\mathcal{M}_{69}+\\
&+16D(D-2)\mathcal{M}_{70}+2D^3(D-2)\mathcal{M}_{73}+4D^2(D-2)\mathcal{M}_{68}\Big]=\\
=&\frac{4}{54\cdot 60480}\frac{46D-67D^2+17D^3+4D^4}{D^3(1-D)^3}\beta^3R^3\\
\left\langle S_2' {S_4}^2\right\rangle_{\mathrm{C}}=&-\frac{R^3}{3\cdot 6^2\beta^2D^3(1-D)^3}\int_{-1}^{0}\mathrm{d}\tau\int_{-1}^{0}\mathrm{d}\sigma\int_{-1}^{0}\mathrm{d}\rho\ \langle\bar{\eta}_\mu\eta^\nu\rangle\times\\
&\times\Big\langle\left[\xi^\mu(\tau)\xi_\nu(\tau)-\delta^\mu{}_\nu\xi_\beta(\tau)\xi^\beta(\tau)\right]\times\\
&\times\left[\xi_\alpha(\sigma)\xi_\beta(\sigma)-\delta_{\alpha\beta}\xi_\beta(\sigma)\xi^\beta(\sigma)\right]\left[\dot{\xi}^\alpha(\sigma)\dot{\xi}^\beta(\sigma)+a^\alpha(\sigma)a^\beta(\sigma)+\right.\\
&\left.+b^\alpha(\sigma)c^\beta(\sigma)\right]\left[\xi_\rho(\rho)\xi_\sigma(\rho)-\delta_{\rho\sigma}\xi_\rho(\rho)\xi^\rho(\rho)\right]\left[\dot{\xi}^\rho(\rho)\dot{\xi}^\sigma(\rho)+\right.\\
&\left.+a^\rho(\rho)a^\sigma(\rho)+b^\rho(\rho)c^\sigma(\rho)\right]\Big\rangle_{\mathrm{C}}=\\
=&\frac{\beta^3R^3}{3\cdot 6^2D^3(1-D)^2}\Big[\left(8D-16D^2+8D^3\right)\mathcal{M}_{74}+\\
&+\left(8D-16D^2+8D^3\right)\mathcal{M}_{75}+\left(-16D+32D^2-16D^3\right)\mathcal{M}_{76}+\\
&+\left(-16D+32D^2-16D^3\right)\mathcal{M}_{77}+\left(8D-16D^2+8D^3\right)\mathcal{M}_{78}+\\
&+\left(-24D+24D^2\right)\mathcal{M}_{79}+\left(24D-24D^2\right)\mathcal{M}_{80}+\\
&+\left(48D-48D^2\right)\mathcal{M}_{81}+\left(16D-32D^2+16D^3\right)\mathcal{M}_{82}+\\
&+\left(-48D+48D^2\right)\mathcal{M}_{83}+\left(8D-16D^2+8D^3\right)\mathcal{M}_{84}+\\
&+\left(8D-16D^2+8D^3\right)\mathcal{M}_{85}+\left(8D-16D^2+8D^3\right)\mathcal{M}_{86}+\\
&+\left(-24D+24D^2\right)\mathcal{M}_{87}+\left(24D-24D^2\right)\mathcal{M}_{88}\Big]=\\
=&\frac{1}{3\cdot 6^2\cdot 7560}\frac{158D-121D^2-37D^3}{D^3(1-D)^2}\beta^3R^3. \qquad (4.77)
\end{aligned}
$$

Summing up all the above terms gives rise to

$$
\begin{aligned}
&-\langle S_8\rangle-\langle S_6'\rangle+\langle S_4S_6\rangle_{\mathrm{C}}-\frac{1}{6}\left\langle {S_4}^3\right\rangle_{\mathrm{C}}-\frac{1}{6}\left\langle {S_2'}^3\right\rangle_{\mathrm{C}}+\left\langle S_2'S_6\right\rangle_{\mathrm{C}}+\\
&+\left\langle S_2'S_4'\right\rangle_{\mathrm{C}}+\left\langle S_4'S_4\right\rangle_{\mathrm{C}}-\frac{1}{2}\left\langle {S'}^2{}_2S_4\right\rangle_{\mathrm{C}}-\frac{1}{2}\left\langle S_2'{S_4}^2\right\rangle_{\mathrm{C}}= \qquad (4.78)\\
&=-\langle S_8\rangle_{\mathrm{DBC}}+\langle S_4S_6\rangle_{\mathrm{C,DBC}}-\frac{1}{6}\left\langle {S_4}^3\right\rangle_{\mathrm{C,DBC}},
\end{aligned}
$$

confirming a perfect agreement between the DBC and SI calculations. Summarizing, the final result for the local trace anomaly computed in a maximally symmetric space

is given by

$$\begin{aligned}\left\langle T^{\mu}{}_{\mu}(\xi)\right\rangle = \lim_{\beta\to 0}\mathcal{Z}(\beta) = \frac{1}{(2\pi\beta)^{\frac{D}{2}}}\exp\Big[\frac{\beta}{4!}(12\xi-2)R+ \\ -\frac{\beta^2}{6!}\frac{D-3}{D(D-1)}R^2+\frac{\beta^3}{8!}\frac{16(D+2)(D-3)}{9D^2(D-1)^2}R^3+o(\beta^3)\Big],\end{aligned} \tag{4.79}$$

or, more explicitly,

$$\begin{aligned}\left\langle T^{\mu}{}_{\mu}(x)\right\rangle_{D=2} &= -\frac{R}{24\pi} \\ \left\langle T^{\mu}{}_{\mu}(x)\right\rangle_{D=4} &= -\frac{R^2}{48\cdot 6!\pi^2} \\ \left\langle T^{\mu}{}_{\mu}(x)\right\rangle_{D=6} &= -\frac{R^3}{60\cdot 9!\pi^3},\end{aligned} \tag{4.80}$$

as DBC-computed in [26].

For completeness, here we report the list of $\mathcal{M}$-integrals used for the previous calculation.

$$\begin{aligned}\mathcal{M}_1 &= \int \mathrm{d}\tau\ \mathcal{B}|_\tau\left(\overset{\bullet}{\mathcal{B}}{}^{\bullet}+\Delta_{\mathrm{gh}}\right)|_\tau = -\frac{1}{12} \\ \mathcal{M}_2 &= \int \mathrm{d}\tau\ \mathcal{B}|_\tau = -\frac{1}{12} \\ \mathcal{M}_3 &= \int \mathrm{d}\tau\ \mathcal{B}|_\tau{}^2\left(\overset{\bullet}{\mathcal{B}}{}^{\bullet}+\Delta_{\mathrm{gh}}\right)|_\tau = \frac{1}{144} \\ \mathcal{M}_4 &= \int \mathrm{d}\tau\ \mathcal{B}|_\tau{}^2 = \frac{1}{144} \\ \mathcal{M}_5 &= \int \mathrm{d}\tau_1\int \mathrm{d}\tau_2\ \mathcal{B}^2 = \frac{1}{720} \\ \mathcal{M}_6 &= \int \mathrm{d}\tau_1\int \mathrm{d}\tau_2\ \mathcal{B}|_1\ \overset{\bullet}{\mathcal{B}}{}^2\left(\overset{\bullet}{\mathcal{B}}{}^{\bullet}+\Delta_{\mathrm{gh}}\right)|_2 = -\frac{1}{144} \\ \mathcal{M}_7 &= \int \mathrm{d}\tau_1\int \mathrm{d}\tau_2\ \mathcal{B}|_1\mathcal{B}|_2\left(\overset{\bullet}{\mathcal{B}}{}^{\bullet 2}-\Delta_{\mathrm{gh}}{}^2\right) = -\frac{1}{144} \\ \mathcal{M}_8 &= \int \mathrm{d}\tau_1\int \mathrm{d}\tau_2\ \mathcal{B}^2\left(\overset{\bullet}{\mathcal{B}}{}^{\bullet}+\Delta_{\mathrm{gh}}\right)|_1\left(\overset{\bullet}{\mathcal{B}}{}^{\bullet}+\Delta_{\mathrm{gh}}\right)|_2 = \frac{1}{720} \\ \mathcal{M}_9 &= \int \mathrm{d}\tau_1\int \mathrm{d}\tau_2\ \mathcal{B}^2\left(\overset{\bullet}{\mathcal{B}}{}^{\bullet 2}-\Delta_{\mathrm{gh}}{}^2\right) = \frac{1}{120} \\ \mathcal{M}_{10} &= \int \mathrm{d}\tau_1\int \mathrm{d}\tau_2\ \mathcal{B}\ \mathcal{B}^{\bullet}\ \overset{\bullet}{\mathcal{B}}\ \overset{\bullet}{\mathcal{B}}{}^{\bullet} = -\frac{11}{1440} \\ \mathcal{M}_{11} &= \int \mathrm{d}\tau_1\int \mathrm{d}\tau_2\ \mathcal{B}^{\bullet 2}\ \overset{\bullet}{\mathcal{B}}{}^2 = \frac{1}{80} \\ \mathcal{M}_{12} &= \int \mathrm{d}\tau_1\int \mathrm{d}\tau_2\ \mathcal{B}^2\left(\overset{\bullet}{\mathcal{B}}{}^{\bullet}+\Delta_{\mathrm{gh}}\right)|_2 = \frac{1}{720} \\ \mathcal{M}_{13} &= \int \mathrm{d}\tau_1\int \mathrm{d}\tau_2\ \mathcal{B}^{\bullet 2}\mathcal{B}|_2 = -\frac{1}{144}\end{aligned} \tag{4.81}$$

$$\mathcal{M}_{14} = \int \mathrm{d}\tau\ \mathcal{B}|_\tau{}^3 \left(\overset{\bullet}{\mathcal{B}}{}^\bullet + \Delta_{\mathrm{gh}}\right)|_\tau = -\frac{1}{1728}$$

$$\mathcal{M}_{15} = \int \mathrm{d}\tau\ \mathcal{B}|_\tau{}^3 = -\frac{1}{1728}$$

$$\mathcal{M}_{16} = \int \mathrm{d}\tau_1 \int \mathrm{d}\tau_2\ \mathcal{B}|_1 \mathcal{B}|_2 \overset{\bullet}{\mathcal{B}}{}^2 \left(\overset{\bullet}{\mathcal{B}}{}^\bullet + \Delta_{\mathrm{gh}}\right)|_2 = \frac{1}{1728}$$

$$\mathcal{M}_{17} = \int \mathrm{d}\tau_1 \int \mathrm{d}\tau_2\ \mathcal{B}|_1 \mathcal{B}|_2{}^2 \left(\overset{\bullet}{\mathcal{B}}{}^{\bullet 2} - \Delta_{\mathrm{gh}}{}^2\right) = \frac{1}{1728}$$

$$\mathcal{M}_{18} = \int \mathrm{d}\tau_1 \int \mathrm{d}\tau_2\ \mathcal{B}^2 \mathcal{B}|_2 \left(\overset{\bullet}{\mathcal{B}}{}^{\bullet 2} - \Delta_{\mathrm{gh}}{}^2\right) = -\frac{1}{1440}$$

$$\mathcal{M}_{19} = \int \mathrm{d}\tau_1 \int \mathrm{d}\tau_2\ \mathcal{B}^2 \mathcal{B}|_2 \left(\overset{\bullet}{\mathcal{B}}{}^\bullet + \Delta_{\mathrm{gh}}\right)|_1 \left(\overset{\bullet}{\mathcal{B}}{}^\bullet + \Delta_{\mathrm{gh}}\right)|_2 = -\frac{1}{8640}$$

$$\mathcal{M}_{20} = \int \mathrm{d}\tau_1 \int \mathrm{d}\tau_2\ \mathcal{B}|_2\ \mathcal{B}\ \overset{\bullet}{\mathcal{B}}{}^\bullet\ \overset{\bullet}{\mathcal{B}}\ \overset{\bullet}{\mathcal{B}}{}^\bullet = \frac{11}{17280}$$

$$\mathcal{M}_{21} = \int \mathrm{d}\tau_1 \int \mathrm{d}\tau_2\ \mathcal{B}^{\bullet 2} \mathcal{B}|_2{}^2 \left(\overset{\bullet}{\mathcal{B}}{}^\bullet + \Delta_{\mathrm{gh}}\right)|_1 = \frac{1}{1728}$$

$$\mathcal{M}_{22} = \int \mathrm{d}\tau_1 \int \mathrm{d}\tau_2\ \mathcal{B}^{\bullet 2}\ \overset{\bullet}{\mathcal{B}}{}^2 \mathcal{B}|_2 = -\frac{1}{960}$$

$$\mathcal{M}_{23} = \int \mathrm{d}\tau_1 \int \mathrm{d}\tau_2 \int \mathrm{d}\tau_3\ \mathcal{B}|_1 \overset{\bullet}{\mathcal{B}}{}_{12}{}^2\ \overset{\bullet}{\mathcal{B}}{}_{23}{}^2 \left(\overset{\bullet}{\mathcal{B}}{}^\bullet + \Delta_{\mathrm{gh}}\right)|_3 = -\frac{1}{1728}$$

$$\mathcal{M}_{24} = \int \mathrm{d}\tau_1 \int \mathrm{d}\tau_2 \int \mathrm{d}\tau_3\ \mathcal{B}|_1{}^2\ \overset{\bullet}{\mathcal{B}}{}_{12}{}^2 \left(\overset{\bullet}{\mathcal{B}}{}^\bullet_{23}{}^2 - \Delta_{\mathrm{gh},23}{}^2\right) = -\frac{1}{1728}$$

$$\mathcal{M}_{25} = \int \mathrm{d}\tau_1 \int \mathrm{d}\tau_2 \int \mathrm{d}\tau_3\ \mathcal{B}|_1\ \overset{\bullet}{\mathcal{B}}{}_{12}\ \mathcal{B}_{23}\ \overset{\bullet}{\mathcal{B}}{}_{23}\ \overset{\bullet}{\mathcal{B}}{}^\bullet_{12} = 0$$

$$\mathcal{M}_{26} = \int \mathrm{d}\tau_1 \int \mathrm{d}\tau_2 \int \mathrm{d}\tau_3\ \mathcal{B}|_1\ \overset{\bullet}{\mathcal{B}}{}_{12}\ \overset{\bullet}{\mathcal{B}}{}_{13}\ \mathcal{B}_{23} \left(\overset{\bullet}{\mathcal{B}}{}^\bullet + \Delta_{\mathrm{gh}}\right)|_2 \left(\overset{\bullet}{\mathcal{B}}{}^\bullet + \Delta_{\mathrm{gh}}\right)|_3 = \frac{1}{8640}$$

$$\mathcal{M}_{27} = \int \mathrm{d}\tau_1 \int \mathrm{d}\tau_2 \int \mathrm{d}\tau_3\ \mathcal{B}|_1\ \overset{\bullet}{\mathcal{B}}{}_{12}\ \overset{\bullet}{\mathcal{B}}{}_{13}\ \mathcal{B}_{23} \left(\overset{\bullet}{\mathcal{B}}{}^\bullet_{23}{}^2 - \Delta_{\mathrm{gh},23}{}^2\right) = \frac{1}{1440}$$

$$\mathcal{M}_{28} = \int \mathrm{d}\tau_1 \int \mathrm{d}\tau_2 \int \mathrm{d}\tau_3\ \mathcal{B}|_1{}^2\ \overset{\bullet}{\mathcal{B}}{}_{12}\ \mathcal{B}^\bullet_{23}\ \overset{\bullet}{\mathcal{B}}{}^\bullet_{13} \left(\overset{\bullet}{\mathcal{B}}{}^\bullet + \Delta_{\mathrm{gh}}\right)|_2 = -\frac{1}{1728}$$

$$\mathcal{M}_{29} = \int \mathrm{d}\tau_1 \int \mathrm{d}\tau_2 \int \mathrm{d}\tau_3\ \mathcal{B}|_1\ \mathcal{B}_{23}{}^2\ \left(\overset{\bullet}{\mathcal{B}}{}^\bullet_{12}{}^2 - \Delta_{\mathrm{gh},12}{}^2\right) \left(\overset{\bullet}{\mathcal{B}}{}^\bullet + \Delta_{\mathrm{gh}}\right)|_3 = \frac{1}{8640}$$

$$\mathcal{M}_{30} = \int \mathrm{d}\tau_1 \int \mathrm{d}\tau_2 \int \mathrm{d}\tau_3\ \mathcal{B}|_1{}^3\ \left(\overset{\bullet}{\mathcal{B}}{}^\bullet_{12}\ \overset{\bullet}{\mathcal{B}}{}^\bullet_{23}\ \overset{\bullet}{\mathcal{B}}{}^\bullet_{13} + \Delta_{\mathrm{gh},12}\ \Delta_{\mathrm{gh},23}\ \Delta_{\mathrm{gh},13}\right) = -\frac{1}{1728}$$

$$\mathcal{M}_{31} = \int \mathrm{d}\tau_1 \int \mathrm{d}\tau_2 \int \mathrm{d}\tau_3\ \mathcal{B}|_1\ \mathcal{B}_{23}{}^2 \left(\overset{\bullet}{\mathcal{B}}{}^\bullet_{12}\ \overset{\bullet}{\mathcal{B}}{}^\bullet_{23}\ \overset{\bullet}{\mathcal{B}}{}^\bullet_{13} + \Delta_{\mathrm{gh},12}\ \Delta_{\mathrm{gh},23}\ \Delta_{\mathrm{gh},13}\right) = \frac{1}{1440}$$

$$\mathcal{M}_{32} = \int \mathrm{d}\tau_1 \int \mathrm{d}\tau_2 \int \mathrm{d}\tau_3\ \mathcal{B}_{12}{}^2\ \overset{\bullet}{\mathcal{B}}{}_{23}{}^2 \left(\overset{\bullet}{\mathcal{B}}{}^\bullet + \Delta_{\mathrm{gh}}\right)|_1 \left(\overset{\bullet}{\mathcal{B}}{}^\bullet + \Delta_{\mathrm{gh}}\right)|_3 = \frac{1}{8640}$$

$$\mathcal{M}_{33} = \int \mathrm{d}\tau_1 \int \mathrm{d}\tau_2 \int \mathrm{d}\tau_3\ \mathcal{B}_{12}{}^2\ \overset{\bullet}{\mathcal{B}}{}_{13}\ \overset{\bullet}{\mathcal{B}}{}_{23}\ \overset{\bullet}{\mathcal{B}}{}^\bullet_{12} \left(\overset{\bullet}{\mathcal{B}}{}^\bullet + \Delta_{\mathrm{gh}}\right)|_3 = -\frac{11}{20160}$$

$$\mathcal{M}_{34} = \int \mathrm{d}\tau_1 \int \mathrm{d}\tau_2 \int \mathrm{d}\tau_3\ \mathcal{B}_{12}{}^2\ \overset{\bullet}{\mathcal{B}}{}_{13}{}^2 \left(\overset{\bullet}{\mathcal{B}}{}^\bullet_{23}{}^2 - \Delta_{\mathrm{gh},23}{}^2\right) = -\frac{1}{4032}$$

$$\mathcal{M}_{35} = \int \mathrm{d}\tau_1 \int \mathrm{d}\tau_2 \int \mathrm{d}\tau_3\ \mathcal{B}_{12}\ \mathcal{B}^\bullet_{12}\ \mathcal{B}_{23}\ \overset{\bullet}{\mathcal{B}}{}_{23} \left(\overset{\bullet}{\mathcal{B}}{}^\bullet + \Delta_{\mathrm{gh}}\right)|_1 \left(\overset{\bullet}{\mathcal{B}}{}^\bullet + \Delta_{\mathrm{gh}}\right)|_3 = 0$$

$$\mathcal{M}_{36} = \int \mathrm{d}\tau_1 \int \mathrm{d}\tau_2 \int \mathrm{d}\tau_3\ \mathcal{B}_{12}\ \mathcal{B}^\bullet_{12}\ \overset{\bullet}{\mathcal{B}}{}_{12}\ \overset{\bullet}{\mathcal{B}}{}_{13}\ \overset{\bullet}{\mathcal{B}}{}_{23} \left(\overset{\bullet}{\mathcal{B}}{}^\bullet + \Delta_{\mathrm{gh}}\right)|_3 = \frac{11}{60480}$$

$$\mathcal{M}_{37} = \int \mathrm{d}\tau_1 \int \mathrm{d}\tau_2 \int \mathrm{d}\tau_3\ \mathcal{B}_{12}\ \mathcal{B}^\bullet_{12}\ \overset{\bullet}{\mathcal{B}}{}_{13}\ \mathcal{B}_{23}\ \overset{\bullet}{\mathcal{B}}{}^\bullet_{12} \left(\overset{\bullet}{\mathcal{B}}{}^\bullet + \Delta_{\mathrm{gh}}\right)|_3 = -\frac{1}{60480}$$

$$\mathcal{M}_{38} = \int \mathrm{d}\tau_1 \int \mathrm{d}\tau_2 \int \mathrm{d}\tau_3\ \mathcal{B}_{12}\ \mathcal{B}^\bullet_{12}\ \mathcal{B}_{23}\ \overset{\bullet}{\mathcal{B}}{}_{23} \left(\overset{\bullet}{\mathcal{B}}{}^\bullet_{13}{}^2 - \Delta_{\mathrm{gh},13}{}^2\right) = \frac{61}{120960}$$

$$\mathcal{M}_{39} = \int \mathrm{d}\tau_1 \int \mathrm{d}\tau_2 \int \mathrm{d}\tau_3\, \mathcal{B}_{12}\, \mathcal{B}_{23}\, \mathcal{B}_{13}\, \left(\overset{\bullet}{\mathcal{B}}{}^{\bullet} + \Delta_{\mathrm{gh}}\right)|_1 \left(\overset{\bullet}{\mathcal{B}}{}^{\bullet} + \Delta_{\mathrm{gh}}\right)|_2 \left(\overset{\bullet}{\mathcal{B}}{}^{\bullet} + \Delta_{\mathrm{gh}}\right)|_3 = -\frac{1}{30240}$$

$$\mathcal{M}_{40} = \int \mathrm{d}\tau_1 \int \mathrm{d}\tau_2 \int \mathrm{d}\tau_3\, \mathcal{B}_{12}\, \mathcal{B}_{23}\, \mathcal{B}_{13}\, \left(\overset{\bullet}{\mathcal{B}}{}^{\bullet} + \Delta_{\mathrm{gh}}\right)|_1 \left(\overset{\bullet}{\mathcal{B}}{}^{\bullet}_{23}{}^{2} - \Delta_{\mathrm{gh},23}{}^{2}\right) = \frac{1}{40320}$$

$$\mathcal{M}_{41} = \int \mathrm{d}\tau_1 \int \mathrm{d}\tau_2 \int \mathrm{d}\tau_3\, \mathcal{B}_{12}\, \mathcal{B}_{13}\, \mathcal{B}^{\bullet}_{23}\, \overset{\bullet}{\mathcal{B}}_{23}\, \overset{\bullet}{\mathcal{B}}{}^{\bullet}_{23}\, \left(\overset{\bullet}{\mathcal{B}}{}^{\bullet} + \Delta_{\mathrm{gh}}\right)|_1 = \frac{13}{120960}$$

$$\mathcal{M}_{42} = \int \mathrm{d}\tau_1 \int \mathrm{d}\tau_2 \int \mathrm{d}\tau_3\, \mathcal{B}_{12}\, \mathcal{B}_{23}\, \mathcal{B}_{13}\, \left(\overset{\bullet}{\mathcal{B}}{}^{\bullet}_{12}\, \overset{\bullet}{\mathcal{B}}{}^{\bullet}_{23}\, \overset{\bullet}{\mathcal{B}}{}^{\bullet}_{13} + \Delta_{\mathrm{gh},12}\, \Delta_{\mathrm{gh},23}\, \Delta_{\mathrm{gh},13}\right) = \frac{143}{120960}$$

$$\mathcal{M}_{43} = \int \mathrm{d}\tau_1 \int \mathrm{d}\tau_2 \int \mathrm{d}\tau_3\, \mathcal{B}_{12}\, \mathcal{B}^{\bullet}_{13}\, \mathcal{B}^{\bullet}_{23}\, \overset{\bullet}{\mathcal{B}}_{23}{}^{2}\, \left(\overset{\bullet}{\mathcal{B}}{}^{\bullet} + \Delta_{\mathrm{gh}}\right)|_1 = -\frac{1}{6720}$$

$$\mathcal{M}_{44} = \int \mathrm{d}\tau_1 \int \mathrm{d}\tau_2 \int \mathrm{d}\tau_3\, \mathcal{B}|_1\, \mathcal{B}|_3\, \overset{\bullet}{\mathcal{B}}_{12}\, \mathcal{B}^{\bullet}_{23}\, \overset{\bullet}{\mathcal{B}}{}^{\bullet}_{12}\, \overset{\bullet}{\mathcal{B}}{}^{\bullet}_{23} = 0$$

$$\mathcal{M}_{45} = \int \mathrm{d}\tau_1 \int \mathrm{d}\tau_2 \int \mathrm{d}\tau_3\, \mathcal{B}|_1\, \overset{\bullet}{\mathcal{B}}_{12}\, \overset{\bullet}{\mathcal{B}}_{13}\, \mathcal{B}^{\bullet}_{23}\, \overset{\bullet}{\mathcal{B}}_{23}\, \overset{\bullet}{\mathcal{B}}{}^{\bullet}_{23} = -\frac{11}{17280}$$

$$\mathcal{M}_{46} = \int \mathrm{d}\tau_1 \int \mathrm{d}\tau_2 \int \mathrm{d}\tau_3\, \mathcal{B}|_1\, \overset{\bullet}{\mathcal{B}}_{12}\, \mathcal{B}_{23}\, \overset{\bullet}{\mathcal{B}}_{23}\, \overset{\bullet}{\mathcal{B}}{}^{\bullet}_{13}\, \overset{\bullet}{\mathcal{B}}{}^{\bullet}_{23} = -\frac{11}{17280}$$

$$\mathcal{M}_{47} = \int \mathrm{d}\tau_1 \int \mathrm{d}\tau_2 \int \mathrm{d}\tau_3\, \mathcal{B}|_1\, \overset{\bullet}{\mathcal{B}}_{12}\, \mathcal{B}^{\bullet}_{23}\, \overset{\bullet}{\mathcal{B}}_{23}{}^{2}\, \overset{\bullet}{\mathcal{B}}{}^{\bullet}_{13} = \frac{1}{960}$$

$$\mathcal{M}_{48} = \int \mathrm{d}\tau_1 \int \mathrm{d}\tau_2 \int \mathrm{d}\tau_3\, \mathcal{B}|_1\, \mathcal{B}_{23}\, \mathcal{B}^{\bullet}_{23}\, \overset{\bullet}{\mathcal{B}}_{23}\, \overset{\bullet}{\mathcal{B}}{}^{\bullet}_{12}\, \overset{\bullet}{\mathcal{B}}{}^{\bullet}_{13} = -\frac{11}{17280}$$

$$\mathcal{M}_{49} = \int \mathrm{d}\tau_1 \int \mathrm{d}\tau_2 \int \mathrm{d}\tau_3\, \mathcal{B}_{12}{}^{2}\, \overset{\bullet}{\mathcal{B}}_{13}\, \overset{\bullet}{\mathcal{B}}_{23}\, \overset{\bullet}{\mathcal{B}}{}^{\bullet}_{13}\, \overset{\bullet}{\mathcal{B}}{}^{\bullet}_{23} = \frac{1}{30240}$$

$$\mathcal{M}_{50} = \int \mathrm{d}\tau_1 \int \mathrm{d}\tau_2 \int \mathrm{d}\tau_3\, \mathcal{B}_{12}\, \mathcal{B}^{\bullet}_{12}\, \overset{\bullet}{\mathcal{B}}_{13}{}^{2}\, \mathcal{B}^{\bullet}_{23}\, \overset{\bullet}{\mathcal{B}}{}^{\bullet}_{23} = \frac{1}{30240}$$

$$\mathcal{M}_{51} = \int \mathrm{d}\tau_1 \int \mathrm{d}\tau_2 \int \mathrm{d}\tau_3\, \mathcal{B}_{12}\, \mathcal{B}^{\bullet}_{12}\, \overset{\bullet}{\mathcal{B}}_{13}\, \mathcal{B}_{23}\, \overset{\bullet}{\mathcal{B}}{}^{\bullet}_{13}\, \overset{\bullet}{\mathcal{B}}{}^{\bullet}_{23} = -\frac{79}{120960}$$

$$\mathcal{M}_{52} = \int \mathrm{d}\tau_1 \int \mathrm{d}\tau_2 \int \mathrm{d}\tau_3\, \mathcal{B}_{12}\, \mathcal{B}^{\bullet}_{12}\, \overset{\bullet}{\mathcal{B}}_{13}\, \overset{\bullet}{\mathcal{B}}_{23}\, \mathcal{B}^{\bullet}_{23}\, \overset{\bullet}{\mathcal{B}}{}^{\bullet}_{13} = -\frac{1}{30240}$$

$$\mathcal{M}_{53} = \int \mathrm{d}\tau_1 \int \mathrm{d}\tau_2 \int \mathrm{d}\tau_3\, \mathcal{B}_{12}\, \mathcal{B}_{13}\, \overset{\bullet}{\mathcal{B}}_{23}\, \mathcal{B}^{\bullet}_{23}\, \overset{\bullet}{\mathcal{B}}{}^{\bullet}_{12}\, \overset{\bullet}{\mathcal{B}}{}^{\bullet}_{13} = -\frac{19}{40320}$$

$$\mathcal{M}_{54} = \int \mathrm{d}\tau_1 \int \mathrm{d}\tau_2 \int \mathrm{d}\tau_3\, \mathcal{B}_{12}\, \mathcal{B}^{\bullet}_{13}\, \overset{\bullet}{\mathcal{B}}{}^{\bullet}_{12}\, \overset{\bullet}{\mathcal{B}}_{13}\, \mathcal{B}^{\bullet}_{23}\, \overset{\bullet}{\mathcal{B}}_{23} = \frac{11}{12096}$$

$$\mathcal{M}_{55} = \int \mathrm{d}\tau_1 \int \mathrm{d}\tau_2 \int \mathrm{d}\tau_3\, \mathcal{B}^{\bullet}_{12}{}^{2}\, \overset{\bullet}{\mathcal{B}}_{13}{}^{2}\, \mathcal{B}^{\bullet}_{23}{}^{2} = \frac{17}{20160}$$

$$\mathcal{M}_{56} = \int \mathrm{d}\tau_1 \int \mathrm{d}\tau_2 \int \mathrm{d}\tau_3\, \mathcal{B}^{\bullet}_{12}\, \mathcal{B}^{\bullet}_{13}\, \overset{\bullet}{\mathcal{B}}_{12}\, \overset{\bullet}{\mathcal{B}}_{13}\, \mathcal{B}^{\bullet}_{23}\, \overset{\bullet}{\mathcal{B}}_{23} = -\frac{17}{20160}$$

$$\mathcal{M}_{57} = \int \mathrm{d}\tau_1 \int \mathrm{d}\tau_2 \int \mathrm{d}\tau_3\, \mathcal{B}|_1\, \mathcal{B}|_2\, \mathcal{B}|_3 = -\frac{1}{1728}$$

$$\mathcal{M}_{58} = \int \mathrm{d}\tau_1 \int \mathrm{d}\tau_2 \int \mathrm{d}\tau_3\, \mathcal{B}|_1\, \mathcal{B}_{23}{}^{2} = -\frac{1}{8640}$$

$$\mathcal{M}_{59} = \int \mathrm{d}\tau_1 \int \mathrm{d}\tau_2 \int \mathrm{d}\tau_3\, \mathcal{B}_{12}\, \mathcal{B}_{23}\, \mathcal{B}_{13} = -\frac{1}{30240}$$

$$\mathcal{M}_{60} = \int \mathrm{d}\tau_1 \int \mathrm{d}\tau_2\, \mathcal{B}^2\, \mathcal{B}|_2\, \left(\overset{\bullet}{\mathcal{B}}{}^{\bullet} + \Delta_{\mathrm{gh}}\right)|_2 = -\frac{1}{8640}$$

$$\mathcal{M}_{61} = \int \mathrm{d}\tau_1 \int \mathrm{d}\tau_2\, \mathcal{B}^{\bullet 2}\, \mathcal{B}|_2 = \frac{1}{1728}$$

$$\mathcal{M}_{62} = \int \mathrm{d}\tau_1 \int \mathrm{d}\tau_2\, \mathcal{B}|_2\, \mathcal{B}^2 = -\frac{1}{8640}$$

$$\mathcal{M}_{63} = \int \mathrm{d}\tau_1 \int \mathrm{d}\tau_2\, \mathcal{B}|_1\, B|_2{}^{2} = -\frac{1}{1728}$$

$$\mathcal{M}_{64} = \int \mathrm{d}\tau_1 \int \mathrm{d}\tau_2\, \mathcal{B}|_1\, \mathcal{B}|_2\, \bullet\!\mathcal{B}^2 = \frac{1}{1728}$$
$$\mathcal{M}_{65} = \int \mathrm{d}\tau_1 \int \mathrm{d}\tau_2\, \mathcal{B}^2\, \mathcal{B}|_2\, (\bullet\!\mathcal{B}^\bullet + \Delta_{\mathrm{gh}})|_1 = -\frac{1}{8640}$$
$$\mathcal{M}_{66} = \int \mathrm{d}\tau_1 \int \mathrm{d}\tau_2 \int \mathrm{d}\tau_3\, \mathcal{B}|_1\, \bullet\!\mathcal{B}_{12}\, \bullet\!\mathcal{B}_{13}\, \mathcal{B}_{23} = \frac{1}{8640}$$
$$\mathcal{M}_{67} = \int \mathrm{d}\tau_1 \int \mathrm{d}\tau_2 \int \mathrm{d}\tau_3\, {\mathcal{B}_{12}}^2\, \bullet\!{\mathcal{B}_{13}}^2 = \frac{1}{8640}$$
$$\mathcal{M}_{68} = \int \mathrm{d}\tau_1 \int \mathrm{d}\tau_2 \int \mathrm{d}\tau_3\, \mathcal{B}_{12}\, \mathcal{B}_{23}\, \mathcal{B}_{13}\, \left(\bullet\!\mathcal{B}^\bullet + \Delta_{\mathrm{gh}}\right)|_1 = -\frac{1}{30240}$$
$$\mathcal{M}_{69} = \int \mathrm{d}\tau_1 \int \mathrm{d}\tau_2 \int \mathrm{d}\tau_3\, \mathcal{B}_{12}\, \mathcal{B}_{13}\, \bullet\!\mathcal{B}_{12}\, \bullet\!\mathcal{B}_{13} = 0$$
$$\mathcal{M}_{70} = \int \mathrm{d}\tau_1 \int \mathrm{d}\tau_2 \int \mathrm{d}\tau_3\, {\mathcal{B}_{13}}^2\, \bullet\!{\mathcal{B}_{12}}^2 = \frac{1}{8640}$$
$$\mathcal{M}_{71} = \int \mathrm{d}\tau_1 \int \mathrm{d}\tau_2 \int \mathrm{d}\tau_3\, \mathcal{B}|_1\, \mathcal{B}|_3\, \bullet\!{\mathcal{B}_{12}}^2 = \frac{1}{1728}$$
$$\mathcal{M}_{72} = \int \mathrm{d}\tau_1 \int \mathrm{d}\tau_2 \int \mathrm{d}\tau_3\, {\mathcal{B}_{12}}^2\, \mathcal{B}|_3\, (\bullet\!\mathcal{B}^\bullet + \Delta_{\mathrm{gh}})|_1 = -\frac{1}{8640}$$
$$\mathcal{M}_{73} = \int \mathrm{d}\tau_1 \int \mathrm{d}\tau_2 \int \mathrm{d}\tau_3\, {\mathcal{B}_{12}}^2\, \bullet\!{\mathcal{B}_{23}}^2\, (\bullet\!\mathcal{B}^\bullet + \Delta_{\mathrm{gh}})|_3 = \frac{1}{8640}$$
$$\mathcal{M}_{74} = \int \mathrm{d}\tau_1 \int \mathrm{d}\tau_2 \int \mathrm{d}\tau_3\, \mathcal{B}|_3\, {\mathcal{B}_{12}}^2 \left(\bullet\!{\mathcal{B}^\bullet_{23}}^2 - {\Delta_{\mathrm{gh},23}}^2\right) = \frac{1}{8640}$$
$$\mathcal{M}_{75} = \int \mathrm{d}\tau_1 \int \mathrm{d}\tau_2 \int \mathrm{d}\tau_3\, \mathcal{B}_{12}\, \mathcal{B}^\bullet_{12}\, \mathcal{B}_{23}\, \bullet\!\mathcal{B}_{23}\, (\bullet\!\mathcal{B}^\bullet + \Delta_{\mathrm{gh}})|_3 = 0$$
$$\mathcal{M}_{76} = \int \mathrm{d}\tau_1 \int \mathrm{d}\tau_2 \int \mathrm{d}\tau_3\, \mathcal{B}_{12}\, \mathcal{B}^\bullet_{12}\, \mathcal{B}^\bullet_{23}\, \bullet\!\mathcal{B}^\bullet_{23}\, \mathcal{B}|_3 = 0$$
$$\mathcal{M}_{77} = \int \mathrm{d}\tau_1 \int \mathrm{d}\tau_2 \int \mathrm{d}\tau_3\, \mathcal{B}_{12}\, \mathcal{B}_{23}\, \mathcal{B}_{13}\, (\bullet\!\mathcal{B}^\bullet + \Delta_{\mathrm{gh}})|_2\, (\bullet\!\mathcal{B}^\bullet + \Delta_{\mathrm{gh}})|_3 = -\frac{1}{30240}$$
$$\mathcal{M}_{78} = \int \mathrm{d}\tau_1 \int \mathrm{d}\tau_2 \int \mathrm{d}\tau_3\, \mathcal{B}_{12}\, \mathcal{B}_{23}\, \mathcal{B}_{13} \left(\bullet\!{\mathcal{B}^\bullet_{23}}^2 - {\Delta_{\mathrm{gh},23}}^2\right) = \frac{1}{40320}$$
$$\mathcal{M}_{79} = \int \mathrm{d}\tau_1 \int \mathrm{d}\tau_2 \int \mathrm{d}\tau_3\, \mathcal{B}_{12}\, \mathcal{B}_{13}\, \bullet\!\mathcal{B}_{23}\, \mathcal{B}^\bullet_{23}\, \bullet\!\mathcal{B}^\bullet_{23} = \frac{13}{120960}$$
$$\mathcal{M}_{80} = \int \mathrm{d}\tau_1 \int \mathrm{d}\tau_2 \int \mathrm{d}\tau_3\, \mathcal{B}_{12}\, \mathcal{B}^\bullet_{13}\, \mathcal{B}_{23}\, \bullet\!\mathcal{B}_{23}\, \bullet\!\mathcal{B}^\bullet_{23} = -\frac{1}{60480}$$
$$\mathcal{M}_{81} = \int \mathrm{d}\tau_1 \int \mathrm{d}\tau_2 \int \mathrm{d}\tau_3\, \mathcal{B}_{12}\, \mathcal{B}^\bullet_{13}\, \mathcal{B}^\bullet_{23}\, \mathcal{B}|_3\, (\bullet\!\mathcal{B}^\bullet + \Delta_{\mathrm{gh}})|_2 = \frac{1}{8640}$$
$$\mathcal{M}_{82} = \int \mathrm{d}\tau_1 \int \mathrm{d}\tau_2 \int \mathrm{d}\tau_3\, \mathcal{B}_{12}\, \mathcal{B}^\bullet_{13}\, \mathcal{B}^\bullet_{23}\, \bullet\!{\mathcal{B}_{23}}^2 = -\frac{1}{6720}$$
$$\mathcal{M}_{83} = \int \mathrm{d}\tau_1 \int \mathrm{d}\tau_2 \int \mathrm{d}\tau_3\, {\mathcal{B}^\bullet_{12}}^2\, {\mathcal{B}_{23}}^2\, (\bullet\!\mathcal{B}^\bullet + \Delta_{\mathrm{gh}})|_3 = \frac{1}{8640}$$
$$\mathcal{M}_{84} = \int \mathrm{d}\tau_1 \int \mathrm{d}\tau_2 \int \mathrm{d}\tau_3\, {\mathcal{B}^\bullet_{12}}^2\, {\mathcal{B}^\bullet_{23}}^2\, \mathcal{B}|_3 = -\frac{1}{1728}$$
$$\mathcal{M}_{85} = \int \mathrm{d}\tau_1 \int \mathrm{d}\tau_2 \int \mathrm{d}\tau_3\, \mathcal{B}|_2\, \mathcal{B}|_3\, \mathcal{B}^\bullet_{12}\, \mathcal{B}^\bullet_{13}\, \bullet\!\mathcal{B}^\bullet_{23} = -\frac{1}{1728}$$
$$\mathcal{M}_{86} = \int \mathrm{d}\tau_1 \int \mathrm{d}\tau_2 \int \mathrm{d}\tau_3\, {\mathcal{B}_{23}}^2\, \mathcal{B}^\bullet_{12}\, \mathcal{B}^\bullet_{13}\, \bullet\!\mathcal{B}^\bullet_{23} = -\frac{11}{20160}$$
$$\mathcal{M}_{87} = \int \mathrm{d}\tau_1 \int \mathrm{d}\tau_2 \int \mathrm{d}\tau_3\, \mathcal{B}^\bullet_{12}\, \mathcal{B}^\bullet_{13}\, \mathcal{B}_{23}\, \mathcal{B}^\bullet_{23}\, \bullet\!\mathcal{B}_{23} = \frac{11}{60480}.$$

This concludes this calculation of the trace anomaly in a maximally symmetric

space using string inspired propagators in dimensional regularization, a BRST gauge fixing of the worldline trajectories and Riemann normal coordinates. String inspired propagators turned out to be quite efficient also because of their translationally invariant nature, unlike the DBC ones. This implies that all diagrams involving equal time propagators with one derivative, are vanishing. This simplification is compensated by the introduction of further vertices, due to the non linear geodesic map, which we computed in closed form for MS spaces. The string inspired formalism can be considered a powerful tool to reduce complexity of standard Feynman diagrams computations, in QFT and string theory: an example is given by the systematic computation of graviton scattering amplitudes and gravitational effective actions.

In the next chapter we will see a direct comparison of calculations performed using mode and dimensional regularization: MR was used in [33] to evaluate the transition amplitude of a scalar particle moving in curved space and that result is taken as a test to confirm the validity of DR for the same problem.

Chapter 5

Dimensional regularization of the particle transition amplitude in curved spaces

As previously discussed, mode and dimensional regularization are two regularization schemes used to operationally compute worldline path integrals. In some cases, DR is preferable as its associated conterterm potential has a simpler (covariant) form (see eq. (3.58) and (3.66)). In this chapter we will compare MR and DR on the same physical problem which is the computation of the particle transition amplitude, proving the equivalence of the two methods [34], thus checking the validity of DR in such context. Actually, the MR calculation was already proven to be equivalent to the one involving time slicing [33]. To complete the picture, we will carry on the calculation with DR.

Here we focus on the dynamics of a non relativistic point-particle in a D-dimensional curved space where an arbitrary scalar potential is included. The associated minkowskian action then reads

$$S[x] = \int_0^t d\tau \left[\frac{1}{2} g_{\mu\nu}(x)\dot{x}^\mu \dot{x}^\nu - V(x)\right] \tag{5.1}$$

At the quantum level, the transition amplitude of such particle satisfies the Wick-rotated Schrödinger equation

$$-\partial_\beta K(x,x';\beta) = \left[-\frac{1}{2}\nabla^2 + V(x)\right] K(x,x';\beta) \tag{5.2}$$

where $\beta = it$ is the Wick-rotated Euclidean propagation time and x, x' are respectively the initial and final points of the propagation. The Euclidean action is actually

$$S[x] = \int_0^\beta d\tau \left[\frac{1}{2} g_{\mu\nu}(x)\dot{x}^\mu \dot{x}^\nu + V(x)\right]. \tag{5.3}$$

An approximated short time solution to (5.2) is given by the so -called heat-kernel expansion which reads

$$K(x,x';\beta)=\frac{1}{(2\pi\beta)^{\frac{D}{2}}}e^{-\frac{\sigma(x,x')}{\beta}}\sum_{n=0}^{\infty}a_n(x,x')\beta^n \tag{5.4}$$

in terms of the Seeley-De Witt coefficients and the Synge function $\sigma(x,x')$ (it measures half the geodesic distance between x and x'). On the other hand, a path integral approach to the transition amplitude provides

$$K(x,x';\beta)=\int DxDaDbDc\; e^{-\int_{-1}^{0}d\tau\left[\frac{1}{2\beta}g_{\mu\nu}(x)(\dot{x}^\mu\dot{x}^\nu+a^\mu a^\nu+b^\mu c^\nu)+\beta(V(x)+V_{\rm DR}(x))\right]} \tag{5.5}$$

where we already included ghost fields a,b,c as done in the previous calculation to account for the $\sqrt{g}$-factor characterizing path integrals' measure in curved space. Boundary conditions are $x^\mu(-1)=x^\mu$, $x^\mu(0)=x'^\mu$ and vanishing for the ghosts. Thus, in the present calculation, the path integral is performed on a line, as opposed to the previous chapter. To the best of our knowledge, this is the first generalization of DR to open line path integrals. In fact, so far DR was proposed and tested in the computation of QFT one-loop effective actions, *i.e.* with periodic boundary conditions. However, recent work on the study of classical black hole scattering [35, 36], and on the computation of scattering amplitudes with gravitons [37], make use of particle path integrals in curved space on the line. Thus, in order to make contact with such work, we considered helpful to extend DR to open line path integrals, and we achieve it by computing the short-time transition amplitude, at three loops, using RNC, which yields the heat kernel expansion at quadratic order in the propagating time. As in most cases, it is useful to adopt a quantum-background splitting of the path $x^\mu(\tau)$, namely

$$x^\mu(\tau)=x^\mu_{\rm bg}(\tau)+q^\mu(\tau),\quad x^\mu_{\rm bg}(\tau)=x'^\mu-\xi^\mu\tau,\quad \xi^\mu=x^\mu-x'^\mu \tag{5.6}$$

with DBC for the quantum fluctuations $q^\mu(\tau)$, together with Riemann normal coordinates z^μ, which allows us to express perturbatively the metric around the origin $x'^\mu|_{\rm RNC}=0$ as

$$\begin{aligned}g_{\mu\nu}(z)=\delta_{\mu\nu}&+\frac{1}{3}R_{\alpha\mu\nu\beta}(0)z^\alpha z^\beta+\frac{1}{6}\nabla_\gamma R_{\alpha\mu\nu\beta}(0)z^\alpha z^\beta z^\gamma+\\&+\left[\frac{1}{20}\nabla_\delta\nabla_\gamma R_{\alpha\mu\nu\beta}(0)+\frac{2}{45}R_{\alpha\mu\sigma\beta}R_{\gamma\nu}{}^{\sigma}{}_{\delta}(0)\right]z^\alpha z^\beta z^\gamma z^\delta+O(z^5).\end{aligned} \tag{5.7}$$

Here we stop the expansion at $o(z^4)$, since this is the needed order to obtain a three-loop (order β^2) amplitude.

As usual we find it convenient to split the action in (5.5) into a quadratic part

$$S_2[\xi;q,a,b,c] = \frac{1}{2\beta}\delta_{\mu\nu}\xi^\mu\xi\nu + \frac{1}{2\beta}\int_{-1}^{0} d\tau\ \delta_{\mu\nu}\left(\dot{q}^\mu\dot{q}^\nu + a^\mu a^\nu + b^\mu c^\nu\right) \tag{5.8}$$

producing propagators for the fields q, a, b, c and an interaction part

$$S_{\rm int}[\xi;q,a,b,c] = S_4 + S_5 + S_6 + \dots, \tag{5.9}$$

with

$$\begin{aligned}
S_4 &= \int_{-1}^{0} d\tau\ \frac{1}{6\beta}R_{\alpha\mu\nu\beta}(0)(-\xi^\alpha\tau + q^\alpha)(-\xi^\beta\tau + q^\beta)\big[(-\xi^\mu + \dot{q}^\mu)(-\xi^\nu + \dot{q}^\nu) + \\
&\quad + a^\mu a^\nu + b^\mu c^\nu\big] + \beta\tilde{V}(0), \\
S_5 &= \int_{-1}^{0} d\tau\ \frac{1}{12\beta}\nabla_\gamma R_{\alpha\mu\nu\beta}(0)(-\xi^\alpha\tau + q^\alpha)(-\xi^\beta\tau + q^\beta)(-\xi^\gamma\tau + q^\gamma)\times \\
&\quad \times\left[(-\xi^\mu + \dot{q}^\mu)(-\xi^\nu + \dot{q}^\nu) + a^\mu a^\nu + b^\mu c^\nu\right] + \beta\int_{-1}^{0} d\tau\ \partial_\alpha\tilde{V}(0)(-\xi^\alpha\tau + q^\alpha) \\
S_6 &= \int_{-1}^{0} d\tau\left(\frac{1}{40\beta}\nabla_\delta\nabla_\gamma R_{\alpha\mu\nu\beta}(0) + \frac{1}{45\beta}R_{\alpha\mu\sigma\beta}R_{\gamma\nu}{}^{\sigma}{}_{\delta}(0)\right)\times \\
&\quad \times(-\xi^\alpha\tau + q^\alpha)(-\xi^\beta\tau + q^\beta)(-\xi^\gamma\tau + q^\gamma)(-\xi^\delta\tau + q^\delta)\times \\
&\quad \times\left[(-\xi^\mu + \dot{q}^\mu)(-\xi^\nu + \dot{q}^\nu) + a^\mu a^\nu + b^\mu c^\nu\right] + \\
&\quad + \int_{-1}^{0} d\tau\ \frac{\beta}{2}\partial_\alpha\partial_\beta\tilde{V}(0)(-\xi^\alpha\tau + q^\alpha)(-\xi^\beta\tau + q^\beta)
\end{aligned} \tag{5.10}$$

and $\tilde{V} = V + V_{\rm DR}$. Propagators for the quantum fields read

$$\begin{aligned}
\langle q^\mu(\tau)q^\nu(\sigma)\rangle &= -\beta\delta^{\mu\nu}\Delta(\tau,\sigma) \\
\langle a^\mu(\tau)a^\nu(\sigma)\rangle &= \beta\delta^{\mu\nu}\Delta_{\rm gh}(\tau,\sigma) \\
\langle b^\mu(\tau)c^\nu(\sigma)\rangle &= -2\beta\delta^{\mu\nu}\Delta_{\rm gh}(\tau,\sigma)
\end{aligned} \tag{5.11}$$

with

$$\begin{aligned}
\Delta(\tau,\sigma) &= \tau(\sigma+1)\theta(\tau-\sigma) + \sigma(\tau+1)\theta(\sigma-\tau) \\
{}^\bullet\Delta(\tau,\sigma) &= \sigma + \theta(\tau-\sigma) \\
\Delta^\bullet(\tau,\sigma) &= \tau + \theta(\sigma-\tau)
\end{aligned}$$

$$
\begin{aligned}
{}^{\bullet\bullet}\Delta(\tau,\sigma) &= \Delta_{\rm gh}(\tau,\sigma) = \delta(\tau,\sigma)\\
\Delta|_\tau &= \tau(\tau+1)\\
{}^{\bullet}\Delta|_\tau &= \tau+\frac{1}{2}
\end{aligned}
\tag{5.12}
$$

Dots on the left (right) refer to derivatives taken with respect to the first (second) variable. Taking into account the free path integral normalization

$$
\int_{q(-1)=0}^{q(0)=0} DqDaDbDc\; e^{-\int_{-1}^{0} d\tau\; \frac{1}{2\beta}\delta_{\mu\nu}(\dot q^\mu \dot q^\nu + a^\mu a^\nu + b^\mu c^\nu)} = \frac{1}{(2\pi\beta)^{\frac{D}{2}}},
\tag{5.13}
$$

the transition amplitude can be written as

$$
\begin{aligned}
K(x,x';\beta) &= \frac{e^{-\frac{1}{2\beta}\delta_{\mu\nu}\xi^\mu\xi^\nu}}{(2\pi\beta)^{\frac{D}{2}}}\left\langle e^{-S_{\rm int}}\right\rangle \\
&= \frac{e^{-\frac{1}{2\beta}\delta_{\mu\nu}\xi^\mu\xi^\nu}}{(2\pi\beta)^{\frac{D}{2}}} e^{-(\langle S_4\rangle+\langle S_5\rangle+\langle S_6\rangle)-\frac{1}{2}\left\langle {S_4}^2\right\rangle_{\rm conn}+\dots} \qquad (5.14)\\
&= \frac{e^{-\frac{1}{2\beta}\delta_{\mu\nu}\xi^\mu\xi^\nu}}{(2\pi\beta)^{\frac{D}{2}}}\left[1-(\langle S_4\rangle+\langle S_5\rangle+\langle S_6\rangle)+\frac{1}{2}\left\langle {S_4}^2\right\rangle_{\rm conn}+\dots\right]. \qquad (5.15)
\end{aligned}
$$

Vertices are given by

$$
\begin{aligned}
\langle S_4\rangle &= -\frac{1}{6}R_{\alpha\beta}\xi^\alpha\xi^\beta I_1+\frac{\beta}{6}RI_2+\beta\tilde V\\
\langle S_5\rangle &= \frac{1}{12}\nabla_\gamma R_{\alpha\beta}\xi^\alpha\xi^\beta\xi^\gamma I_3-\frac{\beta}{6}\nabla_\alpha R\xi^\alpha I_4+\frac{\beta}{2}\nabla_\alpha\tilde V\xi^\alpha\\
\langle S_6\rangle &= -\left(\frac{1}{40}\nabla_\delta\nabla_\gamma R_{\alpha\beta}+\frac{1}{45}R_{\alpha\lambda\sigma\beta}R_\gamma{}^{\lambda\sigma}{}_\delta\right)\xi^\alpha\xi^\beta\xi^\gamma\xi^\delta I_5+\\
&\quad+\left(\frac{\beta}{40}\nabla^2R_{\alpha\beta}+\frac{\beta}{20}\nabla^\lambda\nabla^\sigma R_{\alpha\lambda\sigma\beta}+\frac{\beta}{45}R_{\alpha\lambda}R_\beta{}^\lambda+\frac{\beta}{30}R_{\alpha\lambda\sigma\rho}R_\beta{}^{\lambda\sigma\rho}\right)\xi^\alpha\xi^\beta I_6+\\
&\quad+\Big(\frac{\beta}{20}\nabla_\alpha\nabla_\beta R+\frac{2\beta}{45}R_{\alpha\lambda\sigma\beta}R^{\lambda\sigma}+\frac{\beta}{20}\nabla^\lambda\nabla_\alpha R_{\beta\lambda}+\\
&\quad-\frac{\beta}{20}\nabla^\lambda\nabla^\sigma R_{\alpha\lambda\sigma\beta}-\frac{\beta}{45}R_{\alpha\lambda}R_\beta{}^\lambda+\frac{\beta}{30}R_{\alpha\lambda\sigma\rho}R_\beta{}^{\lambda\sigma\rho}\Big)\xi^\alpha\xi^\beta I_7+\\
&\quad-\left(\frac{\beta^2}{20}\nabla^2R+\frac{\beta^2}{45}R_{\lambda\sigma}^2+\frac{\beta^2}{30}R_{\lambda\sigma\rho\tau}^2\right)I_8-\frac{\beta^2}{2}\nabla^2\tilde V I_9+\frac{\beta}{6}\nabla_\alpha\nabla_\beta\tilde V\xi^\alpha\xi^\beta\\
\left\langle {S_4}^2\right\rangle_{\rm conn} &= \frac{1}{36}R_{\alpha\lambda\sigma\beta}R_\gamma{}^{\lambda\sigma}{}_\delta\xi^\alpha\xi^\beta\xi^\gamma\xi^\delta I_{10}-\frac{\beta}{9}R_{\alpha\lambda}R_\beta{}^\lambda\xi^\alpha\xi^\beta I_{11}-\frac{\beta}{9}R_{\alpha\lambda\sigma\beta}R^{\lambda\sigma}\xi^\alpha\xi^\beta I_{12}+\\
&\quad-\frac{\beta}{6}R_{\alpha\lambda\rho\sigma}R_\beta{}^{\lambda\sigma\rho}\xi^\alpha\xi^\beta I_{13}+\frac{\beta^2}{12}R_{\lambda\sigma}^2I_{14}+\frac{\beta^2}{12}R_{\lambda\sigma\rho\xi}^2I_{15}
\end{aligned}
\tag{5.16}
$$

in terms of the worldline integrals I_i, $i=1,\dots,15$ computed using dimensional regularization. To be precise, we are adding D extra infinite dimensions to the compact worldline direction $-1\le\tau\le 0$ so to have $\tau\to t^a=(\tau,\mathbf{t})$, with $\mathbf{t}=(t^1,\dots,t^D)$.

The kinetic action for the q-fields is then

$$S_2[q] = \frac{1}{2\beta}\int d^{D+1}t\ \delta_{\mu\nu}\partial_a q^\mu \partial_a q^\nu \tag{5.17}$$

with $\partial_a = \frac{\partial}{\partial t^a}$. We apply this new derivative notation to Δ-functions as follows,

$$\begin{aligned}
\frac{\partial}{\partial t^a}\Delta(t,s) &= {}_a\Delta(t,s)\\
\frac{\partial}{\partial s^a}\Delta(t,s) &= \Delta_a(t,s)\\
\frac{\partial^2}{\partial t^a \partial s^b}\Delta(t,s) &= {}_a\Delta_b(t,s)\\
\partial_a\partial_a\Delta(t,s) &= {}_{aa}\Delta(t,s) = \Delta_{\rm gh}(t,s) = \delta(\tau,\sigma)\delta^D(\mathbf{t}-\mathbf{s})
\end{aligned} \tag{5.18}$$

where, in momentum space,

$$\Delta(t,s) = \int \frac{d^Dk}{(2\pi)^D}\sum_{n=1}^{\infty}\frac{-2}{(\pi n)^2+\mathbf{k}^D}\sin(\pi n\tau)\sin(\pi n\sigma)e^{i\mathbf{k}\cdot(\mathbf{t}-\mathbf{s})}. \tag{5.19}$$

We point out the property

$$({}_a\Delta_a + {}_{aa}\Delta)|_t = {}_0({}_0\Delta|_t) = {}^\bullet({}^\bullet\Delta|_t), \tag{5.20}$$

well analyzed in [30]. It will be important for the computation of the integrals I_i. We also notice that, since the extra dimensions are infinite and translationally invariant, we keep the same background of the compact interval, that is

$$\begin{aligned}
x^\mu(t) &= -\xi^\mu\tau + q^\mu(t)\\
\partial_a x^\mu(t) &= -\xi^\mu\delta^0_a + \partial_a q^\mu(t).
\end{aligned} \tag{5.21}$$

The main advantage of using DR (besides the covariant counterterm potential $V_{\rm DR}$) is the use of integrations by part (i.b.p.) within worldline integrals I_i. I.b.p.'s are guaranteed for the extra dimensions due to Poincaré invariance, whereas on the compact dimension, more attention is needed: the propagator $\Delta(t,s)$ vanishes at the endpoints of the compact direction for both τ and σ, so its presence in the integrand guarantees that no boundary terms pop out from i.b.p. However, single dotted propagators ${}^\bullet\Delta(t,s)$, $\Delta^\bullet(t,s)$ only vanish at the boundary of the compact interval of the variable not used in the derivation. When $t=s$, the regulated time derivative vanishes at the endpoints, whereas the unregulated one is discontinuous there. Moreover, the last property of

the group (5.18) can be safely used at the regulated level. Relying on all the previous properties and considerations, we show the list of the I_i worldline integrals used in the expression of the transition amplitude (5.15).

$$I_1 = \int_{-1}^{0} d\tau \left[\tau^2 \left({}^{\bullet}\Delta^{\bullet} + {}^{\bullet\bullet}\Delta\right) + \Delta - 2\tau {}^{\bullet}\Delta\right] |_{\tau} \rightarrow$$
$$\rightarrow \int dt \left[\tau^2 \left({}_a\Delta_a + {}_{aa}\Delta\right) + \Delta - 2\tau_a \Delta\right] |_t = -\frac{1}{2} \tag{5.22}$$
$$I_2 = \int_{-1}^{0} d\tau \left[\Delta \left({}^{\bullet}\Delta^{\bullet} + {}^{\bullet\bullet}\Delta\right) - \left({}^{\bullet}\Delta\right)^2\right] |_{\tau} \rightarrow$$
$$\rightarrow \int dt \left[\Delta \left({}_a\Delta_a + {}_{aa}\Delta\right) - \left({}_a\Delta\right)^2\right] |_t = -\frac{1}{4} \tag{5.23}$$
$$I_3 = \int_{-1}^{0} d\tau \left[\tau^3 \left({}^{\bullet}\Delta^{\bullet} + {}^{\bullet\bullet}\Delta\right) + \tau\Delta - 2\tau^2 {}^{\bullet}\Delta\right] |_{\tau} \rightarrow$$
$$\rightarrow \int dt \left[\tau^3 \left({}_a\Delta_a + {}_{aa}\Delta\right) + \tau\Delta - 2\tau^2 {}_a\Delta\right] |_t = \frac{1}{2} \tag{5.24}$$
$$I_4 = \int_{-1}^{0} d\tau \left[\tau\Delta \left({}^{\bullet}\Delta^{\bullet} + {}^{\bullet\bullet}\Delta\right) - \tau\left({}^{\bullet}\Delta\right)^2\right] |_{\tau} \rightarrow$$
$$\rightarrow \int dt \left[\tau\Delta \left({}_a\Delta_a + {}_{aa}\Delta\right) - \tau\left({}_a\Delta\right)^2\right] |_t = \frac{1}{8} \tag{5.25}$$
$$I_5 = \int_{-1}^{0} d\tau \left[\tau^4 \left({}^{\bullet}\Delta^{\bullet} + {}^{\bullet\bullet}\Delta\right) + \tau^2\Delta - 2\tau^3 {}^{\bullet}\Delta\right] |_{\tau} \rightarrow$$
$$\rightarrow \int dt \left[\tau^4 \left({}_a\Delta_a + {}_{aa}\Delta\right) + \tau^2\Delta - 2\tau^3 {}_a\Delta\right] |_t = -\frac{1}{2} \tag{5.26}$$
$$I_6 = \int_{-1}^{0} d\tau \left[\tau^2\Delta \left({}^{\bullet}\Delta^{\bullet} + {}^{\bullet\bullet}\Delta\right) + \Delta^2 - 2\tau {}^{\bullet}\Delta\Delta\right] |_{\tau} \rightarrow$$
$$\rightarrow \int dt \left[\tau^2\Delta \left({}_a\Delta_a + {}_{aa}\Delta\right) + \Delta^2 - 2\tau_a\Delta\Delta\right] |_t = 0 \tag{5.27}$$
$$I_7 = \int_{-1}^{0} d\tau \left[\tau^2\Delta \left({}^{\bullet}\Delta^{\bullet} + {}^{\bullet\bullet}\Delta\right) - \tau^2\left({}^{\bullet}\Delta\right)^2\right] |_{\tau} \rightarrow$$
$$\rightarrow \int dt \left[\tau^2\Delta \left({}_a\Delta_a + {}_{aa}\Delta\right) - \tau^2\left({}_a\Delta\right)^2\right] |_t = -\frac{1}{12} \tag{5.28}$$
$$I_8 = \int_{-1}^{0} d\tau \left[\Delta^2 \left({}^{\bullet}\Delta^{\bullet} + {}^{\bullet\bullet}\Delta\right) - \left({}^{\bullet}\Delta\right)^2\Delta\right] |_{\tau} \rightarrow$$
$$\rightarrow \int dt \left[\Delta^2 \left({}_a\Delta_a + {}_{aa}\Delta\right) - \left({}_a\Delta\right)^2\Delta\right] |_t = \frac{1}{24} \tag{5.29}$$
$$I_9 = \int_{-1}^{0} d\tau\Delta|_{\tau} = -\frac{1}{6} \tag{5.30}$$
$$I_{10} = \int_{-1}^{0} d\tau \int_{-1}^{0} d\sigma \Big[2\tau^2 \left({}^{\bullet}\Delta^{\bullet}\,{}^{\bullet}\Delta^{\bullet} - {}^{\bullet\bullet}\Delta\Delta^{\bullet\bullet}\right)\sigma^2 + 4\tau^2\left({}^{\bullet}\Delta\right)^2 +$$
$$- 8\tau^2 {}^{\bullet}\Delta\,{}^{\bullet}\Delta^{\bullet}\sigma + 2\Delta^2 - 8\Delta\Delta^{\bullet}\sigma + 4\tau\Delta\,{}^{\bullet}\Delta^{\bullet}\sigma + 4\tau^{\bullet}\Delta\Delta^{\bullet}\sigma\Big] \rightarrow$$
$$\rightarrow \int dt \int ds \Big[2\tau^2 \left({}_a\Delta_b\,{}_a\Delta_b - {}_{aa}\Delta\Delta_{bb}\right)\sigma^2 + 4\tau^2\left({}_a\Delta\right)^2 +$$
$$- 8\tau^2 {}_a\Delta\,{}_a\Delta_b\sigma + 2\Delta^2 - 8\Delta\Delta_b\sigma + 4\tau\Delta\,{}_a\Delta_b\sigma + 4\tau_a\Delta\Delta_b\sigma\Big] = 1 \tag{5.31}$$
$$I_{11} = \int_{-1}^{0} d\tau \int_{-1}^{0} d\sigma \Big[\tau\left({}^{\bullet}\Delta^{\bullet} + {}^{\bullet\bullet}\Delta\right)|_{\tau}\Delta\left({}^{\bullet}\Delta^{\bullet} + {}^{\bullet\bullet}\Delta\right)|_{\sigma}\sigma + \tau\Delta^{\bullet}|_{\tau}\,{}^{\bullet}\Delta^{\bullet}\,\Delta^{\bullet}|_{\sigma}\sigma +$$

$$
\begin{aligned}
&- 2\tau({}^{\bullet}\Delta^{\bullet} + {}^{\bullet\bullet}\Delta)|_{\tau}\Delta^{\bullet}\ \Delta^{\bullet}|_{\sigma}\sigma + \Delta|_{\tau}\ {}^{\bullet}\Delta^{\bullet}\ \Delta|_{\sigma} + \Delta^{\bullet}|_{\tau}\Delta\Delta^{\bullet}|_{\sigma} - 2\Delta|_{\tau}\ {}^{\bullet}\Delta\Delta^{\bullet}|_{\sigma} + \\
&+ 2\tau({}^{\bullet}\Delta^{\bullet} + {}^{\bullet\bullet}\Delta)|_{\tau}\Delta^{\bullet}\ \Delta|_{\sigma} + 2\tau\Delta^{\bullet}|_{\tau}\ {}^{\bullet}\Delta\Delta^{\bullet}|_{\sigma} + \\
&- 2\tau({}^{\bullet}\Delta^{\bullet} + {}^{\bullet\bullet}\Delta)|_{\tau}\Delta\Delta^{\bullet}|_{\sigma} - 2\tau\Delta^{\bullet}|_{\tau}\ {}^{\bullet}\Delta^{\bullet}\ \Delta|_{\sigma}\sigma\Big] \to \\
&\to \int dt \int ds\Big[\tau({}_{a}\Delta_{b} + {}_{aa}\Delta)|_{t}\Delta({}_{a}\Delta_{b} + {}_{aa}\Delta)|_{s}\sigma + \tau\Delta_{b}|_{t}\ {}_{a}\Delta_{b}\ \Delta_{b}|_{s}\sigma + \\
&- 2\tau({}_{a}\Delta_{b} + {}_{aa}\Delta)|_{t}\Delta_{b}\ \Delta_{b}|_{s}\sigma + \Delta|_{t}\ {}_{a}\Delta_{b}\ \Delta|_{s} + \Delta_{b}|_{t}\Delta\Delta_{b}|_{s} - 2\Delta|_{t}\ {}_{a}\Delta\Delta_{b}|_{s} + \\
&+ 2\tau({}_{a}\Delta_{b} + {}_{aa}\Delta)|_{t}\Delta_{b}\ \Delta|_{s} + 2\tau\Delta_{b}|_{t}\ {}_{a}\Delta\Delta_{b}|_{s} + \\
&- 2\tau({}_{a}\Delta_{b} + {}_{aa}\Delta)|_{t}\Delta\Delta_{b}|_{s} - 2\tau\Delta_{b}|_{t}\ {}_{a}\Delta_{b}\ \Delta|_{s}\sigma\Big] = -\frac{1}{12}
\end{aligned}
\tag{5.32}
$$

$$
\begin{aligned}
I_{12} = &\int_{-1}^{0} d\tau \int_{-1}^{0} d\sigma\Big[\tau^{2}\Delta|_{\sigma}\,({}^{\bullet}\Delta^{\bullet}\ {}^{\bullet}\Delta^{\bullet} - {}^{\bullet\bullet}\Delta\Delta^{\bullet\bullet}) + (\Delta^{\bullet})^{2}\Delta|_{\sigma} + \\
&- 2\tau\Delta^{\bullet}\ {}^{\bullet}\Delta^{\bullet}\ \Delta|_{\sigma} + \tau^{2}({}^{\bullet}\Delta)^{2} + \Delta^{2} - 2\tau\Delta\ {}^{\bullet}\Delta - 2\tau^{2}{}^{\bullet}\Delta\ {}^{\bullet}\Delta^{\bullet}\ \Delta^{\bullet}|_{\sigma} + \\
&- 2\Delta\Delta^{\bullet}\ \Delta^{\bullet}|_{\sigma} + 2\tau\Delta\ {}^{\bullet}\Delta^{\bullet}\ \Delta^{\bullet}|_{\sigma} + 2\tau^{\bullet}\Delta\Delta^{\bullet}\ \Delta^{\bullet}|_{\sigma}\Big] \to \\
&\to \int dt \int ds\Big[\tau^{2}\Delta|_{s}\,({}_{a}\Delta_{b}\ {}_{a}\Delta_{b} - {}_{aa}\Delta\Delta_{bb}) + (\Delta_{b})^{2}\Delta|_{s} + \\
&- 2\tau\Delta_{b}\ {}_{a}\Delta_{b}\ \Delta|_{s} + \tau^{2}({}_{a}\Delta)^{2} + \Delta^{2} - 2\tau\Delta\ {}_{a}\Delta - 2\tau^{2}{}_{a}\Delta\ {}_{a}\Delta_{b}\ \Delta_{b}|_{s} + \\
&- 2\Delta\Delta_{b}\ \Delta_{b}|_{s} + 2\tau\Delta\ {}_{a}\Delta_{b}\ \Delta_{b}|_{s} + 2\tau_{a}\Delta\Delta_{b}\ \Delta_{b}|_{s}\Big] = \frac{1}{6}
\end{aligned}
\tag{5.33}
$$

$$
\begin{aligned}
I_{13} = &\int_{-1}^{0} d\tau \int_{-1}^{0} d\sigma\Big[\tau\sigma\Delta\,({}^{\bullet}\Delta^{\bullet}\ {}^{\bullet}\Delta^{\bullet} - {}^{\bullet\bullet}\Delta\Delta^{\bullet\bullet}) - \tau\sigma^{\bullet}\Delta\Delta^{\bullet}\ {}^{\bullet}\Delta^{\bullet} + \\
&+ \Delta^{2}\ {}^{\bullet}\Delta^{\bullet} - \Delta\ {}^{\bullet}\Delta\Delta^{\bullet} + 2\tau\Delta^{\bullet}\ ({}^{\bullet}\Delta)^{2} - 2\tau\Delta\ {}^{\bullet}\Delta\ {}^{\bullet}\Delta^{\bullet}\Big] \to \\
&\to \int dt \int ds\Big[\tau\sigma\Delta\,({}_{a}\Delta_{b}\ {}_{a}\Delta_{b} - {}_{aa}\Delta\Delta_{bb}) - \tau\sigma_{a}\Delta\Delta_{b}\ {}_{a}\Delta_{b} + \\
&+ \Delta^{2}\ {}_{a}\Delta_{b} - \Delta\ {}_{a}\Delta\Delta_{b} + 2\tau\Delta_{b}\ ({}_{a}\Delta)^{2} - 2\tau\Delta\ {}_{a}\Delta\ {}_{a}\Delta_{b}\Big] = 0
\end{aligned}
\tag{5.34}
$$

$$
\begin{aligned}
I_{14} = &\int_{-1}^{0} d\tau \int_{-1}^{0} d\sigma\Big[\Delta|_{\tau}\Delta|_{\sigma}\,({}^{\bullet}\Delta^{\bullet}\ {}^{\bullet}\Delta^{\bullet} - {}^{\bullet\bullet}\Delta\Delta^{\bullet\bullet}) + \\
&- 4\Delta|_{\tau}\ {}^{\bullet}\Delta^{\bullet}\ {}^{\bullet}\Delta\Delta^{\bullet}|_{\sigma} + 2\Delta|_{\tau}\ ({}^{\bullet}\Delta)^{2} + 2\Delta^{\bullet}|_{\tau}\Delta\ {}^{\bullet}\Delta^{\bullet}\ \Delta^{\bullet}|_{\sigma} + \\
&+ 2\Delta^{\bullet}|_{\tau}\ {}^{\bullet}\Delta\Delta^{\bullet}\ \Delta^{\bullet}|_{\sigma} - 4\Delta^{\bullet}|_{\tau}\Delta\ {}^{\bullet}\Delta + \Delta^{2}\Big] \to \\
&\to \int dt \int ds\Big[\Delta|_{t}\Delta|_{s}\,({}_{a}\Delta_{b}\ {}_{a}\Delta_{b} - {}_{aa}\Delta\Delta_{bb}) + \\
&- 4\Delta|_{t}\ {}_{a}\Delta_{b}\ {}_{a}\Delta\Delta_{b}|_{s} + 2\Delta|_{t}\ ({}_{a}\Delta)^{2} + 2\Delta_{b}|_{t}\Delta\ {}_{a}\Delta_{b}\ \Delta_{b}|_{s} + \\
&+ 2\Delta_{b}|_{t}\ {}_{a}\Delta\Delta_{b}\ \Delta_{b}|_{s} - 4\Delta_{b}|_{t}\Delta\ {}_{a}\Delta + \Delta^{2}\Big] = -\frac{1}{12}
\end{aligned}
\tag{5.35}
$$

$$
\begin{aligned}
I_{15} = &\int_{-1}^{0} d\tau \int_{-1}^{0} d\sigma\Big[\Delta^{2}\,({}^{\bullet}\Delta^{\bullet}\ {}^{\bullet}\Delta^{\bullet} - {}^{\bullet\bullet}\Delta\Delta^{\bullet\bullet}) + ({}^{\bullet}\Delta)^{2}(\Delta^{\bullet})^{2} - 2\Delta\ {}^{\bullet}\Delta\Delta^{\bullet}\ {}^{\bullet}\Delta^{\bullet}\Big] \to \\
&\to \int dt \int ds\Big[\Delta^{2}\,({}_{a}\Delta_{b}\ {}_{a}\Delta_{b} - {}_{aa}\Delta\Delta_{bb}) + ({}_{a}\Delta)^{2}(\Delta_{b})^{2} - 2\Delta\ {}_{a}\Delta\Delta_{b}\ {}_{a}\Delta_{b}\Big] = 0.
\end{aligned}
\tag{5.36}
$$

The arrow means the passage from the unregulated compact time interval to the regulated $D+1$-dimensional one.

Putting things together, it is possible to reconstruct the transition amplitude (5.15) in the DR scheme and notice that the result is the same as the MR one obtained in [33].

This calculation shows how dimensional regularization can be easily used to compute path integrals on the line, that is with open boundary conditions. We stress that one of the main advantages of using this regularization scheme is the simplicity of the associated counterterm, which is covariant. This method is an optimal candidate to obtain master formulas with an arbitrary number of graviton insertions, for instance. However, one of the main complications for such application, comes from the fact that the particle coordinates are coupled to the curved metric in a generic non linear way. Moreover, the scalar potential may involve couplings to the scalar curvature which is renormalized by a counterterm $\tilde{V} = (\alpha + \frac{1}{8})R$. Hence, graviton vertex operators get more and more complicated as the number of gravitons grows. Anyway, a particularly simple case occurs when the scalar potential compensates the counterterm, that is $\alpha = -\frac{1}{8}$, producing a linear coupling to gravity and making this method quite helpful.

Here we conclude our analytical studies of particle path integrals in curved space, and from the next chapter on we will focus on numerical methods to evaluate such quantities, firstly in flat space— whose theory is pretty well known— to get familiar with the techniques, and then in curved space, where we present our new idea to estimate worldline path integral on a non trivial (curved) background.

Chapter 6

A numerical approach to σ-models: Worldline Monte Carlo

6.1 Introduction

Given the established relations between classes of QFT observables and particle path integrals, it is natural to explore methods which can provide results beyond perturbation theory. These methods rely upon numerical approaches rather than (only) analytical ones. In particular, due to their quantum mechanical direct analogy, σ-models are particularly suitable for numerical interpretation when expressed in terms of point-particle path integrals. The idea at the basis of this construction is actually very intuitive and dates back to the Feynman's original quantum mechanical path integral representation of particle propagation [5]. In this perspective, a point-particle travelling through spacetime from an initial point x_A to a final point x_B actually moves simultaneously along any possible allowed paths joining x_A and x_B with a probability amplitude distribution assigned to each (quantum) trajectory, which is specifically weighed according to how such path deviates from the classical one (the geodesic linking x_A and x_B). In order to translate this idea to the numerical realm, one has to simulate the spacetime trajectories as discrete collections of points on top of which the action for a scalar particle is computed. The main issue, however, is the generation of these numerical trajectories. In 2001, Gies and Langfeld [38] proposed a first algorithm relying on a weighed Monte Carlo sampling of the paths as an improvement of a previous work by Nieuwenhuis and Tjon [39]. Monte Carlo[1] is a widespread method to provide numerical estimates of mathematical quantities which has found more and

[1] This name is due to N. C. Metropolis and refers to the well-known casino.

more approval through recent years. Its actual formalization dates back to the forties by E. Fermi, J. von Neumann and S. M. Ulam in the context of the Manhattan Project. This method relies on the use of random variables which are selected according to some convenient probability distribution. A famous example of application of the Monte Carlo idea is the estimate of the π-value: if we assume to know the relation between π and the area of a circle of radius 1, we can randomly extract couples (x, y) such that $0 < x < 1$ and $0 < y < 1$ and take note of those couples for which $x^2 + y^2 \leq 1$, *i.e.* they lay inside a sector of the circle. All other points are outside the sector and inside a square of side 1. Since the area of the sector is $\pi/4$ and that of the square is 1, a ratio between the number of couples for which $x^2 + y^2 \leq 1$ and the total number of draws provides an estimate of $\pi/4$ (see Figure 6.1). As we can imagine, the

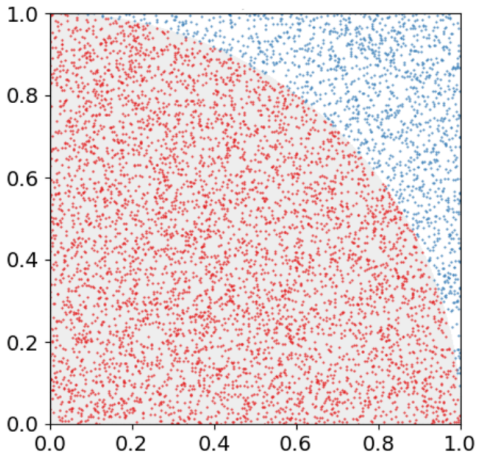

FIGURE 6.1: An estimate of $\pi/4$ can be performed by counting the number N_π points for which $x^2 + y^2 \leq 1$ (red points), compared to the total number N of draws (red and blue points). Hence, as $N \to \infty$, $\frac{N_\pi}{N} \to \frac{\pi}{4}$. Image from Wikipedia.

larger the sample of draws, the more accurate the estimate. Other applications span a lot of fields, from statistical physics, computational biology and computer graphics, to artificial intelligence, finance and the study of climate change [40].

Here, we want to apply the Monte Carlo idea to the worldline realm of theoretical physics: this combination goes under the name of Worldline Monte Carlo (WLMC) method, and it has then been used for several QFT applications, such as the Casimir effect [41, 42], Schwinger pair production in inhomogeneous fields [43], quantum effective actions [44] and strongly coupled large-N fermion models [45]. The sampling routine for the worldlines has also been improved through the years and has been

inspiration for other algorithms. The most popular ones are the *VLOOPS* [41], the *DLOOPS* [44], the *YLOOPS* and *LSOL* [46]. All the above algorithms model the worldline sampling according to the Brownian motion of the scalar particle, hence considering only the kinetic contribution to the action at this stage. The potential contribution is then evaluated once all worldline are produced, and determines the final result for the particle propagation. One of the main goals of this thesis is to use the WLMC machinery to numerically explore the realm of curved spacetime calculations, relying on the algorithm previously introduced. No routine has ever been proposed to directly sample trajectories on a curved manifold, however, with some shrewdness, we will show that the flat space construction can be suitable also for curved space problems [47].

6.2 Worldline Monte Carlo in flat space

To become familiar with the WLMC formalism, first it is useful to review how this method works on simple flat space models in order to better understand how it can be extended to more involved curved space problems. Let us consider a D-dimensional heat kernel for a scalar particle moving from x to x' in an Euclidean flat space and subjected to a potential $V(x)$. Its path integral representation is

$$I(x,x';\beta) = \int_{x(0)=x}^{x(\beta)=x'} Dx\, e^{-S[x]} \tag{6.1}$$

where β is the propagation time in Euclidean signature and

$$Dx = \prod_{\tau=0,\dots,\beta} dx(\tau), \tag{6.2}$$

$$S[x] = \int_0^\beta d\tau \left(\frac{1}{2}\delta_{\mu\nu}\dot{x}^\mu\dot{x}^\nu + V(x)\right). \tag{6.3}$$

Eq. (6.1) can be interpreted as a sum over all possible worldlines $x^*(\tau)$ joining the endpoints x and x' in a time interval β, where each path is weighed according to the factor $e^{-S[x^*]}$ (see Figure 6.2 for a visual representation). To numerically realize this idea, we are restricted to consider only a finite set of N_{WL} worldlines, each of which contains a finite number N of spacetime points. We point out that this second

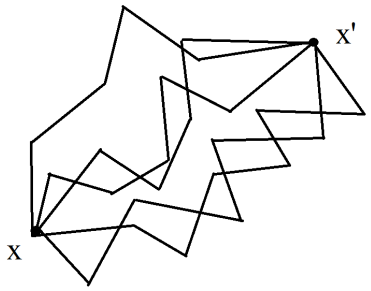

FIGURE 6.2: Example of an ensamble of five discretized paths joining x and x' on a plane.

discretization involves the affine parameter τ parametrizing the worldline [46], rather than blindly dividing the spacetime in a set of discrete points $x(\tau)$ (this construction is commonly used in Lattice Field Theories). Moreover, WLMC approaches [38, 41, 43, 44, 46] aim to compute WLMC averages of the kind

$$\left\langle e^{-S_{POT}} \right\rangle = \frac{\int_{x(0)=x}^{x(\beta)=x'} Dx\; e^{-S_{KIN}[x]-S_{POT}[x]}}{\int_{x(0)=x}^{x(\beta)=x'} Dx\; e^{-S_{KIN}[x]}} \tag{6.4}$$

where $S_{KIN}[x]$ and $S_{POT}[x]$ denote respectively the first and the second contributions to the action (6.3). Looking at (6.4) we realize that $e^{-S_{KIN}[x]}$ assumes the meaning of a weight factor for each trajectory contributing with $e^{-S_{POT}[x]}$ to the average. More in detail, this weighing is realized via one of the Monte Carlo algorithms which assigns a probability for each path to be realized according to the Brownian motion of the associated scalar particle. Hence, once all trajectories have been produced (and weights have then been considered), we are allowed to turn the above weighed average to an arithmetic one, *i.e.* to each selected worldline is assigned a weight 1. This choice is due to a universality requirement [46] for worldlines, which are thus model-independent, as the potential part of the action is not involved in their sampling. Let us call $\left\{x_i^{(s)}\right\}_{i=1,\dots,N}$ with $s = 1, \dots, N_{WL}$ the discrete set of spacetime points which represents the worldline s. The potential part of the action then reads

$$S_{POT}^{(s)}(\beta) = \int_0^\beta d\tau\; V\left(x^{(s)}\right) \simeq \frac{\beta}{N} \sum_{i=1}^{N} V\left(x_i^{(s)}\right), \quad s = 1, \dots, N_{WL}. \tag{6.5}$$

Expression (6.4) is then written as

$$\left\langle I(x,x';\beta)\right\rangle = \frac{\sum_{s=1}^{N_{WL}} e^{-S^{(s)}_{POT}(\beta)}}{N_{WL}}, \quad N_{WL} = \sum_{s=1}^{N_{WL}} 1, \tag{6.6}$$

where the larger N and N_{WL}, the more accurate is the estimate. An important point is the generation of closed worldlines, also denoted by loops, since each of them carries probabilistic information for the particle to travel such worldline: here we review a generalized version of the original *YLOOPS* algorithm [46], including a further mass-like term which will turn out to be relevant for later calculations in curved spacetime. We will refer to the original algorithm as *YLOOPS*$^{(0)}$ and to the generalized one as *YLOOPS*$^{(\alpha)}$. In order to diagonalize the kinetic term in (6.3), we define the backward difference as

$$\dot{x}^\mu \simeq \frac{N}{\beta}(x^\mu_k - x^\mu_{k-1}), \tag{6.7}$$

where the k-index discretizes the x-points in the same way as the affine parameter τ parametrizes the continuous worldline $x(\tau)$. Note that k plays the same role as it does in the TS regularization scheme. The full kinetic term will then be proportional to the difference

$$\Upsilon^{(0)} = \sum_{k=2}^{N}(x_k - x_{k-1})^2, \tag{6.8}$$

which we generalize to

$$\Upsilon^{(\alpha)} = \sum_{k=2}^{N}\left[(x_k - x_{k-1})^2 + \alpha x_k^2\right], \quad \alpha > 0. \tag{6.9}$$

Following the same path as in [46]

$$\begin{aligned}
\Upsilon^{(\alpha)} &= \sum_{k=2}^{N}\left[(x_k - x_{k-1})^2 + \alpha x_k^2\right] \\
&= \sum_{k=3}^{N-1}\left[(x_k - x_{k-1})^2 + \alpha x_k^2\right] + x_2^2 + x_{N-1}^2 + \alpha x_2^2 \\
&= \sum_{k=1}^{N-2}\left(x_{N-k} - \frac{1}{C_k^{(\alpha)}}x_{N-k-1}\right)^2 \\
&= \sum_{K=2}^{N-1} C^{(\alpha)}_{N-k}\bar{x}_k^2
\end{aligned} \tag{6.10}$$

with

$$\bar{x}_k = x_k - \frac{1}{C^{(\alpha)}_{N-k}} x_{k-1}, \tag{6.11}$$

and

$$\begin{aligned} C^{(\alpha)}_1 &= 2 + \alpha \\ C^{(\alpha)}_k &= C^{(\alpha)}_1 - \frac{1}{C^{(\alpha)}_{k-1}}, \quad k = 2, \dots, N-2. \end{aligned} \tag{6.12}$$

Hence, the algorithm can be summarized as follows.

1. Produce $N-2$ vectors $\omega_i, \quad i = 1, \dots, N-2$ (with Box-Muller algorithm [48] for instance) distributed according to $\frac{1}{(2\pi)^{D/2}} e^{-{\omega_i}^2}$.

2. Compute
$$\bar{x}_i = \sqrt{\frac{2}{N} \frac{1}{C^{(\alpha)}_{N-i}}} \omega_{i-1}, \quad i = 2, \dots, N-1. \tag{6.13}$$

3. Build the loop according to

$$\begin{aligned} x_1 &= x_N = 0 \\ x_2 &= \bar{x}_2 \\ x_i &= \bar{x}_i + \frac{1}{C^{(\alpha)}_{N-1}} x_{i-1}, \quad i = 3, \dots, N-1. \end{aligned} \tag{6.14}$$

For a quick check, we notice that the coefficients $C^{(\alpha)}_k$ coincide with those of [46] once α is set to zero, that is $C^{(0)}_k = \frac{k+1}{k}$. The above procedure allows to obtain discretized loops whose points are distributed according to $S_{KIN}[x]$; to get an open loop on can simply linearly shift each point x_i by a coefficient $\frac{i}{N}$, which idea is at the basis of the algorithm *LSOL*.

To warm up, let us now apply the WLMC method to a simple case, *i.e.* the propagator of a bosonic harmonic oscillator with null endpoints in a D-dimensional Euclidean space. Such quantity con be expressed by the following path integral

$$\tilde{G}(\beta) = \int_{x(0)=0}^{x(\beta)=0} Dx \; e^{-\frac{1}{2}\int_0^\beta d\tau \, (\dot{x}^2 + x^2)}, \tag{6.15}$$

where, for simplicity, we fixed $\omega = 1 = m$. This propagator has a well-known analytical result which reads

$$\tilde{G}(\beta) = \left[\frac{1}{2\pi \sinh(\beta)}\right]^{\frac{D}{2}}. \tag{6.16}$$

Multiplying and dividing by the potential-free theory

$$\tilde{G}(\beta) = \oint_0 Dx\, e^{-\frac{1}{2}\int_0^\beta d\tau\, \dot{x}^2} \frac{\oint_0 Dx\, e^{-\frac{1}{2}\int_0^\beta d\tau\, (\dot{x}^2+x^2)}}{\oint_0 Dx\, e^{-\frac{1}{2}\int_0^\beta d\tau\, \dot{x}^2}} \tag{6.17}$$

with simplified notation $\oint_0 = \int_{x(0)=0}^{x(\beta)=0}$ and using that

$$\oint_0 Dx\, e^{-\frac{1}{2}\int_0^\beta d\tau\, \dot{x}^2} = \left[\frac{1}{2\pi\beta}\right]^{\frac{D}{2}}, \tag{6.18}$$

we can express (6.17) as

$$\tilde{G}(\beta) = \left[\frac{1}{2\pi\beta}\right]^{\frac{D}{2}} \left\langle e^{-\frac{1}{2}\int_0^\beta d\tau\, x^2} \right\rangle \tag{6.19}$$

where we brought up the path integral average $\langle \ldots \rangle$. Combining (6.16) and (6.19) we get

$$G(\beta) = \left\langle e^{-\frac{1}{2}\int_0^\beta d\tau\, x^2} \right\rangle = \left[\frac{\beta}{\sinh(\beta)}\right]^{\frac{D}{2}} \tag{6.20}$$

which we can estimate by means of WLMC simulations.

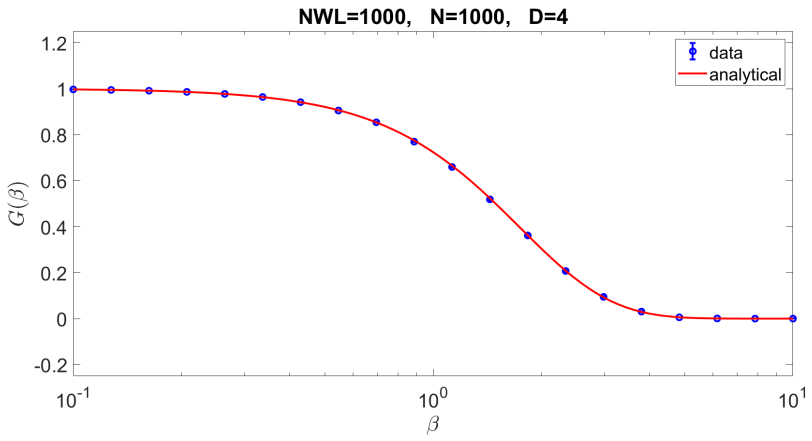

FIGURE 6.3: Comparison between a WLMC simulation and the known result for a null endpoints bosonic harmonic oscillator in a 4-dimensional Euclidean flat spacetime with $(N_{WL}, N) = (1000, 1000)$.

Fig. 6.3 shows an optimal agreement between our data and the analytical curve

over three orders of magnitude of the propagation time β. For this quite simple simple calculation we used a different set of worldlines for each β-value, which choice removes correlation between points. We used the above discussed algorithm with coefficients $C_k^{(\alpha=0)}$ to generate all the worldlines used here. Even though difficult to notice, in fig. 6.3 we also reported error bars for each computed point; they have been calculated—as it has been done for all WLMC error bars throughout this thesis—using the standard error mean [46]

$$SEM = \sqrt{\sum_{s=1}^{N_{WL}} \frac{\left[(\dots)_s - \langle(\dots)\rangle\right]^2}{N_{WL}(N_{WL}-1)}} \tag{6.21}$$

which is commonly accepted as the maximum source of error for WLMC calculations. The choice of parameters $(N_{WL}, N) = (1000, 1000)$ in this case has been made by quality of life considerations: we noticed that by further increasing these two values—which makes the calculation more accurate actually—the result doesn't change appreciably, but the machine-time cost can easily increase. Hence $(N_{WL}, N) = (1000, 1000)$ is a good compromise between accuracy and sources involved for this specific case.

Even though relatively simple, this prototypical calculation shows all the main features of the WLMC technique; in fact, it will be widely exploited for almost all the subsequent computations, in particular for those in curved spacetime, which constitute a novelty for numerical worldline applications. As we will see in the next chapter, the apparatus is pretty much the same as the one in flat spacetime, with a deep complication emerging in the form of the potential, which ultimately encodes all the information brought by curvature.

Chapter 7

Worldline Monte Carlo in curved space

7.1 Set-up

In the present chapter we move from flat space to curved space considering a non trivial background. At the very first stage, a substantial change in the form of the kinetic term of the theory, with the inclusion of the curved spacetime metric $g_{\mu\nu}(x)$, needs to be taken into account. If we consider the classical Hamiltonian of a bosonic scalar point particle moving in a D-dimensional Euclidean curved space, it can be expressed in momentum space as

$$H(x,p) = \frac{1}{2} g^{\mu\nu}(x) p_\mu p_\nu + V(x). \tag{7.1}$$

The associated Einstein invariant operator reads

$$\hat{H}(\hat{x},\hat{p}) = \frac{1}{2} g^{-\frac{1}{4}}(\hat{x}) \hat{p}_\mu g^{\frac{1}{2}}(\hat{x}) g^{\mu\nu}(\hat{x}) \hat{p}_\nu g^{-\frac{1}{4}}(\hat{x}) + V(\hat{x}), \tag{7.2}$$

where all operator symbols are expressed using hats and $g(x) = \det g_{\mu\nu}(x)$. The advantage of expressing the Hamiltonian as the operator (7.2) is that in this way it is possible to apply the same procedure reviewed in Chapter 2 to define and regularize by time-slicing the associated path integral. A complete treatment of this procedure was extensively developed in [15]. Thus, the heat kernel of the Hamiltonian (7.2) can be expressed in terms of the worldline path integral

$$I(x,x';\beta) = \int_{x(0)=x}^{x(\beta)=x'} \mathcal{D}x \; e^{-S[x]} \tag{7.3}$$

with Einstein-invariant measure

$$\mathcal{D}x = \prod_{\tau=0,\dots,\beta} \sqrt{g(x(\tau))}dx(\tau) \tag{7.4}$$

and action

$$S[x] = \int_0^\beta d\tau \left(\frac{1}{2}g_{\mu\nu}(x)\dot{x}^\mu\dot{x}^\nu + V_{CT}(x) + V(x)\right) \tag{7.5}$$

which results in a one-dimensional non-linear sigma model. We can easily detect three main differences between the flat space case and the curved one: the $\sqrt{g}$ measure factor in (7.4), the metric tensor $g_{\mu\nu}(x)$ and the counterterm potential $V_{CT}(x)$ appearing in (7.5). Whereas the first two ingredients are quite intuitive, the latter requires more effort to be justified [15]; it naturally emerges from the time-slicing procedure which leads to the construction of the action $S[x]$ if we start from the Hamiltonian (7.2) (where $\hat{p}$- and $\hat{x}$-operators are mixed) and extrapolate the kinetic term $g_{\mu\nu}(x)\dot{x}^\mu\dot{x}^\nu$. $V_{CT}(x)$ hence contains curved space information as well as metric factors and its form depends on the regularization scheme which is adopted. Nonetheless, this arbitrary choice does not affect the result of the path integral (as discussed in Chapter 3), since each specific choice of the regularization scheme implies a list of rules to compute unambiguously all Feynman integrals emerging from a perturbative treatment. Some of these perturbative contributions are divergent, but are remarkably compensated by the ones which arise from $\sqrt{g}$, leading to a finite, unique result for $I(x,x';\beta)$. Our WLMC numerical construction, however, will produce a non-perturbative result (so no cancellations of divergences are explicitly expected), but a choice of the regularization scheme has to be done anyway, and since the WLMC trajectory discretization reflects a time-slicing procedure, this scheme will be chosen to shape V_{CT}. Namely,

$$V_{CT}(x) = V_{TS}(x) = -\frac{1}{8}\left[R(x) + g^{\mu\nu}\Gamma^\rho{}_{\mu\sigma}\Gamma^\sigma{}_{\nu\rho}(x)\right]. \tag{7.6}$$

Action (7.5) shows a non trivial kinetic term which is hard to envisage how to directly implemented into numerical worldline generating algorithms[1]. In order to re-conduct ourselves to the easier flat space treatment, the key idea is to split $g_{\mu\nu}(x)\dot{x}^\mu\dot{x}^\nu$

[1] A priori one could try to include the metric $g_{\mu\nu}(x)$ directly into the *YLOOPS* algorithm for instance; however the diagonalization procedure which is then required makes this idea pretty much unaffordable.

into a flat space part plus what remains, *i.e.*

$$g_{\mu\nu}(x)\dot{x}^\mu\dot{x}^\nu = \delta_{\mu\nu}\dot{x}^\mu\dot{x}^\nu + (g_{\mu\nu}(x) - \delta_{\mu\nu})\dot{x}^\mu\dot{x}^\nu. \tag{7.7}$$

We will use the $\delta\dot{x}\dot{x}$ term to sample flat space worldlines and the rest of (7.7) is considered part of the interaction potential under the label V_{KIN}. In this way we map the curved space problem into a flat space one, once we also take into account the counterterm potential and the measure factor. Precisely, the numerical path integral average we will compute is given by

$$K(x,x';\beta) \simeq \frac{\sum_{s=1}^{N_{WL}} \sqrt{g^{(s)}} e^{-S^{(s)}_{POT}(\beta)}}{N_{WL}}, \tag{7.8}$$

with

$$\begin{aligned}
\sqrt{g^{(s)}} &= \prod_{n=2}^{N} \sqrt{g\left(\bar{x}^{(s)}_{n-\frac{1}{2}}\right)} \\
S^{(s)}_{POT}(\beta) &= \frac{\beta}{N-1} \sum_{n=2}^{N} \left[V_{KIN}\left(\bar{x}^{(s)}_{n-\frac{1}{2}}\right) + V_{TS}\left(\bar{x}^{(s)}_{n-\frac{1}{2}}\right) + V\left(\bar{x}^{(s)}_{n-\frac{1}{2}}\right)\right]
\end{aligned} \tag{7.9}$$

and

$$\bar{x}^{(s)}_{n-\frac{1}{2}} = \frac{x^{(s)}_n + x^{(s)}_{n-1}}{2} \tag{7.10}$$

being the middle point between consecutive points on the worldline s. The first term of the series of potentials in (7.9) reads

$$V_{KIN}\left(\bar{x}^{(s)}_{n-\frac{1}{2}}\right) = \frac{(N-1)^2}{\beta^2}\left(g_{\mu\nu}\left(\bar{x}^{(s)}_{n-\frac{1}{2}}\right) - \delta_{\mu\nu}\right)\left(x^{(s)\mu}_n - x^{(s)}_{n-1}{}^{\mu}\right)\left(x^{(s)\nu}_n - x^{(s)}_{n-1}{}^{\nu}\right) \tag{7.11}$$

whereas the counterterm potential is

$$V_{TS}\left(\bar{x}^{(s)}_{n-\frac{1}{2}}\right) = -\frac{1}{8}\left[R\left(\bar{x}^{(s)}_{n-\frac{1}{2}}\right) + g^{\mu\nu}\Gamma^\rho{}_{\mu\sigma}\Gamma^\sigma{}_{\nu\rho}\left(\bar{x}^{(s)}_{n-\frac{1}{2}}\right)\right]. \tag{7.12}$$

In the following we will apply this construction to numerically study a model which perfectly adapts to this treatment: it is the case of the free heat kernel of a scalar point particle constrained on maximally symmetric spaces. We will adopt Riemann Normal Coordinates (RNC) since, as it was shown in [49] (see also [50]), it is possible to map this problem into the one of a flat space heat kernel with an effective potential which encodes maximally symmetric space effects. It was also shown in [26] that,

for such a curved space, the RNC expression for the metric tensor can be expressed in closed form as the flat space contribution plus a correction due to curvature. Thus, our numerical problem can be analyzed from a pure flat space point of view, using the potential deduced in [49] and the numerical machinery presented in 6, and using the WLMC in curved space shown here. The effective flat space set-up will be a benchmark to test our curved space construction.

7.2 Free scalar heat kernel on a sphere

The model we are focusing on is deeply discussed in [51] and here quickly reviewed, before being numerically studied with WLMC techniques [47]. Let us consider the Hamiltonian operator of a free scalar particle in a background curved space,

$$\hat{\mathcal{H}}_0(\hat{x},\hat{p}) = \frac{1}{2} g^{-\frac{1}{4}}(\hat{x})\hat{p}_\mu g^{\frac{1}{2}}(\hat{x}) g^{\mu\nu}(\hat{x})\hat{p}_\nu g^{-\frac{1}{4}}(\hat{x}), \tag{7.13}$$

which is used to build the associated heat kernel

$$\hat{I}(\beta) = e^{-\beta\hat{\mathcal{H}}_0} \tag{7.14}$$

satisfying the equation of motion

$$-\frac{\partial \hat{I}(\beta)}{\partial\beta} = \hat{\mathcal{H}}_0 \hat{I}(\beta). \tag{7.15}$$

Our curved space conventions are

$$\begin{aligned} \left[\nabla_\mu, \nabla_\nu\right] V^\lambda &= R_{\mu\nu}{}^\lambda{}_\sigma V^\sigma \\ R_{\mu\nu} &= R_\mu{}^\rho{}_{\nu\rho}. \end{aligned} \tag{7.16}$$

The configuration space representation of the heat kernel is given by the matrix elements

$$I(x,x';\beta) = \langle x|\, \hat{I}\, |x'\rangle \tag{7.17}$$

satisfying

$$\frac{\partial I(x,x';\beta)}{\partial\beta} = \frac{1}{2}\nabla_x{}^2 I(x,x';\beta). \tag{7.18}$$

If we define

$$\bar{I}(x,x';\beta) = g^{\frac{1}{4}}(x) I(x,x';\beta) g^{\frac{1}{4}}(x') \tag{7.19}$$

and apply Riemann Normal Coordinates (RNC) for maximally symmetric (MS) spaces, equation (7.18) turns into the flat space heat equation

$$-\frac{\partial \bar{I}(x,x';\beta)}{\partial\beta} = \left[-\frac{1}{2}\delta^{\mu\nu}\partial_\mu\partial_\nu + V_{eff}(x)\right]\bar{I}(x,x';\beta). \tag{7.20}$$

To be precise, the MS space we are considering here is the one of a D-dimensional sphere for which

$$R_{\mu\nu\rho\sigma} = M^2\left(g_{\mu\rho}g_{\nu\sigma} - g_{\mu\sigma}g_{\nu\rho}\right) \tag{7.21}$$

where M is the sectional curvature of the sphere[2]. If this is the case, in [51] authors proved the following properties,

$$\begin{aligned}
g_{\mu\nu}(x) &= \delta_{\mu\nu} + f(x)P_{\mu\nu}(x), \quad x = \sqrt{\delta_{\mu\nu}x^\mu x^\nu} \\
f(x) &= \frac{1-2M^2x^2-\cos(2Mx)}{2M^2x^2}, \quad P_{\mu\nu}(x) = \delta_{\mu\nu} - \frac{x_\mu x_\nu}{x^2} \\
g(x) &= \left[1+f(x)\right]^{D-1} \\
V_{eff}(x) &= \frac{D(1-D)}{12}M^2 + \frac{(D-1)(D-3)}{48}\frac{5M^2x^2-3+(M^2x^2+3)\cos(2Mx)}{x^2\sin^2(Mx)}.
\end{aligned} \tag{7.22}$$

The first equation of (7.22), in particular, allows to split the full metric $g_{\mu\nu}(x)$ into a flat space part plus a curved space correction, exactly what we needed for the construction (7.7). However, in the heat kernel $\bar{I}$ above the curvature effects are entirely taken care of by the effective potential. At this point we can provide a path integral representation of the heat kernel (7.19), namely

$$\bar{I}(x,x';\beta) = \int_{x(0)=x}^{x(\beta)=x'} Dx\, e^{-S[x]}, \quad S[x] = \int_0^\beta d\tau\, \left[\frac{1}{2}\delta_{\mu\nu}\dot{x}^\mu\dot{x}^\nu + V_{eff}(x)\right], \tag{7.23}$$

which represents a curved space problem in terms of a flat space computation where curvature effects are hidden in the effective potential V_{eff}. We will perform this calculation from two different perspectives:

1. we refer to "Effective Potential Method" (EPM) for the pure flat space evaluation of the heat kernel (7.23) making use of the last expression of (7.22) for V_{eff};

2. we refer to "Non-linear Sigma Model Method" (NSMM) and compute the same quantity by using the discretized potentials (7.11) and (7.12) and the first three

[2] In our conventions, $R = g^{\nu\rho}g_{\mu\sigma}R_{\mu\nu\rho\sigma} = -D(D-1)M^2$.

lines of (7.22). In appendix C we report an example of the MATLAB code we used for curved space applications of the WLMC theory.

Point 1 is a benchmark to test point 2. We also found it convenient to use different versions of the *YLOOPS* routine: we use $YLOOPS^{(0)}$ for EPM and $YLOOPS^{(\alpha)}$ for NSMM. The use of $YLOOPS^{(\alpha)}$ in EPM would be irrelevant, whereas, as we will see, it is an important ingredient in the NSMM case. The reasons for these choices will be detailed later.

	Eff. Pot. Method (EPM)	Non-linear σ-Model Method (NSMM)
WL algo.	$YLOOPS^{(0)}$	$YLOOPS^{(\alpha)}, \quad 0 < \alpha \ll 1$
quantity	$\langle I(0,0;\beta)\rangle \simeq \frac{\sum_{s=1}^{N_{WL}} e^{-S^{(s)}_{POT}(\beta)}}{N_{WL}}$	$\langle I(0,0;\beta)\rangle \simeq \frac{\sum_{s=1}^{N_{WL}} \sqrt{g^{(s)}}\, e^{-S^{(s)}_{POT}(\beta)}}{N_{WL}}$
WL action	$S^{(s)}_{POT}(\beta) = \frac{\beta}{N}\sum_{n=1}^{N} V_{eff}(x^{(s)}_n)$	$S^{(s)}_{POT}(\beta) = \frac{\beta}{N-1}\sum_{n=2}^{N}\left[V_{KIN}(\bar{x}^{(s)}_{n-\frac{1}{2}}) + V_{TS}(\bar{x}^{(s)}_{n-\frac{1}{2}})\right]$
potential	eq. (7.22)	eqs. (7.11) and (7.12)

TABLE 7.1: Details of the two types of computation performed for the same heat kernel expansion, with a linear sigma model and with a non-linear sigma model respectively.

In Table 7.1 we summarize the details of the two calculations, both computed at null endpoints for simplicity.

In Figure 7.1 we report the results of two calculations with fixed parameters $D = 4$ and $M = 1$. In the following, we have adopted the notations $\bar{K} = \langle I \rangle$. Both figures show a comparison between the data of NSMM (blue), of EPM (green) and an overall control curve (red) (we refer to it as "analytical") with the theoretical, pertubative and analytical solution obtained in [51]. In particular Figure 7.1(a) and Figure 7.1(b) refer to couples of discretization parameters $(N_{WL}, N) = (100, 100)$ and $(1000, 3000)$. We notice that, as expected, EPM is a lot more precise than NSMM, surely because of the form of the associated potential: in the first case, it is expressed by the regular form (7.22) (last line), whereas NSMM makes use of numerical derivatives (7.11). On the other hand EPM requires a knowledge of V_{eff} which is not always affordable for more complicated cases, whilst NSMM could be straightforwardly applied to such cases. In

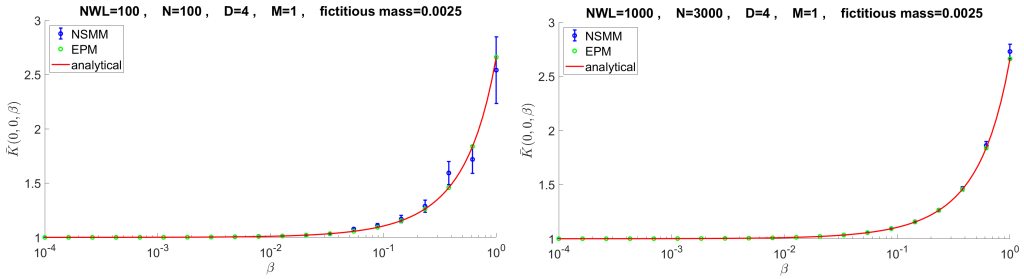

(a) (b)

FIGURE 7.1: Calculations of the heat kernel of a free scalar particle in a D=4 sphere with endpoints $x = x' = 0$ for various parameters (N_{WL}, N) both using the effective potential method (green data) with known potential and using the non-linear sigma model method (blue data). The red curve is the analytical and perturbative computation for small β performed in [51].

other words, the applicability of EPM seems to be tightly linked to MS spaces, for which the effectively flat heat kernel $\bar{I}$ can be constructed. On the other hand, NSMM is certainly less efficient than EPM, in MS spaces, but there is a priori no obstruction to extend its applicability to more generic geometries. We will return to this issue in the subsequent sections. For the moment let us stick to MS spaces. Assuming the green points as benchmarks for the blue ones, we point out that the agreement between the two calculations improves as the discretized approximation does, *i.e.* when N_{WL} and N get large. Indeed the absolute value of the maximum relative discrepancy between them passes from $\sim$ 35% with $(N_{WL}, N) = (100, 100)$ (Fig. 7.1(a)) to $\sim$ 4% with $(N_{WL}, N) = (3000, 3000)$ (Fig. 7.1(b)). We also recognize the overall *undersampling* numerical phenomenon detected and studied in [46], which manifests at large β-values as a result of the difficulty for extended worldlines to interact with localized potentials (at the origin). Even though the benchmark solution always falls within the data errorbars, for large β-values we denote a systematic discrepancy between the data and the theory, which we ascribe to the aforementioned *undersampling* phenomenon. Another possible source of error which could explain such discrepancy is due to the level of precision we use to represent derivatives. The whole numerical construction we presented (including *YLOOPS*$^{(\alpha)}$) makes use of simple backward derivatives: maybe, adopting a more accurate discretization could improve the results, even though new algorithms based on it should be found.

Figure 7.2 shows a calculation with higher precision with respect to the ones of Figures 7.1, namely with $(N_{WL}, N) = (3000, 10000)$ for values $\beta \in (0.3, 1)$, that

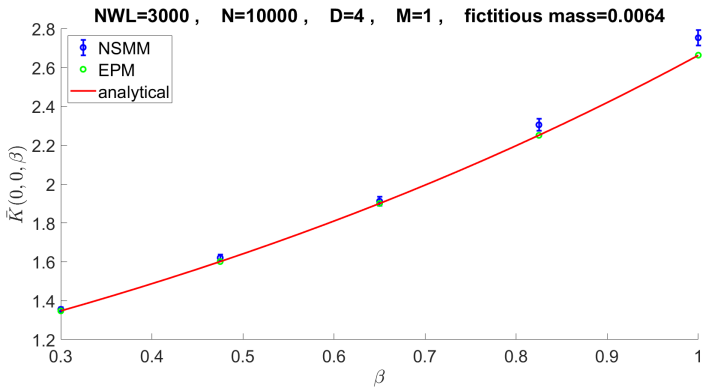

FIGURE 7.2: High precision calculation of the heat kernel for the free scalar particle on the sphere with $(N_{WL}, N) = (3000, 10000)$.

is the tail of Figures 7.1. Here an appreciable suppression of WLMC fluctuations are noticeable due to the increasing values of N_{WL} and N. At this point it is also interesting to see the effect of the α-parameter (which we can refer to as a "fictitious mass") on the latter high precision case.

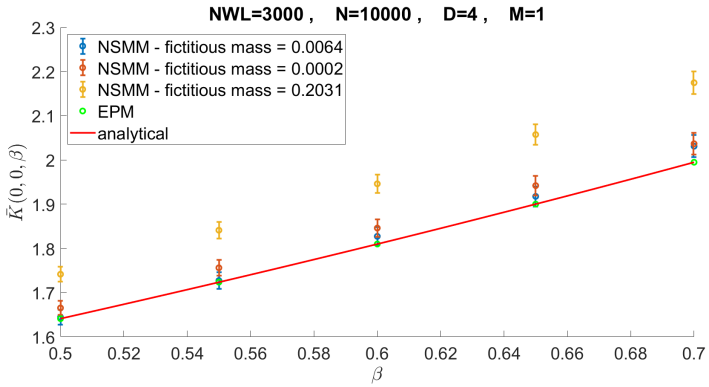

FIGURE 7.3: Calculations of the heat kernel for the free scalar particle on the sphere with $(N_{WL}, N) = (3000, 10000)$ and or different values of the fictitious mass.

Figure 7.3 shows the comparison between NSMM calculations for three different values of α, *i.e.* $\alpha_{min} = 0.0064$, $\alpha_- = 0.0002$ and $\alpha_+ = 0.2031$. The choice of α_{min} is actually explained in Appendix B: it is given by the α-value which minimizes the average discrepancy between NSMM and EPM. In Figure 7.3, α_- and α_+ lie on the left and on right respectively of α_{min} on a logarithmic scale.

We studied this model also for different curvature parameters M. In Figures 7.4 we fixed $M = 1$ and $M = 0.1$, reporting also the relative errors between NSMM and EPM. This is to point out that when the curvature of the sphere decreases, the relative error decreases too, due to the fact the we are locally moving from a more curved geometry to a flatter one, where discrepancies arising from curvature effects

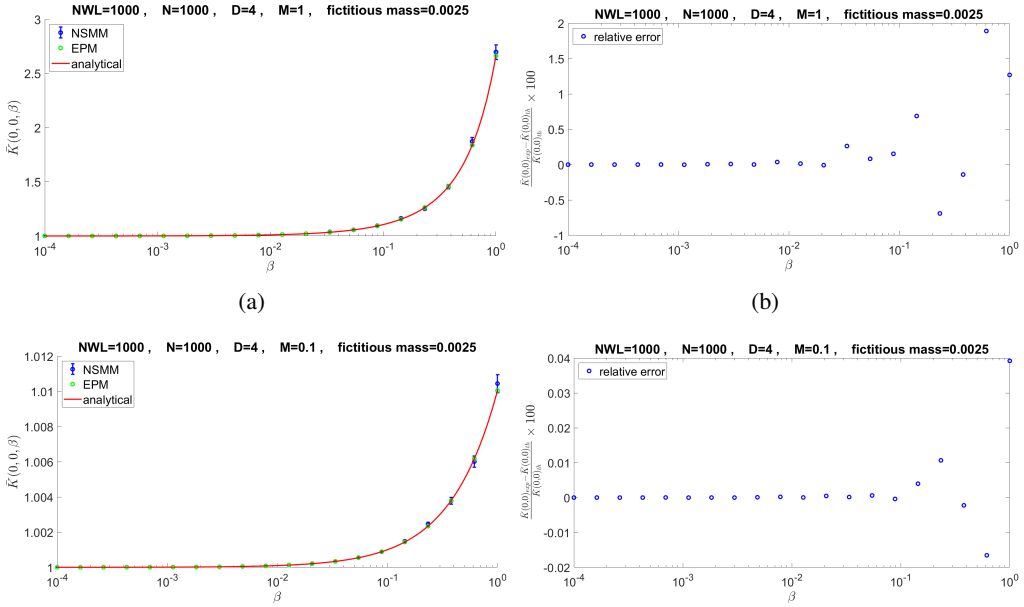

FIGURE 7.4: Calculations of the heat kernel for the free scalar particle on the sphere with $M = 1$ (top) and $M = 0.1$ (bottom). The relative errors between the blue and the green data have been shown in the figures on the right. All other parameters are kept fixed.

(hidden in the discretized representation of derivative in curvature potential terms) are less relevant. In fact, the maximum relative error between NSMM and EPM passes from $\sim 2\%$ to $\sim 0.04\%$ going from $M = 1$ to $M = 0.1$.

7.3 Free scalar heat kernel on a hyperboloid

The very same calculation described above can be performed in the case of a positive curvature MS space, in our case a 4-hyperboloid. Following [51], we thus consider $M^2 < 0$ and, defining $|M| = \sqrt{-M^2}$, we write the metric as

$$g_{\mu\nu}(x) = \delta_{\mu\nu} + \tilde{f}(x) P_{\mu\nu}(x) \tag{7.24}$$

with

$$\tilde{f}(x) = \frac{-1 - 2(|M|x)^2 + \cosh\big(2|M|x\big)}{2(|M|x)^2}. \tag{7.25}$$

All other quantities in (7.22) are defined analogously, whereas for the potential V_{eff} the replacement $M \to iM$ has to be performed.

Figure 7.5 shows a very good agreement between NSMM and EPM for $(N_{WL}, N) = (1000, 1000)$ and $\beta \in (0.01, 10)$.

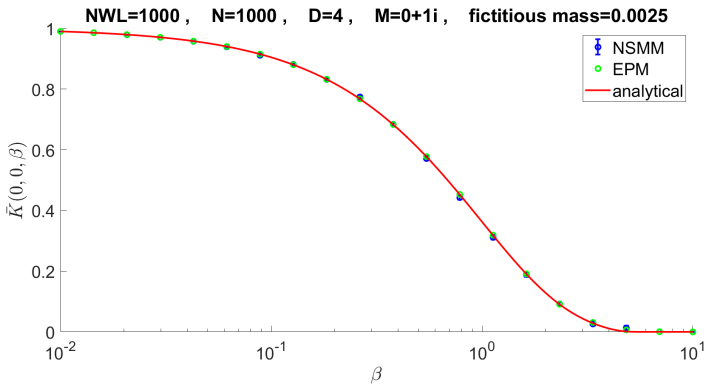

FIGURE 7.5: Calculations of the heat kernel for the free scalar particle on a hyperboloid with $D = 4$ and $|M| = 1$.

7.4 An extension to open worldlines

So far we studied the heat kernel of a point-particle looping around the origin, that is $x(0) = x(\beta) = 0$. It is however possible to extend the WLMC method to the open-line case, where $x(0) \neq x(\beta)$. Let us call $x(0) = y$ and $x(\beta) = z$. The expression for the path integral representing the heat kernel is then

$$I(y,z;\beta) = \int_{x(0)=y}^{x(\beta)=z} \mathcal{D}x\, e^{-S[x]}, \tag{7.26}$$

with

$$\mathcal{D}x = \prod_{\tau=0,\dots,\beta} \sqrt{g(x(\tau))}dx(\tau), \quad S[x] = \int_0^\beta d\tau \left(\frac{1}{2} g_{\mu\nu}(x)\dot{x}^\mu \dot{x}^\nu + \tilde{V}(x).\right) \tag{7.27}$$

$\tilde{V}(x)$ includes the counterterm potential $V_{TS}(x)$ and a possible external potential. We now split the worldline into the classical path $x_{cl}(\tau)$ (it is the straight line joining y and z) plus quantum fluctuations $q(\tau)$,

$$x^\mu(\tau) = x^\mu_{cl}(\tau) + q^\mu(\tau), \quad x^\mu_{cl}(\tau) = y^\mu + \frac{\tau}{\beta}(z^\mu - y^\mu), \tag{7.28}$$

where $q(0) = q(\beta) = 0$. The average path integral assumes the form

$$\langle I(y,z;\beta)\rangle = e^{-\frac{(y-z)^2}{2\beta}} \left\langle \int_{q(0)=0}^{q(\beta)=0} \mathcal{D}q\, e^{-S_{KIN}[x_{cl},q]-S_{POT}[x_{cl},q]} \right\rangle \tag{7.29}$$

with

$$\mathcal{D}q = \prod_{\tau=0,\dots,\beta} \sqrt{g(x_{cl}(\tau)+q(\tau))}dq(\tau), \tag{7.30}$$

$$S_{KIN}[x_{cl},q] = \int_0^\beta d\tau \left[\frac{1}{2}(g_{\mu\nu}(x_{cl}+q)-\delta_{\mu\nu})\left(\frac{1}{\beta}(z^\mu-y^\mu)+\dot{q}^\mu\right)\left(\frac{1}{\beta}(z^\nu-y^\nu)+\dot{q}^\nu\right)\right], \tag{7.31}$$

$$S_{POT}[x_{cl},q] = \int_0^\beta d\tau \tilde{V}(x_{cl}+q). \tag{7.32}$$

Equations (7.29)-(7.32) show that it is possible to express the averaged path integral $\langle I(y,z;\beta)\rangle$ having non-vanishing boundary conditions in terms of another one with null boundaries, like those studied all through this chapter. The price to pay is just a few displacements with respect of the classical trajectory and an overall factor in front of the average.

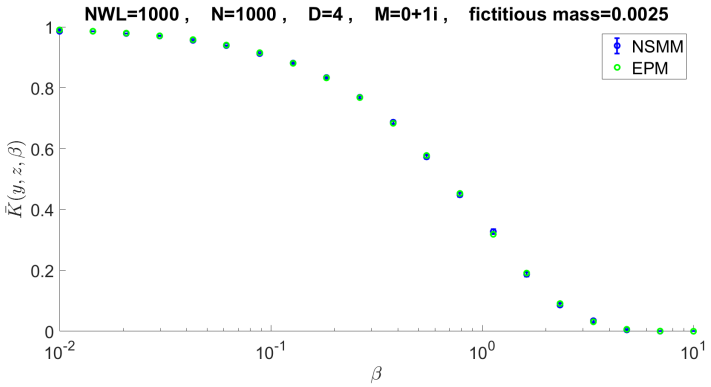

FIGURE 7.6: Calculations of the heat kernel for the free scalar particle propagating from $y = (0,0,0,0)$ to $z = (5,5,5,5)$ on a hyperboloid with $D = 4$ and $|M| = 1$. The blue points show a calculation performed with the non-linear sigma model method, whereas the green points are referred to a benchmark calculation obtained with the flat space setup.

Figure 7.6 shows the calculation of the heat kernel of a free scalar point-particle propagating on a 4-hyperboloid from $y = (0,0,0,0)$ to $z = (5,5,5,5)$ using NSMM and EPM. Also in this case, the agreement is quite positive.

7.5 Conclusions

In this chapter we saw how a method to implement the WLMC formalism to the case of a maximally symmetric curved space, for which analytical perturbative results already known from literature have been used to test our method. It amounts to separate

the curved metric tensor into a flat part and a curvature correction: the first one is used to generate flat space worldlines according to the generalized algorithm *YLOOPS*$^{(\alpha)}$, whereas the correction is considered as part of the potential, as well as the associated time-slicing counterterm. Considering positive and negative curvature spaces, such method proves to be effective and easy to implement. There can be further possible applications beyond scalar theories in MS spaces: QFT effective actions can be numerically studied without treating gravity perturbatively, as for instance in the derivation of gravitational corrections to the Euler-Heisenberg Lagrangians [20]. Another example is the effect of curvatures in strongly-coupled fermionic models, such as the Gross Neveu model, which describes the low-energy limit of different physical systems. In fact, flat space worldline Monte Carlo studies for large N fermionic models where already successfully taken into consideration [45], whilst, at the perturbative level, the heat kernel expansion of the Gross-Neveu model in 3d curved spaces at fixed curvature was studied in [52]. A desirable extension of the present method certainly involves the inclusion of spinorial degrees of freedom: this problem can be tackled either with the inclusion of suitable matrix-valued potentials (spin factors) or in terms of spinning particle models, which involve Grassmann odd coordinates. In Chapter 9 we will see this last possibility in action, whereas, in the next chapter, we will consider a bunch of physical problems and review how to extend the WLMC in curved space machinery to them. We will consider the calculation of Casimir energies [41, 42] for specific geometries and the case of a scalar particle in presence of a magnetic field [38, 43].

Chapter 8

Further applications of the WLMC technique

In this chapter we study a few scenarios where the new worldline Monte Carlo tools described above can be fruitfully employed. We will study the application of the WLMC formalism to numerically study Casimir energies for different geometries and the scalar propagator in presence of a Maxwell background.

8.1 Casimir energies

The study of Casimir configurations energies was the primary reason why H. Gies and collaborators introduced Monte Carlo techniques in the worldline formalism [41, 42]. The main important advantage of the model is its independence in the shape (and number) of boundaries. The main drawback is that the model, so far, has only been introduced for scalar field with DBC. Here we review the basics of their construction and possible developments.

Let us consider a scalar field $\phi(x)$ in a D-dimensional Euclidean space subjected to a potential $V(x)$ which models the Casimir configuration geometry, *i.e.* the set of points x where $V(x)$ is not zero is occupied by rigid bodies whose interaction via ϕ gives the associated Casimir energy. The scalar field vanishes (DBC) at the location of these boundaries. The Lagrangian of this system is given by

$$L = \frac{1}{2}\partial_\mu\phi\partial^\mu\phi + \frac{1}{2}m^2\phi^2 + \frac{1}{2}V(x)\phi^2 \tag{8.1}$$

which is used to get the effective action

$$\Gamma[V] = \frac{1}{2}\mathrm{Tr}\,\ln\frac{-\partial^2 + m^2 + V(x)}{-\partial^2 + m^2}$$

$$= -\frac{1}{2}\int_{0^+}^{\infty}\frac{d\beta}{\beta}\int d^D x\,\left[\langle x|\, e^{-\beta(-\partial^2+m^2+V(x))}\,|x\rangle - \frac{1}{(4\pi\beta)^{D/2}}e^{-m^2\beta}\right]. \quad (8.2)$$

Eq. (8.2) contains a contraction which is represented by a worldline path integral,

$$\begin{aligned}&\int d^D x\ \langle x|\, e^{-\beta(-\partial^2+m^2+V(x))}\,|x\rangle = \\ &= \int d^D x_{CM}\frac{1}{(4\pi\beta)^{D/2}}\int_{x(0)=x(\beta)} Dx\ e^{-\int_0^\beta d\tau\ \dot{x}^2/4-\int_0^\beta d\tau\ V(x_{CM}+x(\tau))}\end{aligned} \quad (8.3)$$

where we have extracted from all trajectories their centers of mass x_{CM} and then path integrated over closed loops of length β. Now, rescaling the proper time parameter τ so that it ranges in $[0,1]$ rather than $[0,\beta]$, we introduce new unit loop trajectories $y(\tau)$ satisfying

$$\int_0^\beta d\tau\ \dot{x}^2(\tau) = \int_0^1 d\tau\ \dot{y}^2(\tau) \quad (8.4)$$

which we can use to compute the effective action[1]

$$\Gamma[V] = -\frac{1}{2}\frac{1}{(4\pi)^{D/2}}\int_{0^+}^{\infty}\frac{d\beta}{\beta^{1+D/2}}e^{-m^2\beta}\int d^D x\left[\langle W_V[y(\tau);x]\rangle_y - 1\right] \quad (8.5)$$

where

$$W_V[y(\tau);x] = e^{-\beta\int_0^1 d\tau\ V(x+\sqrt{\beta}y(\tau))}. \quad (8.6)$$

In case of time independent Casimir configuration we also divide by the time volume $L_{x_0} = \int dx_0$, and obtain the Casimir energy

$$\mathcal{E}_V = \frac{\Gamma[V]}{L_{x_0}}. \quad (8.7)$$

Most of the interesting Casimir problems involve the computation of the interaction between rigid bodies, each of which here we can model by a certain potential $V_k(x)$. The full Casimir interaction energy between such bodies will be then[2]

$$E = \mathcal{E}_{\sum_k V_k} - \sum_k \mathcal{E}_{V_k}. \quad (8.8)$$

Formula (8.8) will be used to compute the Casimir energy of interaction between rigid bodies. For such a purpose, we now focus on the potential $V(x)$ which geometrically

[1] Here we drop the notation x_{CM} in place of x, for simplicity.
[2] A more detailed discussion about this point can be found in [41].

defines the rigid bodies. A smart choice is the use of δ-function,

$$V(x) = \lambda \int_\Sigma d\sigma \, \delta^{D-1}(x - x_\sigma) \tag{8.9}$$

where Σ represents the body surface, x_σ are its space points and the positive coupling λ can be seen as a plasma frequency of the body: smaller values of λ make the body transparent whereas larger ones identify a conducting object, hence DBC for the field ϕ at the body surface. Integrating this potential over the proper time, we end up with

$$\begin{aligned} I_V[y(\tau);\beta,x] &= \int_0^1 d\tau \, V(x + \sqrt{\beta} y(\tau)) \\ &= \lambda \int_0^1 \int_\Sigma d\sigma \, \delta(\sqrt{\beta} y(\tau) + x - x_\sigma) \\ &= \frac{\lambda}{\sqrt{\beta}} \int_\Sigma d\sigma \sum_{\{\tau_i | \sqrt{\beta} y(\tau_i) + x = x_\sigma\}} \frac{1}{|\dot{y}(\tau_i)|}. \end{aligned} \tag{8.10}$$

Eq. (8.10) prescribes to consider all worldline points parametrized by τ_i which intercept the Casimir body Σ at x_σ, compute the modulus of the inverse derivative of the unit loop at that point, sum over all these contributions and over all the volume Σ. A remarkable property of the above construction is that we have to consider only those worldlines which intercept all the bodies of the Casimir configuration, since all other trajectories give a null contribution to the energy (8.8).

An easy example of application of this numerical Casimir construction is the one of two parallel plates spaced by a transverse distance a. Let's locate them at $z = \pm\frac{a}{2}$ orthogonal to the z-axis, as depicted in Fig. 8.1.

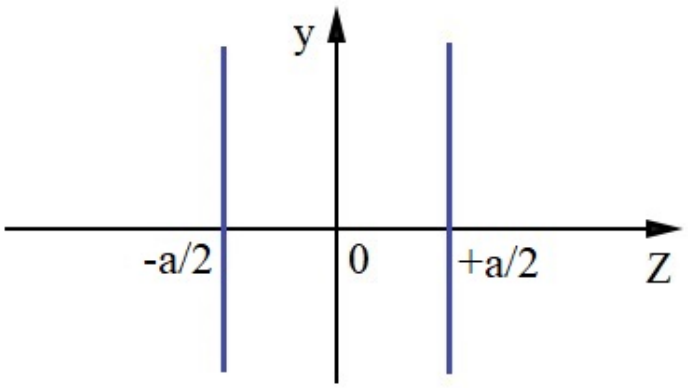

FIGURE 8.1: Graphical representation of the parallel plates Casimir configuration. The two vertical lines at $z = \pm\frac{\delta}{2}$ are the intersections between the two plates and the yz-plane.

Thus, the associated potential will be

$$V(x) = V(z) = \lambda \left[\delta\left(z + \frac{a}{2}\right) + \delta\left(z - \frac{a}{2}\right) \right]. \tag{8.11}$$

Reference [53] provides an analytical computation of the Casimir interaction energy between parallel plates versus the product λa and it is a perfect benchmark for this numerical calculation.

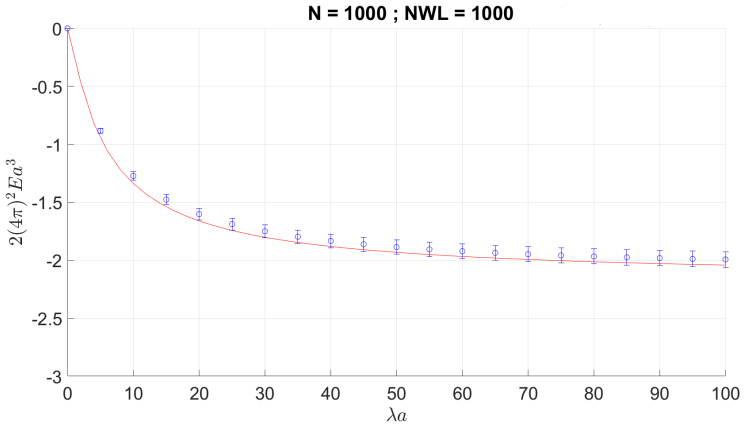

FIGURE 8.2: Numerical calculation of the (rescaled) Casmir interacting energy between two parallel plates separated by a with $m = 1$ in terms of the product between a and the potential coupling λ. As $\lambda a \to \infty$, the rescaled Casimir energy tends to $-\frac{\pi^4}{45}$.

Figure 8.2 shows a replica of the calculation presented in [41] of the rescaled Casimir interacting energy between parallel plates in terms of the product λa and with $m = 1$. The asymptotic value to which the curves tend as $\lambda a \to \infty$ is $-\frac{\pi^4}{45} \simeq -2.16$. We see an optimal agreement between the numerical estimate (blue points) and the analytical reference (red line) even for relatively small numerical parameters $(N_{WL}, N) = (1000, 1000)$. Here the limit $\lambda a \to 0$ corresponds to transparent plates (no plates), whereas $\lambda a \to \infty$ corresponds to perfectly conducting plates.

Let us stress that the little offset between the blue data and the reference curve which slightly increases as λa increases, is due to numerical reasons: further optimizing the values N, N_{WL}, the β-integral and the grid of centers of mass, would make the two curve coincide. Clearly, greater the effort, better the result. In fact, we point out that Casimir calculations like this one are much more involved and time-consuming than those of the previous chapter: looking back at equation (8.5) we notice that to obtain an estimate of the effective action we need to numerically integrate over all the

centers of mass x considered (those which a priori are considered relevant for the specific Casimir configuration) and over the total proper time length β (over a numerically significant range). Typically, for $m = 1$, β is ranged in $(0^+, \sim 5)$, whereas the centers of mass are sampled obviously according to the geometry of the system: in the case of parallel plates we took advantage of the cylindrical symmetry and chose to consider centers of mass with $z \in (-a, a)$. In fact, although some loops have a center of mass which is at the left (right) of the left (right) plate, they can put in contact both plates, as long as they are not too far from them. We checked that expanding the center of mass interval $(-a, a)$ brings no significant contribution for the Casimir energy.

An, a priori, simple setup which combines Casimir effect with a curved spacetime can be the following. We take on a 4-sphere like the one considered in Chapter 7 and insert two parallel plates on its surface, distanced by a. They are positioned symmetrically with respect to the north pole (assumed as the origin). Thus we end up with a configuration that resembles that of a baseball, as it is sketched in Fig. 8.3.

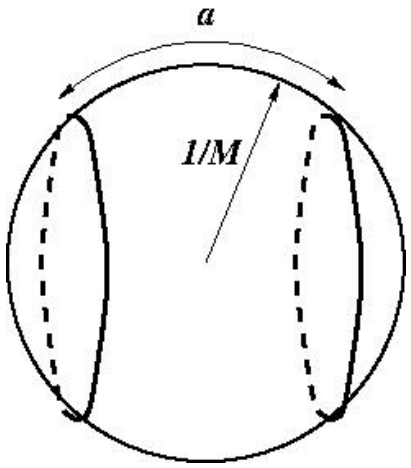

FIGURE 8.3: Geometry of two parallel plates defined on the surface a sphere.

Now, we fix the curvature of the sphere and study the Casimir interaction energy versus a, expecting to recover asymptotically the flat space result for small a, that is $-\frac{\pi^4}{45}$ in these units.

Figure 8.4 shows how numerical data (blue points) approach the flat space theoretical value (in these rescaled units it is $\simeq -2.16$), which is represented by the red line being meaningful for small a. We fixed the curvature of the sphere at $M = r^{-1} = 0.01$ to see this locally flat behaviour increased at the origin of the RNC system (the north pole of the sphere). Even though data error bars do not get close enough to intersect the analytical reference (as one should expect to recover the flat space limit), the trend

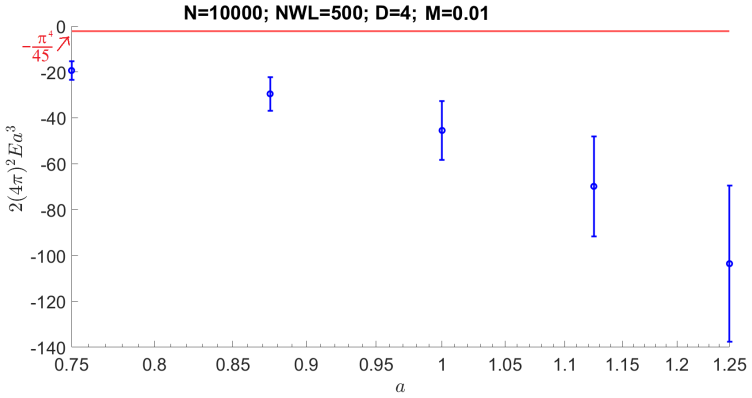

FIGURE 8.4: Numerical calculation of the (rescaled) Casimir interacting energy between two parallel plates on a 4-sphere separated by a with $m = 1$ versus a. As the plates get closer, the Casimir energy tends to the one computed in flat space, that is $-\frac{\pi^4}{45}$.

is quite clear[3]. To see in a more direct way the effect of the curvature on the Casimir energy, we can define a function

$$g(a) = \frac{E_{SPHERE}(a)}{E_{PLANE}(a)}, \tag{8.12}$$

where $E_{SPHERE}(a)$ and $E_{PLAN}(a)$ are the Casimir energies of interaction between the two plates in curved and in flat space respectively, versus a. We can then plot $g(a)$ for the points of Fig. 8.4. The result in Fig. 8.5 shows how $g(a)$ increases with a, suggesting that curvature effects tend to increase the associated force between the plates.

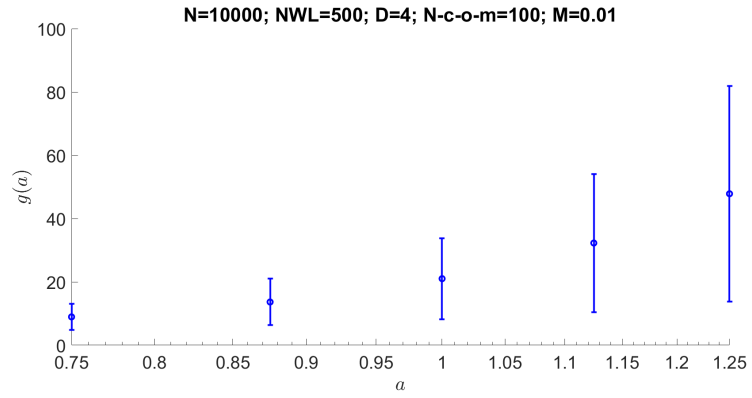

FIGURE 8.5: Plot of the function $g(a) = \frac{E_{SPHERE}(a)}{E_{PLAN}(a)}$. $g(a)$ increases as the curvature effects increase (this occurs at large values of a).

[3] As previously pointed out, due to multiple numerical integrations, Casimir WLMC calculations are a lot more expensive than other WLMC estimates, hence in most cases large values of both N_{WL} and N may be prohibitive.

8.2 Magnetic field background

In the present section we instead apply the worldline representation of the open line particle path integral introduced in section 7.4. Here we show how the numerical method correctly reproduces the particle transition amplitude in the presence of a Maxwell background. We consider the case of a constant magnetic field. The general Euclidean field strength tensor associated to electromagnetism is given by

$$F_{ij} = \begin{bmatrix} 0 & B_3 & -B_2 & iE_1 \\ -B_3 & 0 & B_1 & iE_2 \\ B_2 & -B_1 & 0 & iE_3 \\ -iE_1 & -iE_2 & -iE_3 & 0 \end{bmatrix}, \tag{8.13}$$

which, setting $\vec{B} = B(0,0,1)$ and $\vec{E} = 0$, reduces to

$$F_{ij} = \begin{bmatrix} 0 & B & 0 & 0 \\ -B & 0 & 0 & 0 \\ 0 & 0 & 0 & 0 \\ 0 & 0 & 0 & 0 \end{bmatrix}. \tag{8.14}$$

Let us now consider a $D = 4$ Euclidean massive scalar field theory coupled to electromagnetism as a constant background without quantum radiation and in particular let us focus on its propagator on an open line. This is expressed by

$$D^{xx'}[A] = \int_0^\infty d\beta\, e^{-m^2\beta} \int_{x(0)=x'}^{x(\beta)=x} Dx\, e^{-\int_0^\beta d\tau \left[\frac{1}{4}\dot{x}^2 + ie\dot{x}\cdot A(x)\right]}, \tag{8.15}$$

where for A we choose the gauge potential in the covariant Fock-Schwinger gauge

$$A_\mu(y) = -\frac{1}{2} F_{\mu\nu} \left(y - x'\right)^\nu. \tag{8.16}$$

Decomposing the arbitrary trajectory into a straight line and a fluctuation part $q(\tau)$ with $q(0) = q(\beta) = 0$

$$x(\tau) = x' + \frac{\tau}{\beta}(x - x') + q(\tau), \tag{8.17}$$

we get to

$$D^{xx'}(F) = \int_0^\infty d\beta\, e^{-m^2 T} e^{-\frac{(x-x')^2}{4\beta}} \times \\ \times \oint_0 Dq(\tau)\, e^{-\int_0^\beta d\tau\, \frac{\dot{q}^2}{4} + \frac{ie}{2}\int_0^\beta d\tau\, \dot{q}^\mu F_{\mu\nu} q^\nu + \frac{ie}{\beta}(x-x')^\mu F_{\mu\nu}\int_0^\beta d\tau\, q^\mu(\tau)} \tag{8.18}$$

with

$$\oint_0 Dq(\tau)\, e^{-\int_0^\beta d\tau\, \frac{1}{4}\dot{q}^2} = (4\pi\beta)^{-\frac{D}{2}}\,. \tag{8.19}$$

Expression (8.18) can then be written as

$$D^{xx'}(F) = \int_0^\infty d\beta\, e^{-m^2\beta} e^{-\frac{(x-x')^2}{4\beta}}\, (4\pi\beta)^{-\frac{D}{2}} \left\langle W^{xx'}(\beta, F)\right\rangle \tag{8.20}$$

with

$$\left\langle W^{xx'}(\beta, F)\right\rangle = \frac{\oint_0 Dq(\tau)\, e^{-\int_0^\beta d\tau\, \frac{\dot{q}^2}{4} + \frac{ie}{2}\int_0^\beta d\tau\, \dot{q}^\mu F_{\mu\nu} q^\nu + \frac{ie}{\beta}(x-x')^\mu F_{\mu\nu}\int_0^\beta d\tau\, q^\mu(\tau)}}{\oint_0 Dq(\tau)\, e^{-\int_0^\beta d\tau\, \frac{\dot{q}^2}{4}}}. \tag{8.21}$$

A known result for $D^{xx'}[F]$ can be found in [55] and reads

$$D^{xx'}[F] = \int_0^\infty d\beta\, e^{-m^2\beta}\, (4\pi\beta)^{-\frac{D}{2}} \sqrt{\det\left(\frac{Z}{\sin Z}\right)} e^{-\frac{(x-x')\cdot Z\cdot\cot Z\cdot(x-x')}{4\beta}} \tag{8.22}$$

where $Z_{\mu\nu} = e\beta F_{\mu\nu}$. Comparing equations (8.20) and (8.22) we have

$$\left\langle W^{xx'}(\beta, F)\right\rangle = \sqrt{\det\left(\frac{Z}{\sin Z}\right)} e^{-\frac{(x-x')\cdot(Z\cdot\cot Z - \mathbb{1})\cdot(x-x')}{4\beta}} \tag{8.23}$$

which we can express with our WLMC method in the case of a pure magnetic field background.

Figure 8.6 shows a WLMC calculation of the scalar averaged propagator in presence of a magnetic field as a background. Parameters values are specified in the figure. We notice a very satisfactory agreement between the reference analytical result and our numerical computation. Given the previous very satisfactory result, it would be interesting to include the coupling to gravity, *i.e.* embed the previous model in a curved space. We leave it for future work.

In this chapter we studied a few applications of the worldline Monte Carlo method, namely: the Casimir interaction energy between two parallel plates in flat space (recovering known results) and in curved space (applying the machinery presented in the

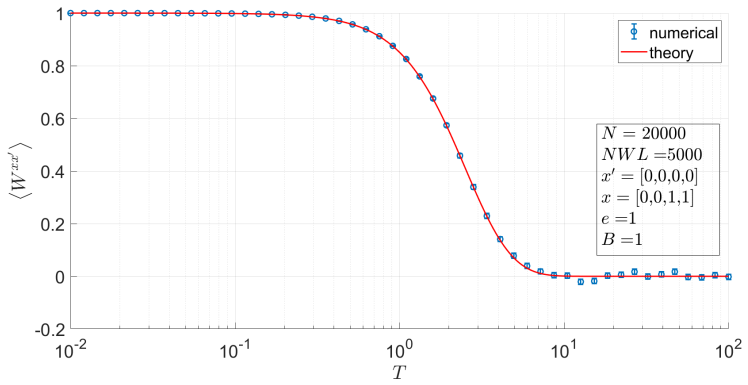

FIGURE 8.6: WLMC calculation of the propagator for a scalar particle in presence of a background magnetic field.

previous chapter); a magnetic field background coupled to a scalar field. The WLMC technique proved to be able to describe accurately the behaviour of the computed quantities in all these cases. However, an important point which often has emerged is the need of reaching the best numerical optimization possible to get a result which reproduces the correct solution. In some cases, like flat space calculations, estimates of propagators, the numerical parameters which control the calculation can be chosen relatively high; for what concerns more involved calculations, like those in curved space and the ones involving effective actions, multiple integrals have to be performed on top of the particle path integrals (β-integration, center of mass integration), and this massively contributes to slow down the computation. An important future challenge for the applications of WLMC method in curved space is certainly optimizing the known algorithms to be able to perform demanding calculations (like the last ones cited) in a reasonable amount of time.

Here we conclude the pure WLMC part of this thesis and, in the next chapter, we move to the study of Grassmannian particle path integrals, in particular we will focus on a numerical method to evaluate such quantities.

Chapter 9

A numerical approach to supersymmetric nonlinear σ-models: Creutz algorithm

9.1 Introduction

So far, we focused our efforts on the numerical study of scalar σ-models, *i.e.* world-line path integrals representing the propagation of scalar particles. Besides the fact that scalar theories are often easier than spinorial ones and that for them a consistent number of theoretical result are known and can be taken as a reference for numerical simulations, the main advantage of numerical implementation of such models lies in the fact that we can provide an intuitive geometrical interpretation to path integrals of scalar particles. As already pointed out, they can be seen as a sum of spacetime trajectories defined on a specific background and the WLMC formalism exactly uses this intuition (apart from subtleties due to the paths sampling and the curved space treatment previously seen). However, a brunch of interesting physical problems can as well be expressed in terms of path integrals which (also) involve anticommuting coordinates, for which a numerical implementation is a lot more involved.

An example is given by the effective action of a massless fermion in curved space-time, for which a path integral representation can be written in terms of the following supersymmetric non-linear σ-model [15]— this formalism, upon dimensional reduction, can also be applied to a massive spinning particle—

$$\Gamma \sim \int_0^\beta \frac{d\beta}{\beta} \int_{PBC} Dx \, \sqrt{g(x)} \int_{ABC} D\psi \; e^{-\int_0^\beta d\tau \left(\frac{1}{2} g_{\mu\nu}(x)\dot{x}^\mu \dot{x}^\nu + \frac{1}{2}\psi^a(\delta_{ab}\partial_\tau + \dot{x}^\mu \omega_{\mu ab}(x))\psi^b + V_{CT}(x)\right)}. \tag{9.1}$$

In eq. (9.1) we identify:

- a curved space bosonic kinetic term $g\dot{x}\dot{x}$, which we already know;
- a flat space fermionic kinetic term $\psi\dot{\psi}$ expressed using Grassmann variables ψ, with tangent space (flat) indices;
- a term which couples bosonic and fermionic coordinates x and ψ through a spacetime-dependent 1-form spin connection $\omega_{\mu ab}(x)$, which encodes curvature information;
- a PBC integration for the x-coordinates and an ABC for ψ, denoting periodic and antiperiodic boundary coordinates respectively.

Hence a whole new dynamics involving anticommuting variables emerges in this scenario and it can be studied regardless of the x-sector. In this chapter we will try to provide a numerical implementation of the Euclideanized path integral

$$\tilde{Z}(\beta) = \int_{ABC} D\psi \; e^{\int_0^\beta d\tau \; \frac{1}{2}\psi^a \dot{\psi}_a + V(\psi)}, \tag{9.2}$$

where an irrelevant minus sign has been removed from the fermionic action. A first comment is the following. In the case of bosonic scalar particles we used to identify the particle $x(\tau)$ directly with its spacetime coordinate representation $x^\mu(\tau)$ having a clear and intuitive geometrical meaning: assuming a 4-dimensional Euclidean space, the particle x at proper time τ has coordinates (x^0, x^1, x^2, x^3) which can be simulated on the computer for each τ. The ordered succession of these vectors gives the trajectory of the bosonic scalar particle. However, if the particle has fermionic nature, we don't have an intuitive geometrical space on which trajectories can be simulated, mainly due to the anticommutativity property of each coordinate. Thus, the WLMC machinery which we studied for bosonic particles cannot be straightforwardly extended to Grassmann variables.

Nonetheless, the path integral (9.2) can be given a discrete approximation by using a numerical algorithm first developed by M.J. Creutz [56] in 1998. We will review his idea and apply it on a simple prototypical case.

Let us then focus on the quantity

$$\tilde{Z} = \int_{ABC} D\psi \; e^{S[\psi]} \simeq \int_{ABC} d\psi_1 \dots d\psi_N \; e^{S[\psi_1, \dots \psi_N]} \tag{9.3}$$

where the continuous $\psi(\tau)$ variable is discretized in terms of N variables $\{\psi_i\}_{1\leq i\leq N}$. Now we move to Fock space where we assume a vacuum state $|0\rangle$, a 1-particle state $|1\rangle$ and assign to each ψ_i a creation-annihilation pair $(a_i^\dagger, a_i)$ with properties

$$\begin{aligned} a\,|0\rangle &= 0 \\ a^\dagger\,|0\rangle &= |1\rangle \\ \left\{a_i^\dagger, a_j\right\} &= \delta_{ij} \\ \left\{a_i^\dagger, a_j^\dagger\right\} &= \{a_i, a_j\} = 0 \\ \int d\psi\psi &= 1 \\ \int d\psi &= 0 \\ e^{f(a)} &= 1 + f(a) \end{aligned} \tag{9.4}$$

with f linear in a. If we want to fill an empty state with different anticommuting particles ψ_i we proceed caring about their ordering because of the anticommuting properties of (9.4)

$$|F\rangle = a_1^\dagger a_2^\dagger \ldots a_{N-1}^\dagger a_N^\dagger\,|0\rangle = |1_1, 1_2, \ldots, 1_{N-1}, 1_N\rangle\,. \tag{9.5}$$

For example, if we want to remove the particle ψ_N from the full state, we act as follows

$$\begin{aligned} a_N\,|F\rangle &= a_N a_1^\dagger a_2^\dagger \ldots a_{N-1}^\dagger a_N^\dagger\,|0\rangle = (-1)^{N-1} a_1^\dagger a_2^\dagger \ldots a_{N-1}^\dagger a_N a_N^\dagger\,|0\rangle = \\ &= (-1)^{N-1} a_1^\dagger a_2^\dagger \ldots a_{N-1}^\dagger (1 - a_N^\dagger a_N)\,|0\rangle = (-1)^{N-1} a_1^\dagger a_2^\dagger \ldots a_{N-1}^\dagger\,|0\rangle = \\ &= (-1)^{N-1}\,|1_1, 1_2, \ldots, 1_{N-1}, 0_N\rangle\,. \end{aligned} \tag{9.6}$$

where a negative sign pops out for even N.

A Fock-representation of the path integral (9.3) that Creutz proposed is

$$\tilde{Z} \sim \langle 0|\, e^{S(a_1,\ldots,a_N)}\,|F\rangle \tag{9.7}$$

where $S(a_1, \ldots, a_N) = S(\psi_1 \to a_1, \ldots, \psi_N \to a_N)$ (without ordering issues, as there are no creation operators.) and arises directly from the integration rules in (9.4). The latter can be easily understood by considering simple example, such as $N = 2$, for which $S(\psi_1, \psi_2; \alpha_1, \alpha_2, \beta) = \alpha_1\psi_1 + \alpha_2\psi_2 + \beta\psi_1\psi_2$ where α_i are Grassmann-odd and

β Grassmann-even. Thus,

$$\tilde{Z}(\alpha_1, \alpha_2, \beta) = \int d\psi_1 d\psi_2 \, e^S = -\beta + \alpha_1\alpha_2. \tag{9.8}$$

On the other hand,

$$\left\langle 0|e^S|1_1 1_2\right\rangle = \langle 0|(\beta a_1 a_2 + \alpha_1 a_1 \alpha_2 a_2)|1_1 1_2\rangle = -\beta + \alpha_1\alpha_2. \tag{9.9}$$

The main goal now is to expand the exponential in (9.7) to get an easier formula to be numerical implemented. Let's define S_i as all the contributions to S having one a_i within. The complementary part is denoted by $\tilde{S}_i$. Hence for each i, $S = S_i + \tilde{S}_i$ and since all the S are Grassmann-even and only involve a's (no $a^\dagger$'s!) we have $[\tilde{S}_i, S_i] = 0$,

$$\tilde{Z} = \langle 0| \, e^{\tilde{S}_i} e^{S_i} \, |F\rangle = \langle 0| \, e^{\tilde{S}_i}(1 - n_i) e^{S_i} \, |F\rangle \, , \quad n_i = a_i^\dagger a_i. \tag{9.10}$$

In the second step we used $\langle 0|e^{\tilde{S}_i}(1 - n_i) = \langle 0|(1 - n_i)e^{\tilde{S}_i} = \langle 0|e^{\tilde{S}_i}$. Since $1 - n_i$ projects in the 0_i occupation part of $e^{S_i}|F\rangle$, in (9.10) we can make the replacement $\tilde{S}_i \to S$ to restore the original full action,

$$\tilde{Z} = \langle 0| \, e^S (1 - n_i) e^{S_i} \, |F\rangle \, . \tag{9.11}$$

Repeating this process for all other Grassmann variables and applying for each the last property of (9.4), we finally get to

$$\tilde{Z} = \langle 0| \prod_{i=1}^{N} (1 - n_i)(1 + S_i) \, |F\rangle \tag{9.12}$$

which can be implemented numerically. In fact what we will do is to start from a fully occupied state $|F\rangle$ and apply the operators $(1 - n_i)(1 + S_i)$ for each i until the state gets empty. Assuming normalization $\langle 0|0\rangle = 1$, the numerical coefficient in front of the contraction will be our estimate for the path integral Z. Let us get more into detail by focusing on a specific problem, that is the calculation of the propagator of the 1-dimensional fermionic harmonic oscillator.

9.2 The fermionic harmonic oscillator

Fixing $\omega = 1 = \hbar$, the quantum Hamiltonian operator of the fermionic harmonic oscillator is

$$\hat{H} = a^\dagger a - \frac{1}{2} \tag{9.13}$$

having eigenstates $|0\rangle$ and $|1\rangle$ with energies $\pm\frac{1}{2}$. Let us call β the transition time as usual. The partition function is then

$$Z(\beta) = \sum_{n=1,2} e^{\beta E_n} = e^{-\frac{\beta}{2}} + e^{\frac{\beta}{2}} = 2\cosh\frac{\beta}{2} \tag{9.14}$$

which, on the other hand, can be expressed with Grassmannian path integrals

$$\tilde{Z}(\beta) = \mathrm{Tr}\ e^{-\beta\hat{H}} = \int d\psi^* d\psi\ \left\langle -\psi | e^{-\beta\hat{H}} | \psi \right\rangle e^{-\psi^*\psi}. \tag{9.15}$$

In order to operate a time-slicing of the exponential propagation operator with N intermediate steps, we make use of the exponential property

$$e^{-\beta\hat{H}} = \lim_{N\to\infty}\left(1 - \frac{\beta H}{N}\right)^N \tag{9.16}$$

which we use inside (9.15) together with identities $\int d\psi_i^* d\psi_i\ e^{-\psi_i^*\psi_i}\ |\psi_i\rangle\langle\psi_i|$ at intermediate steps,

$$\begin{aligned}
\tilde{Z}(\beta) = &\lim_{N\to\infty}\int d\psi^* d\psi e^{-\psi^*\psi}\prod_{k=1}^{N-1} d\psi_k^*\psi_k e^{-\sum_{n=1}^{N-1}\psi_n^*\psi_n} \\
&\times \langle -\psi|1 - \frac{\beta}{N}\hat{H}|\psi_{N-1}\rangle\ \langle\psi_{N-1}|1 - \frac{\beta}{N}\hat{H}|\psi_{N-2}\rangle \dots \langle\psi_1|1 - \frac{\beta}{N}\hat{H}|\psi\rangle = \\
&= \lim_{N\to\infty}\int d\psi^* d\psi e^{-\psi^*\psi}\prod_{k=1}^{N-1} d\psi_k^*\psi_k e^{-\sum_{n=1}^{N-1}\psi_n^*\psi_n} \\
&\times \langle\psi_N|1 - \frac{\beta}{N}\hat{H}|\psi_{N-1}\rangle\ \langle\psi_{N-1}|1 - \frac{\beta}{N}\hat{H}|\psi_{N-2}\rangle \dots \langle\psi_1|1 - \frac{\beta}{N}\hat{H}|-\psi_N\rangle
\end{aligned} \tag{9.17}$$

with $\psi = -\psi_N = \psi_0$ and $\psi^* = -\psi_N^* = \psi_0^*$. Each contraction can be expressed as

$$\begin{aligned}
&\langle\psi_k|1 - \frac{\beta}{N}\hat{H}|\psi_{k-1}\rangle = \langle\psi_k|\psi_{k-1}\rangle\left(1 - \frac{\beta}{N}\frac{\langle\psi_k|\hat{H}|\psi_{k-1}\rangle}{\langle\psi_k|\psi_{k-1}\rangle}\right) = \\
&\simeq \langle\psi_k|\psi_{k-1}\rangle\, e^{-\frac{\beta}{N}\frac{\langle\psi_k|\hat{H}|\psi_{k-1}\rangle}{\langle\psi_k|\psi_{k-1}\rangle}} = e^{\psi_k^*\psi_{k-1}} e^{-\frac{\beta}{N}\left(\psi_k^*\psi_{k-1} - \frac{1}{2}\right)} = e^{\frac{\beta}{2N}} e^{\left(1-\frac{\beta}{N}\right)\psi_k^*\psi_{k-1}}.
\end{aligned} \tag{9.18}$$

Hence the partition function reads

$$\tilde{Z}(\beta) = e^{\frac{\beta}{2}} \lim_{N\to\infty} \prod_{k=1}^{N} \int d\psi_k^* d\psi_k \; e^{-\sum_{n=1}^{N} \psi_n^* \psi_n} e^{\left(1-\frac{\beta}{N}\right) \sum_{n=1}^{N} \psi_n^* \psi_{n-1}} =$$
$$= e^{\frac{\beta}{2}} \lim_{N\to\infty} \prod_{k=1}^{N} \int d\psi_k^* d\psi_k \; e^{-\sum_{n=1}^{N} \left[\psi_n^*(\psi_n - \psi_{n-1}) + \frac{\beta}{N} \psi_n^* \psi_{n-1}\right]} \tag{9.19}$$

which has the desired form of (9.3) with $N \to 2N$, and we can apply Creutz's formula (9.12). More to the numerical perspective, we fix a (possibly large) value N and a value β. Then we start from a full state $|F\rangle$ where all N Grassmannian particles ψ_i are present and apply $O_i = (1 - n_i)(1 + S_i)$ for each i and get to the vacuum $|0\rangle$. Thus we need to keep track of the current Fock state and its numerical coefficient which change each time we apply O_i. We can represent it by the $(N+1)$-row in Figure 9.1.

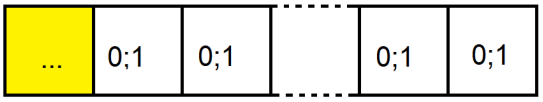

FIGURE 9.1: Graphical representation of each N-Fock state with its numerical coefficient in front.

It is important to notice that the main difficulty that this algorithm imposes is to deal with superpositions of Fock states in general. Each application of O_i on a state may in principles produce a combination of more than one state, each of which is then object of the following application O_{i+1}. In Figure 9.2 we show the diagrammatic application of the Creutz's algorithm for the case of the harmonic oscillator with reduced parameters $N = 4$ and $\beta = 1$, just to sketch the mechanism. The output is actually the rescaled partition function

$$Z(\beta) = e^{-\frac{\beta}{2}} \tilde{Z}(\beta) \tag{9.20}$$

with outcome $Z(\beta = 1, N = 4) = 1.56 \, \langle 0|0\rangle = 1.56$.

As we may figure out from figure 9.2, the repeated application of operators O_i contributes to generate a tree-structure which of course gets more and more complicated as N grows. For simplicity, in the figure all N-tuples with null coefficients have been removed. This situation happens when an annihilation operator a_i hits a state $|\ldots 0_i \ldots\rangle$ and this can occur also for different values of the current iteration i. What makes a tree complicated to be calculated (hence a flourishing tree, with a low number of cut branches) is essentially the form of the discretized action S and the number N: a

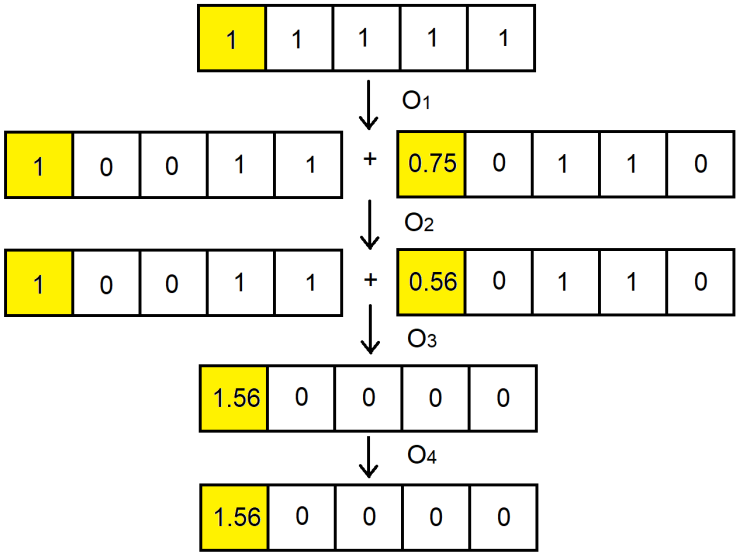

FIGURE 9.2: Diagrammatic representation of the Creutz's algorithm to numerically estimate the value of the reduced partition function $Z(\beta)$ for illustrative values $\beta = 1$ and $N = 4$.

large value N increases the length of the tree's trunk, whereas a complicated structure of the interactions S_i causes each tree's level to produce increasing non-null branches.

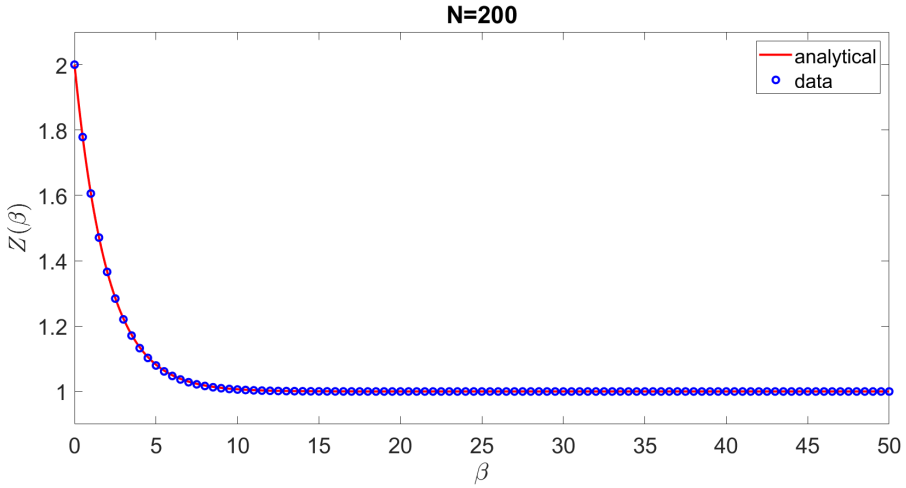

FIGURE 9.3: Calculation of the reduced partition function $z(\beta)$ for the fermionic harmonic oscillator with $\omega = 1 = \hbar$ and with fixed discretization value $N = 200$.

Figure 9.3 shows the calculation of the rescaled partition function $z(\beta)$ for the fermionic harmonic oscillator with fixed discretization value $N = 200$ within a range of total proper time lengths $\beta \in [0, 50]$ (blue data), compared with the theoretical curve (red line). In Appendix D we report the MATLAB code we used to generate this calculation. This calculation has been performed using a self-consistent routine

which cumulatively accounts for the coefficient of each branch by exploring all the tree. We notice an excellent agreement between the data and the analytical result even for a N-value which is smaller compared to the ones usually taken in WLMC calculation. However the main downside of this construction lies in the tree structure itself, which produces an exponential growing of branches as N increases. The rate of growing is determined by the form of the interactions S_i, which as pointed out, rules how flourished the tree expands at each iteration $i \in [1, N]$. The length of the tree (N) can be controlled by the user, rather its flourishing rate (S_i structure) cannot, as it substantially is part of the physical model we are dealing with. This makes this method a bit difficult to be adopted when the form of the interaction gets more complicated. A good idea could be to focus a priori only on those branches which are known to give non-null contribution to the final result, based on the knowledge of each S_i interaction. This could save a lot of calculation time for arid trees, but the problem remains an exponential one. Anyway, this simple algorithm is promising and allows for numerical Grassmannian calculations which otherwise would be unaffordable. In the next section we will concentrate on a physical model which, in theory, could be studied by matching the consolidated WLMC machinery and the Creutz's method for fermionic degrees of freedom, namely the Gross-Neveu model. Even though for the current state of numerical routine optimization a full significant numerical calculation cannot be brought on, we highlight the procedural path.

9.3 The Gross-Neveu model

In this section we present a possible recipe to study (analytically and numerically) a specific example of a supersymmetric nonlinear σ-model, the Gross-Neveu model [57]. It can be used to study strongly coupled fermions on a non-planar surface when a curved space geometry is implemented into the theory by analyzing its chiral phase structure [58].

Let us then consider a D-dimensional Gross-Neveu model

$$L = \bar{\Psi} i \not{\nabla} \Psi + G(\bar{\Psi}\Psi)^2 \tag{9.21}$$

which is chirally symmetric, i.e. invariant under transformation

$$\begin{cases} \Psi \to \gamma_5 \Psi \\ \bar{\Psi} \to \bar{\Psi} \gamma_5, \end{cases} \tag{9.22}$$

which induces

$$\begin{cases} \bar{\Psi}\Psi \to -\bar{\Psi}\Psi \\ \bar{\Psi}\gamma_\mu \Psi \to \bar{\Psi}\gamma_\mu \Psi, \end{cases} \tag{9.23}$$

with γ_5 satisfying

$$\begin{cases} \gamma_5^\dagger = \gamma_5 \\ \{\gamma^\mu, \gamma_5\} = 0 \\ {\gamma_5}^2 = \mathbf{1}. \end{cases} \tag{9.24}$$

Here, a explicit mass term of the kind $m\bar{\Psi}\Psi$ is not allowed as it would formally break the aforementioned chirality conditions. However, the four fermion interaction in (9.21) can break dynamically the chiral symmetry allowing for a non-null vacuum expectation value

$$\langle \bar{\Psi}\Psi \rangle \neq 0. \tag{9.25}$$

With this trick, fermions dynamically acquire a mass. A possible way to show that is by means of a Hubbard-Stratonovich transformation of Lagrangian (9.21): let's introduce the Gaussian path integral

$$C = \int DM'(x)\, e^{i\int d^D x \sqrt{g}(-\frac{1}{4G}M'(x)^2)} \tag{9.26}$$

and shift the field $M'(x)$

$$M'(x) \to M(x) = M'(x) - 2G\bar{\Psi}\Psi \tag{9.27}$$

to get

$$C = \int DM(x)\, e^{i\int d^D x \sqrt{g}[-\frac{1}{4G}(M+2G\bar{\Psi}\Psi)^2]}. \tag{9.28}$$

Now we can introduce the partition function in Minkowski space

$$Z = \int D\Psi D\bar{\Psi}\, e^{iS} \tag{9.29}$$

with

$$S = \int d^D x \, \sqrt{g} L. \tag{9.30}$$

Plugging (9.28) into (9.29) we obtain

$$Z = \frac{1}{C} \int D\Psi D\bar{\Psi} DM \, e^{iS_y} \tag{9.31}$$

where

$$S_y = \int d^D x \, \sqrt{g} \left[\bar{\Psi}(i\nabla\!\!\!/ - M)\Psi - \frac{1}{4G} M^2 \right]. \tag{9.32}$$

We notice that the fermion has acquired a mass expressed by a spacetime-dependent scalar field $M(x)$. Such field is quantized under the path integral in (9.31), but, if we want to treat $M(x)$ as an ordinary parameter to study the chiral symmetry breaking, we have to remove such path integration. A possibility, which is also considered in [58] is to ultimately treat M in the mean field approach. Hence, up to an irrelevant constant, we move to Euclidean space and define a mean field effective action associated to (9.32), defined by

$$e^{-\Gamma} = \int D\Psi D\bar{\Psi} \, e^{-S_y}, \tag{9.33}$$

where the covariant derivative

$$\nabla_\mu = \partial_\mu + \frac{1}{4} \omega_{\mu ab}(x) \gamma^a \gamma^b \tag{9.34}$$

includes curvature information via the spin connection 2-form $\omega_{\mu ab}(x)$. Isolating the effective action in (9.33) and performing the integration over fermion fields, we get [13]

$$\begin{aligned} \Gamma[M] = & - \text{Log Det}(\nabla\!\!\!/ + M(x)) + \frac{1}{4G} \int d^D x \, \sqrt{g} M^2(x) \\ & - \text{Log}[\text{Det}(\nabla\!\!\!/ + M(x))(-\nabla\!\!\!/ + M(x))]^{1/2} + \frac{1}{4G} \int d^D x \, \sqrt{g} \, M^2(x) \\ & - \frac{1}{2} \text{Tr Log}\big[- \nabla\!\!\!/^2 + M^2(x) + \nabla\!\!\!/ M(x) \big] + \frac{1}{4G} \int d^D x \, \sqrt{g} \, M^2(x) \\ & - \frac{1}{2} \text{Tr Log}\big[- \nabla^2 + \frac{1}{4} R + M^2(x) + \nabla\!\!\!/ M(x) \big] + \frac{1}{4G} \int d^D x \, \sqrt{g} \, M^2(x). \end{aligned} \tag{9.35}$$

Note that, in the classical action, the equation of motion for $M(x)$ gives $M(x) = -2G\bar{\Psi}\Psi$. Therefore, the equation of motion in (9.35) yields $M(x) = -2G \langle \bar{\Psi}\Psi \rangle$. The first term in the last line of (9.35) is now written as the worldline of a point-particle

in curved spacetime, namely

$$\Gamma[M] = \frac{1}{2}\int_0^\infty \frac{d\beta}{\beta} \int_{\text{PBC}} \mathcal{D}x^\mu \int_{\text{ABC}} \mathcal{D}\psi^a \; e^{-S[x^\mu,\psi^a,\omega_{\mu ab}]} + \frac{1}{4G}\int d^D x \; \sqrt{g}\; M^2(x) \quad (9.36)$$

with

$$S[x^\mu,\psi^a,\omega_{\mu ab}] = \int_0^1 d\tau \; \Big[\frac{1}{4\beta} g_{\mu\nu}(x)\dot{x}^\mu\dot{x}^\nu + \frac{1}{4\beta}\psi^a\big(\delta_{ab}\partial_\tau + \dot{x}^\mu\omega_{\mu ab}(x)\big)\psi^b + \\ + \beta\left(M^2(x) + \sqrt{2}\psi^a\nabla_a M(x)\right)\Big], \quad (9.37)$$

where the gamma-matrix in $\not{\nabla} M$ has been written in terms of the spinning variables. We notice that, upon choosing dimensional regularization to regularize the worldline path integral as done in [15], there is a perfect cancellation of the term $\frac{1}{4}R$ in (9.35) due to the DR-counterterm which has to be included in the action. Eq. (9.36) is the worldline representation of the effective action where the path integrals over bosonic coordinates x^μ and the fermionic supercoordinates ψ^a are taken with periodic and antiperiodic boundary conditions respectively. This theory can be studied in the same way as done in chapter 4, that is introducing Riemann normal coordinates ξ^μ,

$$x^\mu(\tau) = x_0^\mu + \xi^\mu(\tau) \quad (9.38)$$

and using BRST transformations. The effective action gets the form

$$\Gamma[M] = \frac{1}{2}\int_0^\infty \frac{d\beta}{\beta}\int dx_0\, d\bar{\eta}\, d\eta\, d\pi \oint_{\text{PBC}} D\xi\, Da\, Db\, Dc \oint_{\text{ABC}} D\psi\, D\bar{\psi}\; e^{-S_q} + \\ + \frac{1}{4G}\int dx_0\; \sqrt{g(x_0)}M^2(x_0) \quad (9.39)$$

with

$$S_q = S_{gf} + S_{gh}$$
$$S_{gf} = S[\xi^\mu,\psi^a,\omega_{\mu ab}] + i\pi_\mu\int_0^1 d\tau\; \xi^\mu(\tau) - \bar{\eta}^\mu\eta^\nu\int_0^1 d\tau\; Q_{\mu\nu}(x_0,\xi(\tau))$$
$$S_{gh} = \int_0^1 d\tau \frac{1}{4\beta} g_{\mu\nu}(x)\big(a^\mu a^\nu + b^\mu c^\nu\big). \quad (9.40)$$

Here we report what we obtain for the effective action,

$$\Gamma[M] = \frac{1}{2}\int d^D x_0 \int_{0^+}^{\infty} \frac{d\beta}{\beta} \frac{\sqrt{g(x_0)}}{(4\pi\beta)^{\frac{D}{2}}} 2^{\frac{D}{2}} \left\langle e^{-S_q^{(f)}} \right\rangle + \frac{1}{4G}\int d^D x_0 \sqrt{g(x_0)} M^2(x_0), \tag{9.41}$$

where $\langle \dots \rangle$ is a Wick-contraction with respect to all quantum fields involved and

$$S_q^{(int)} = S_q\left[g_{\mu\nu}(x_0,\xi) \to g_{\mu\nu}(x_0,\xi) - g_{\mu\nu}(x_0), Q_{\mu\nu}(x_0,\xi) \to Q_{\mu\nu}(x_0,\xi) - \delta_{\mu\nu}\right]. \tag{9.42}$$

Moreover, field contributions come also from the massive term of (9.36) when $M(x)$ is RNC-expanded,

$$M(x_0,\xi) = M(x_0) + \nabla_\mu M(x_0)\xi^\mu + \frac{1}{2}\nabla_\nu\nabla_\mu M(x_0)\xi^\nu\xi^\mu + \dots. \tag{9.43}$$

Expansion (9.43) is correct up to quadratic term: from the cubic term on, covariant derivatives start acting non trivially among themselves, producing further contributions which can be non-null at the origin x_0.

An effective Lagrangian can be defined from

$$\Gamma = \int d^D x_0 \ \sqrt{g(x_0)}\mathcal{L}(x_0) \tag{9.44}$$

reading

$$\mathcal{L}(x_0) = \int_{0^+}^{\infty} \frac{d\beta}{2\beta} \frac{1}{(4\pi\beta)^{\frac{D}{2}}} \left\langle e^{-S_q^{(int)}} \right\rangle + \frac{1}{4G} M^2(x_0). \tag{9.45}$$

All the interacting terms are obtained by RNC-expanding the metric tensor, the Jacobian Q [8] and the spin-connection about x_0 [59],

$$\begin{aligned}
g_{\mu\nu}(x_0,\xi) &= g_{\mu\nu}(x_0) + \frac{1}{3}R_{\mu\alpha\beta\nu}(x_0)\xi^\alpha\xi^\beta + \frac{1}{6}\nabla_\gamma R_{\mu\alpha\beta\nu}(x_0)\xi^\alpha\xi^\beta\xi^\gamma + \\
&+ \left(\frac{1}{20}\nabla_\delta\nabla_\gamma R_{\mu\alpha\beta\nu}(x_0) + \frac{2}{45}R_{\mu\alpha\beta}{}^\rho R_{\rho\gamma\delta\nu}(x_0)\right)\xi^\alpha\xi^\beta\xi^\gamma\xi^\delta + \dots \\
Q_{\mu\nu}(x_0,\xi) &= \delta_{\mu\nu} + \frac{1}{3}R_{\mu\alpha\beta\nu}(x_0)\xi^\alpha\xi^\beta + \frac{1}{12}\nabla_\gamma R_{\mu\alpha\beta\nu}(x_0)\xi^\alpha\xi^\beta\xi^\gamma + \\
&+ \left(\frac{1}{60}\nabla_\delta\nabla_\gamma R_{\mu\alpha\beta\nu}(x_0) - \frac{1}{45}R_{\mu\alpha\beta}{}^\rho R_{\rho\gamma\delta\nu}(x_0)\right)\xi^\alpha\xi^\beta\xi^\gamma\xi^\delta + \dots \\
\omega_{\mu ab}(x_0,\xi) &= \frac{1}{2}\xi^\nu R_{ab\nu\mu}(x_0) + \frac{1}{3}\xi^\nu\xi^\rho\nabla_\rho R_{ab\nu\mu}(x_0) + \\
&+ \frac{1}{8}\xi^\nu\xi^\rho\xi^\sigma\nabla_\rho\nabla_\sigma R_{ab\nu\mu}(x_0) + \dots
\end{aligned} \tag{9.46}$$

from which we use the constant pieces to build up the SI-Green's functions, namely

$$\begin{aligned}
\langle \xi^\mu(\tau)\xi^\nu(\sigma)\rangle &= -2\beta\delta^{\mu\nu}\Delta(\tau-\sigma)\\
\langle a^\mu(\tau)a^\nu(\sigma)\rangle &= 2\beta\delta^{\mu\nu}\Delta_{gh}(\tau-\sigma)\\
\langle b^\mu(\tau)c^\nu(\sigma)\rangle &= -4\beta\delta^{\mu\nu}\Delta_{gh}(\tau-\sigma)\\
\langle \psi^a(\tau)\psi^b(\sigma)\rangle &= 2\beta\delta^{ab}\Delta_{AF}(\tau-\sigma)
\end{aligned} \tag{9.47}$$

where

$$\begin{aligned}
\Delta(\tau-\sigma) &= \frac{1}{2}\,|\tau-\sigma| - \frac{1}{2}(\tau-\sigma)^2 - \frac{1}{12}\\
\Delta_{gh}(\tau-\sigma) &= \delta_P(\tau-\sigma)\\
\Delta_{AF} &= \frac{1}{2}\epsilon(\tau-\sigma)
\end{aligned} \tag{9.48}$$

with properties

$$\begin{aligned}
{}^{\bullet\bullet}\Delta(\tau-\sigma) &= \delta_P(\tau-\sigma) - 1\\
{}^{\bullet}\Delta_{AF}(\tau-\sigma) &= \delta_A(\tau-\sigma)\\
{}^{\bullet}\Delta(0) &= 0.
\end{aligned} \tag{9.49}$$

δ_P and δ_A are $1D$-Dirac delta functions on the spaces of periodic and antiperiodic functions in $[0,1]$ respectively, while a left (right) dot on a Δ-propagator indicates a derivative taken on the first (second) variable. The worldline integrals are computing using dimensional regularization.

Defining

$$\bar{S}_q^{(int)} = S_q^{(int)} - \beta M^2(x_0), \tag{9.50}$$

it's worth reporting its explicit form, so to better organize the calculation,

$$\begin{aligned}
\bar{S}_q^{(int)} = \int_0^1 d\tau\, \Bigg\{ & \frac{1}{4\beta}\left[\frac{1}{3}R_{\mu\alpha\beta\nu}\xi^\alpha\xi^\beta + \frac{1}{6}\nabla_\gamma R_{\mu\alpha\beta\nu}\xi^\alpha\xi^\beta\xi^\gamma + \right.\\
& \left. + \left(\frac{1}{20}\nabla_\delta\nabla_\gamma R_{\mu\alpha\beta\nu} + \frac{2}{45}R_{\mu\alpha\beta}{}^\rho R_{\rho\gamma\delta\nu}\right)\xi^\alpha\xi^\beta\xi^\gamma\xi^\delta + \dots\right]\left(\dot\xi^\mu\dot\xi^\nu + a^\mu a^\nu + b^\mu c^\nu\right) +\\
& + \frac{1}{4\beta}\dot\xi^\mu\left[\frac{1}{2}\xi^\nu R_{ab\nu\mu} + \frac{1}{3}\xi^\nu\xi^\rho\nabla_\rho R_{ab\nu\mu} + \frac{1}{8}\xi^\nu\xi^\rho\xi^\sigma\nabla_\rho\nabla_\sigma R_{ab\nu\mu} + \dots\right]\psi^a\psi^b +\\
& - \bar\eta^\mu\eta^\nu\left[\delta_{\mu\nu} + \frac{1}{3}R_{\mu\alpha\beta\nu}\xi^\alpha\xi^\beta + \frac{1}{12}\nabla_\gamma R_{\mu\alpha\beta\nu}\xi^\alpha\xi^\beta\xi^\gamma + \right.
\end{aligned}$$

$$
\begin{aligned}
&+\left(\frac{1}{60}\nabla_\delta\nabla_\gamma R_{\mu\alpha\beta\nu}-\frac{1}{45}R_{\mu\alpha\beta}{}^{\rho}R_{\rho\gamma\delta\nu}\right)\xi^\alpha\xi^\beta\xi^\gamma\xi^\delta+\dots\Big]+\\
&+\beta\Big[2M\nabla_\mu M\xi^\mu+\sqrt{2}\nabla_a M\psi^a+\\
&+\left(M\nabla_\mu\nabla_\nu M+\nabla_\mu M\nabla_\nu M\right)\xi^\mu\xi^\nu+\sqrt{2}\nabla_a\nabla_\mu M\psi^a\xi^\mu+\dots\Big]\Big\},
\end{aligned}
\tag{9.51}
$$

where Riemann tensors and the order parameter M are evaluated at x_0. In the last line of (9.51) we used that RNC satisfy $\nabla\xi=0$ in the expansion of $\nabla_a M(x_0,\xi)$.

Now, the effective Lagrangian

$$
\mathcal{L}(x_0)=\int_0^\infty\frac{d\beta}{4\beta}\frac{1}{(2\pi\beta)^{\frac{D}{2}}}e^{-\beta M^2(x_0)}\left\langle e^{-\bar{S}_q^{(int)}}\right\rangle+\frac{1}{4G}M^2(x_0).
\tag{9.52}
$$

can be computed in two steps:

1. by evaluating
$$
\left\langle e^{-\bar{S}_q^{(int)}}\right\rangle
\tag{9.53}
$$
as a polynomial in β with coefficients depending on curvature's and M's invariants;

2. performing the β-integral as an Euler's Γ-function.

Thus, we have

$$
\left\langle e^{-\bar{S}_q^{(int)}}\right\rangle=1-\left\langle\bar{S}_q^{(int)}\right\rangle+\frac{1}{2}\left\langle\bar{S}_q^{(int)2}\right\rangle-\frac{1}{3!}\left\langle\bar{S}_q^{(int)3}\right\rangle+\dots.
\tag{9.54}
$$

At this point, some names to the various terms in (9.51) can be provided,

$$
\begin{aligned}
\bar{S}_q^{(int)}=&\,S_{1-1}+S_{1-1.5}+S_{1-2}+\dots\\
&+S_{2-1}+S_{2-1.5}+S_{2-2}+\dots\\
&+S_{3-1}+S_{3-1.5}+S_{3-2}+\dots\\
&+S_{4-1.5}+S_{4-2}+\dots,
\end{aligned}
\tag{9.55}
$$

in particular:

- $S_{1-\dots}$ are terms of lines 1 and 2 of (9.51);
- $S_{2-\dots}$ are terms of line 3 of (9.51);

- $S_{3-\dots}$ are terms of lines 4 and 5 of (9.51);
- $S_{4-\dots}$ are terms of lines 6 and 7 of (9.51).

The second index (where the dots are) indicates the β-order brought by that piece of action, remembering that (just by looking at the propagators (9.47))

$$\begin{aligned} &\xi \sim a \sim b \sim c \sim \psi \sim \beta^1 \\ &\eta \sim \beta^0. \end{aligned} \tag{9.56}$$

For instance, the first term is

$$S_{1-1} = \frac{1}{12\beta} R_{\mu\alpha\beta\nu} \int_0^1 d\tau \; \xi^\alpha \xi^\beta \left(\dot{\xi}^\mu \dot{\xi}^\nu + a^\mu a^\nu + b^\mu c^\nu \right), \tag{9.57}$$

which is linear in β. Here we report the values of the contractions needed up to β^2,

$$\begin{aligned} \left\langle S_{1-1} \right\rangle &= \frac{1}{36} R\beta \\ \left\langle S_{2-1} \right\rangle &= 0 \\ \left\langle S_{3-1} \right\rangle &= \frac{1}{18} R\beta \\ \left\langle S_{1-2} \right\rangle &= \frac{1}{360} \left[\frac{1}{2} \nabla^2 R - \frac{2}{9} {R_{\mu\nu}}^2 - \frac{1}{3} {R_{\mu\nu\rho\sigma}}^2 \right] \beta^2 \\ \left\langle S_{2-2} \right\rangle &= 0 \\ \left\langle S_{3-2} \right\rangle &= \frac{1}{540} \left[\frac{1}{2} \nabla^2 R - \frac{1}{3} {R_{\mu\nu}}^2 + \frac{1}{2} {R_{\mu\nu\rho\sigma}}^2 \right] \beta^2 \\ \left\langle S_{4-2} \right\rangle &= \frac{1}{6} \left[M \nabla^2 M + \left(\nabla_\mu M \right)^2 \right] \beta^2 \\ \left\langle {S_{1-1}}^2 \right\rangle |_{conn} &= \frac{1}{216} \left[\frac{1}{6} R^2 - \frac{19}{90} {R_{\mu\nu}}^2 + \frac{13}{5} {R_{\mu\nu\rho\sigma}}^2 \right] \beta^2 \\ \left\langle {S_{2-1}}^2 \right\rangle |_{conn} &= -\frac{1}{48} {R_{\mu\nu\rho\sigma}}^2 \beta^2 \\ \left\langle {S_{3-1}}^2 \right\rangle |_{conn} &= \frac{1}{108} \left[\frac{1}{3} R^2 - \frac{1}{5} {R_{\mu\nu}}^2 - \frac{1}{10} {R_{\mu\nu\rho\sigma}}^2 \right] \beta^2 \\ \left\langle S_{1-1} S_{2-1} \right\rangle |_{conn} &= 0 \\ \left\langle S_{1-1} S_{3-1} \right\rangle |_{conn} &= \frac{1}{324} \left[\frac{1}{2} R^2 + \frac{1}{5} {R_{\mu\nu}}^2 \right] \beta^2 \\ \left\langle S_{2-1} S_{3-1} \right\rangle |_{conn} &= 0, \end{aligned} \tag{9.58}$$

where, again, all quantities are evaluated at x_0. Putting everything together, we have

$$\mathcal{L}(x_0) = \frac{M^2}{4G} + \frac{1}{2(4\pi)^{\frac{D}{2}}} \int_0^\infty d\beta\, \beta^{-\frac{D}{2}-1} e^{-\beta M^2} \left[1 + \mathcal{A}_1\beta + \mathcal{A}_2\beta^2 + \dots\right], \tag{9.59}$$

with

$$\begin{aligned}
\mathcal{A}_1 &= -\frac{1}{12}R \\
\mathcal{A}_2 &= \frac{1}{288}R^2 + \frac{17}{38880}R_{\mu\nu}{}^2 - \frac{7}{1440}R_{\mu\nu\rho\sigma}{}^2 - \frac{1}{432}\nabla^2 R - \frac{1}{6}M\nabla^2 M - \frac{1}{6}\left(\nabla_\mu M\right)^2.
\end{aligned} \tag{9.60}$$

Integrating out β we get

$$\begin{aligned}
\bar{\Gamma}(x_0) = \frac{M^2}{4G} + \frac{1}{2(4\pi)^{\frac{D}{2}}}\Bigg[&\left(M^2\right)^{\frac{D}{2}} \Gamma\left(-\frac{D}{2}\right) + \mathcal{A}_1 \left(M^2\right)^{\frac{D}{2}-1} \Gamma\left(-\frac{D}{2}+1\right) + \\
&+ \mathcal{A}_2 \left(M^2\right)^{\frac{D}{2}-2} \Gamma\left(-\frac{D}{2}+2\right) + \dots\Bigg].
\end{aligned} \tag{9.61}$$

It's possible to see that the expansion (9.61), to the lowest order, reduces to equation (31) of [57] in flat space and to equations (69-70) therein in weakly curved spacetime, confirming the validity of the method. Hence, the discussion about spontaneous chiral symmetry breaking follows the same steps, for instance, of [57]. A clear advantage of the WL method is that it allows for a quite easy computation of the terms appearing in (9.61) when one wants to go beyond the linear contribution in the scalar curvature R, and/or consider inhomogeneous condensates $M(x)$. Obviously the evaluation of the mean field, *i.e.* the solution of $\int d^D x \sqrt{g}\mathcal{L}$ ought to be done numerically.

However one may also tackle the problem from a fully numerical view point, using a combination of WLMC and Creutz's algorithms. Focusing on equations (9.36) and (9.37), which we report here for simplicity

$$\begin{aligned}
\Gamma[M] =& \frac{1}{2}\int_0^\infty \frac{d\beta}{\beta} \int_{\text{PBC}} \mathcal{D}x^\mu \int_{\text{ABC}} \mathcal{D}\psi^a\, e^{-S[x^\mu,\psi^a,\omega_{\mu ab}]} + \frac{1}{4G}\int d^D x\, \sqrt{g}\, M^2(x) \\
S[x^\mu,\psi^a,\omega_{\mu ab}] =& \int_0^1 d\tau \left[\frac{1}{4\beta} g_{\mu\nu}(x)\dot{x}^\mu\dot{x}^\nu + \frac{1}{4\beta}\psi^a\left(\delta_{ab}\partial_\tau + \dot{x}^\mu\omega_{\mu ab}(x)\right)\psi^b + \right. \\
&\left. + \beta\left(M^2(x) + \sqrt{2}\psi^a\nabla_a M(x)\right) + V_{CT}(x)\right],
\end{aligned} \tag{9.62}$$

we can get rid of a volume integration over x_0 and consider the effective action density $\mathcal{L}(x_0)$ at fixed $x_0 = 0$ for instance. Now we can act as follows.

1. Sample WLMC points with the *YLOOPS*$^{(\alpha)}$ algorithm (with $\alpha \neq 0$ if needed) to generate loops with coinciding endpoints at zero.

2. For each point x, compute the spin-connection $\omega_{\mu ab}(x)$ and perform a Gaussian integration
$$\int_{ABC} D\psi^a \; e^{-\int_0^1 d\tau \; \frac{1}{4\beta}\psi^a(\delta_{ab}\partial_\tau + \dot{x}^\mu \omega_{\mu ab}(x))\psi^b}. \tag{9.63}$$

3. Perform the WLMC average.

Even restricting on a single point x_0, this calculation is huge: each point x of each worldline s requires a complete Creutz's integration and finally a global β-integration over the proper time length has to be done. With the actual means, an acceptably optimized numerical calculation for the effective action density of this model is not viable in reasonable times, hence we keep here this idea for possible future work, possibly after that the algorithms involved (in particular Creutz's one) finds a better and faster numerical optimization. Note also that, as pointed in Chapter 7, the suitable regularization to be adopted in WLMC is the time-slicing. Thus, the counterterm does not completely cancel against the $R/4$ term: there remains the $\Gamma\Gamma$ part, which is followed by a similar $\omega\omega$ contribution, associated to the regularization of the fermionic sector, in curved space (see [15]).

Chapter 10

A perturbative method for a particle on a rotating ring

In the present chapter we describe a project we collaborated on, where several of the ingredients discussed previously, such as effective actions and numerical approaches, are applied to a scalar QFT model representation of a cold atom system. Specifically we present a perturbative calculation for the effective action associated to a scalar particle living on a one-dimensional rotating ring in presence of a cut (constituting a barrier for the particle itself). This theoretical study [60] is motivated by the growing interest towards systems which involve confining optical traps. The scalar model setup that we will consider can be in principle adapted to study in an alternative way interacting atoms at very low temperatures, in presence of a spacial confinement inducing boundary conditions.

The starting point is to consider a scalar quantum field living on a ring. In this simple case it is quite obvious that a reciprocal rotation between the field and the ring does not produce any physical effect due to gauge invariance. The situation is substantially different when this invariance is broken by adding a defect (a barrier) along the ring, producing physical boundary conditions for the field. In this case, it is possible for a laboratory observer to detect an effective rotation of the ring, in opposition to a co-rotating observer who can't, by definition. Physically, this genuine rotation induces an artificial gauge field that can lead to the appearance of a persistent current along the ring. Examples of this phenomena involve the creation of Josephson junctions on toroidal Bose-Einstein condensates [61], toroidal Bose-Einstein condensate stirred by a rotating optical barrier [62], and spinor (^{87}Rb) condensates [63]. A similar study has been performed in [64] for an interacting non-relativistic scalar field on a ring in presence of a delta-function defect, and shows how the persistent current gets affected

by the barrier strength. Here we adopt a different strategy: firstly we focus on the field ground state rather than the current; secondly, interaction effects are imposed by a constraint on the field and the delta-function potential is replaced by boundary conditions. To do that, we make use of $O(N)$ nonlinear sigma models and employ zeta-function regularization on the effective action.

Let us now introduce the setup by defining a non-relativistic complex Schrödinger field Φ,

$$\Phi = \frac{1}{\sqrt{2}}\left(\phi_1 + i\phi_2\right) \tag{10.1}$$

for real fields ϕ_1 and ϕ_2. Its dynamics is given by the action

$$\begin{aligned} S_0 = \int dt \int dx \Big[\frac{i}{2}\left(\Phi^\dagger\dot{\Phi} - \Phi\dot{\Phi}^\dagger\right) - \frac{1}{2mR^2}\left|\frac{\partial\Phi}{\partial\varphi}\right|^2 - V(x)\left|\Phi\right|^2 + \\ + \frac{i\Omega}{2R}\left(\Phi^\dagger\Phi' - \Phi\Phi'^\dagger\right) - \frac{m}{2}\Omega^2\left|\Phi\right|^2\Big] \end{aligned} \tag{10.2}$$

with $x = \varphi R$ and m, R, V, Ω and φ being the mass, the ring radius, a generic scalar potential, the ring angular rotation velocity and the field angular velocity respectively. Such action is obtained starting from the one at $\Omega = 0$ and performing a coordinates change from the co-rotating frame ($\Omega = 0$) to the lab frame ($\Omega \neq 0$), $(t_0, \varphi_0) \to (t, \varphi)$,

$$t = t_0, \quad \varphi = \varphi_0 + \Omega t_0 \tag{10.3}$$

and

$$\frac{\partial}{\partial t_0} = \frac{\partial}{\partial t} + \Omega\frac{\partial}{\partial\varphi}, \quad \frac{\partial}{\partial\varphi_0} = \frac{\partial}{\partial\varphi} \tag{10.4}$$

together with

$$\Phi \to e^{i\frac{m}{2}\Omega^2 t}\Phi. \tag{10.5}$$

Already from eq. (10.2), we can assign to the rotation the role of a constant gauge (synthetic) field $A_\varphi = m\Omega R$. Before proceeding with the interacting theory, we briefly study the simpler non interacting case in absence of scalar potential. The equation of motion for the field Φ is given by

$$i\frac{\partial\Phi}{\partial t} + i\frac{\Omega}{R}\frac{\partial\Phi}{\partial\varphi} + \frac{1}{\rho}\frac{\partial^2\Phi}{\partial\varphi^2} - \frac{m\Omega^2}{2}\Phi = 0 \tag{10.6}$$

where we introduced $\rho = 2mR^2$. The time-independent version of (10.6) provides an equation for the eigenfunction $f_p(\varphi)$,

$$\frac{1}{\rho}\frac{\partial^2 f_p(\varphi)}{\partial\varphi^2} + i\frac{\Omega}{R}\frac{\partial f_p(\varphi)}{\partial\varphi} = \left(\frac{m\Omega^2}{2} - \lambda_p\right) f_p(\varphi) \tag{10.7}$$

with solution

$$f_p(\varphi) = N_p e^{-i\frac{\rho\Omega}{2R}\varphi}\sin(\varphi\Delta), \quad \Delta^2 = \lambda_p\rho. \tag{10.8}$$

where we imposed $f_p(0) = 0$. The continuity condition $f_p(2\pi) = 0$ sets

$$\Delta = \frac{p}{2}, \quad p \in \mathbb{N} \tag{10.9}$$

and consequently

$$\lambda_p = \frac{p^2}{4\rho}. \tag{10.10}$$

The one-loop effective action may be obtained moving to Euclidean time, $t \to -i\tau$ and integrating over quantum fluctuations $\delta\Phi$. In fact, the full field can be written as $\Phi = \bar{\Phi} + \delta\Phi$, where $\bar{\Phi}$ is a background field. In such way, the effective action reads

$$\Gamma[\bar{\Phi}] = \int_0^\beta d\tau \int dx\, \bar{\Phi}^\dagger \left[\frac{\partial}{\partial\tau} - \frac{1}{\rho}\frac{\partial^2}{\partial\varphi^2} - \frac{i\Omega}{R}\frac{\partial}{\partial\varphi} + \frac{m\Omega^2}{2}\right]\bar{\Phi} + \delta\Gamma \tag{10.11}$$

where

$$\delta\Gamma = \log\det\left(\frac{\partial}{\partial\tau} - \frac{1}{\rho}\frac{\partial^2}{\partial\varphi^2} - \frac{i\Omega}{R}\frac{\partial}{\partial\varphi} + \frac{m\Omega^2}{2}\right). \tag{10.12}$$

We notice that the background field $\bar{\Phi}$ does not appear in $\delta\Gamma$ whereas it does in the interacting case as we will see. Assuming periodic boundary conditions in Euclidean time, the complete eigenfunctions read $e^{-i\omega_n\tau}f_p(\varphi)$ with frequencies given by $\omega_n = 2\pi n/\beta$, $n \in \mathbb{Z}$. Physically, the quantity β is intended as the inverse temperature of the system or as the size of the box in the Euclidean time direction, which ultimately is set to infinity according to the zero temperature limit. The eigenvalues of the operator (10.12) can be written as

$$\varepsilon_{np} = i\omega_n + \lambda_p \tag{10.13}$$

and used within the zeta-regularization for the action,

$$\zeta(s) = \sum_{n=-\infty}^{\infty}\sum_p \varepsilon_{np}^{-s}, \tag{10.14}$$

so that

$$\delta\Gamma = 2\pi R\beta \left(\zeta(0)\log\ell - \zeta'(0)\right), \tag{10.15}$$

where ℓ indicates a renormalization scale with dimension of a length. Rewriting the zeta-function as the zero-temperature plus all the rest, gives

$$\zeta(s) = \sum_{p>0} \lambda_p^{-s} + \sigma(s), \quad \sigma(s) = \frac{\beta^2}{\Gamma(s)} \sum_{n=1}^{\infty} \sum_{\lambda_p>0} \frac{e^{-n\beta\lambda_p}}{n^{1-s}}, \tag{10.16}$$

where, as we said, $\lim_{T\to 0}\sigma = 0$. Thus only the first term in (10.16) contributes for zero temperatures. The vacuum energy contribution can be expressed in terms of Riemann zeta functions ζ_R,

$$\xi(s) = (4\rho)^s \sum_{p=1}^{\infty} p^{-2s} = (4\rho)^s \zeta_R(2s) \tag{10.17}$$

yielding

$$\delta\Gamma = 2\pi R\beta \frac{1}{2}\log\left(\frac{16\pi^2\rho}{\ell}\right). \tag{10.18}$$

We point out that imposing Dirichlet boundary conditions leads to a Ω-independent vacuum energy and thus a null persistent current. This comes with no surprise as DBCs suppress any flux through the boundary, as also found in [64].

The simplest way to introduce interactions is by enforcing a constraint on the field. We thus consider the action

$$S_\lambda = S_0 - \int dt \int dx\ \lambda(x)\left(|\Phi|^2 - z^2\right) \tag{10.19}$$

for a positive constant z. Extremizing with respect to the Lagrange multiplier, we have

$$0 = \frac{\delta S_\lambda}{\delta\lambda} = |\Phi|^2 - z^2 \tag{10.20}$$

which enforces interaction between the components of the multiplet Φ. Since the norm is kept fixed, any change in , say, ϕ_1 is reflected upon ϕ_2. Proceeding as before the one-loop Euclidean effective action reads

$$\Gamma = \int_0^\beta d\tau \int dx\ \bar\Phi^\dagger \left[\frac{\partial}{\partial\tau} - \frac{1}{\rho}\mathcal{D}^2\right]\bar\Phi + \lambda(x)\left(|\Phi|^2 - z^2\right) + \delta\Gamma \tag{10.21}$$

where now

$$\delta\Gamma = \log\det\left(\frac{\partial}{\partial\tau} - \frac{1}{\rho}\mathcal{D}^2 + \lambda(x)\right), \quad \mathcal{D} = \frac{\partial}{\partial\varphi} + i\frac{\rho}{2R}\Omega. \tag{10.22}$$

What prevents us from straightforwardly apply the same derivation of the non-interacting case is the fact that we don't know the form of the Lagrange multiplier function $\lambda(x)$, which plays the role of a fake mass (function), and does not correspond to any dynamical degree of freedom. We will use a mean field approximation. Hence, we express the determinant in (10.22) as

$$\delta\Gamma = -\lim_{s\to 0}\frac{d}{ds}\frac{1}{\Gamma(s)}\sum_{n=-\infty}^{\infty}\int_0^\infty \frac{dt}{t^{1-s}}e^{-i\omega_n t}\mathrm{Tr}\, e^{-\frac{t}{\rho}D} \tag{10.23}$$

with a new differential operator

$$D = -\mathcal{D}^2 + \rho\lambda(x). \tag{10.24}$$

Setting $t = \rho u$, $\eta = \frac{\beta}{\rho}$ and $\bar{\omega} = \frac{2\pi n}{\eta}$, we have

$$\delta\Gamma = -\lim_{s\to 0}\frac{d}{ds}\frac{\rho^2}{\Gamma(s)}\sum_{n=-\infty}^{\infty}\int_0^\infty \frac{du}{u^{1-s}}e^{-i\bar{\omega}_n u}\mathrm{Tr}\, e^{-uD}. \tag{10.25}$$

The functional trace can then be written in terms of the eigenvalues of D,

$$\mathrm{Tr}\, e^{-uD} = \sum_{\xi_p>0} e^{-\xi_p u}. \tag{10.26}$$

Assuming non-negative eigenvalues, we perform a heat-kernel expansion

$$\mathrm{Tr}\, e^{-uD} \simeq K(u) = \sqrt{\frac{1}{2\pi u}}\sum_{k\in\mathbb{N}} a_k(\lambda)u^k + \text{boundary terms} \tag{10.27}$$

and consider only bulk terms. Boundary terms can be added later. The one-loop effective action hence reads

$$\delta\Gamma = -\lim_{s\to 0}\frac{d}{ds}\frac{\rho^s}{\Gamma(s)}\sum_{n=-\infty}^{\infty}\int_0^\infty \frac{du}{u^{1-s}}e^{-i\bar{\omega}_n u}K(u). \tag{10.28}$$

It turns out to be useful to rewrite the exponential term using the following identity

$$\sum_{n=-\infty}^{\infty} e^{inu} = \eta\sum_{n=-\infty}^{\infty}\delta(u-\eta n) \tag{10.29}$$

to get

$$\delta\Gamma = -\lim_{s\to 0}\frac{d}{ds}\frac{\eta\rho^s}{\Gamma(s)}\sum_{n=-\infty}^{\infty}\int_0^\infty \frac{du}{u^{1-s}}\delta(u-\eta n)K(u)\theta_{\text{reg}}(u), \tag{10.30}$$

where a regularizing θ_{reg}-function ($\theta_{\text{reg}} \to \theta$) is included in order to perform the integration over u will keeping the integrand continuous at $u = 0$. Proceeding with the calculation, we get

$$\begin{aligned}\delta\Gamma = &-\lim_{s\to 0}\lim_{n\to 0}\frac{d}{ds}\frac{(\rho\eta)^s}{\Gamma(s)}n^{s-1}K(\eta n)\theta_{\text{reg}}(\eta n)+\\ &-\lim_{s\to 0}\frac{d}{ds}\frac{(\rho\eta)^s}{\Gamma(s)}\sum_{n=1}^{\infty}n^{s-1}K(\eta n)\end{aligned} \tag{10.31}$$

where the first term ($n = 0$) is independent on λ and $\bar{\Phi}$. We then get

$$\begin{aligned}\delta\Gamma =& -\lim_{n\to 0}\left[\frac{a_0}{n^{3/2}}+\eta\frac{a_1}{\sqrt{n}}\right]\frac{\theta_{\text{reg}(0)}}{\sqrt{2\pi\eta}}+\\ &-\frac{1}{\sqrt{2\pi\eta}}\lim_{s\to 0}\frac{d}{ds}\frac{(\rho\eta)^s}{\Gamma(s)}\sum_{k\in\mathbb{N}}\zeta_R\left(\frac{3}{2}-k-s\right)\eta^k a_k\\ =&-\sqrt{\frac{\eta}{2\pi}}a_1\lim_{n\to 0}\frac{\theta_{\text{reg}}(0)}{\sqrt{n}}-\frac{1}{\sqrt{2\pi n}}\sum_{k=1}^{\infty}\zeta\left(\frac{3}{2}-k\right)\eta^k a_k\end{aligned} \tag{10.32}$$

where, in the last line, the a_0-term has been dropped since it does not depend on the background field or λ and disappears from the equation of motion. The first four coefficients are given by

$$\begin{aligned}a_0 =&\beta\int dx\ 1\\ a_1 =&\beta\int dx\ (-\lambda)\\ a_2 =&\beta\int dx\ \left(\frac{1}{2}\lambda^2-\frac{1}{6}\mathcal{D}^2\lambda\right)\\ a_3 =&\beta\int dx\ \left(-\frac{1}{6}\lambda^3+\frac{1}{12}(\mathcal{D}\lambda)^2+\frac{1}{6}\lambda\mathcal{D}\lambda-\frac{1}{60}\mathcal{D}^6\lambda\right)\end{aligned} \tag{10.33}$$

and can be used inside (10.32) to have en explicit expression for $\delta\Gamma$ which can be used to derive the equations of motion for $\bar{\Phi}$, its conjugate and λ. As a result, we have a system of nonlinear coupled differential equations,

$$\begin{aligned}X_1' =&X_2\\ X_2' =&\frac{m\rho\Omega^2}{2}X_1+\rho Z_1 X_1+\frac{\rho\Omega}{R}Y_2\end{aligned}$$

$$
\begin{aligned}
Y_1' =& Y_2 \\
Y_2' =& \frac{m\rho\Omega^2}{2} Y_1 + \rho Z_1 Y_1 - \frac{\rho\Omega}{R} X_2 \\
Z_1' =& Z_2 \\
Z_2' =& 3Z_1^2 - \mathcal{M} Z_1 - \mathcal{U}
\end{aligned}
\tag{10.34}
$$

where

$$
\begin{aligned}
X_1 =& \text{Re}\,\bar{\Phi}, \quad Y_1 = \text{Im}\,\bar{\Phi}, \quad Z_1 = \lambda, \\
X_2 =& \text{Re}\,\bar{\Phi}', \quad Y_2 = \text{Im}\,\bar{\Phi}', \quad Z_2 = \lambda', \\
\mathcal{U} =& \frac{\pi\rho^3\Omega^2\zeta(3/2)}{3R^2\beta\zeta(5/2)} - \frac{6\rho^2\zeta(1/2)}{\beta^2\zeta(-3/2)} + \\
& - 6\sqrt{\frac{2\pi\rho^5}{\beta^5}} \frac{\left(X_1^2 + X_2^2 - z_{\text{ren}}^2\right)}{\zeta(-3/2)} - \frac{1}{10}\left(\frac{\rho\Omega}{2R}\right)^4, \\
\mathcal{M} =& 8\pi\frac{\zeta(3/2)\rho}{\zeta(5/2)\beta} - 3\left(\frac{\rho\Omega}{2R}\right)^2,
\end{aligned}
\tag{10.35}
$$

with z_{ren} being the renormalized coupling. The above equations have been solved using *Python* routines by fixing left boundary conditions at $\varphi = 0$ and shooting to the right. A tolerance of $\epsilon = 10^{-2}$ is kept for the right boundary condition. The left boundary values have been varied according to the intervals: $10^{-3} \leq \text{Re}\,\bar{\Phi}_{\varphi=0} \leq 1.4$, $10^{-3} \leq \text{Im}\,\bar{\Phi}_{\varphi=0} \leq 1.4$, $-10^{-3} \leq \text{Re}\,\bar{\Phi}'_{\varphi=0} \leq 1.1$, $-10^{-3} \leq \text{Im}\,\bar{\Phi}'_{\varphi=0} \leq 1.1$, $-1.90 \leq \lambda'_{\varphi=0} \leq 0.81$. The value of $\lambda_{\varphi=0}$ has been rescaled to 1. For the boundary conditions on the right we have aimed at solutions satisfying continuity and (anti-) periodicity for the real and imaginary part, so that the squared modulus Φ^2 was periodic. This was done with a tolerance of 1%. Physical parameters have been set as follows: $mR = 0.3$, $\beta/R = 10$, $z = 0.1$. In our simulations we also set $R = 1$. These choices where made in order to keep mass and temperature at small values, accordingly to our theoretical assumptions. Fig. 10.1 shows illustrative results for numerical solutions of Φ^2 and λ for values of $\Omega = 0, 0.5, 1$. Attempts for intermediate values of Ω have been explored without finding any satisfying solution. We remark that our system, within our approximations, is analogous to a second order equation with a delta-potential representing the boundary. Upon integration across the left boundary, we get the jump on the first derivative; if the field is continuous, we have $\partial\Phi|_{\varphi=0^+} - \partial\Phi|_{\varphi=0^-} \propto \xi\Phi(0)$, where ξ encodes the height of the barrier. To sum up, the jump of the first derivative gives a measure of the strength of the barrier. We finally point out that our solutions of

Fig. 10.1 show a behaviour which is similar to those of [64]: solutions are peaked at $\varphi = \pi$ and slowly descend towards boundaries. We also found out-of-phase solutions having larger amplitudes and peaked at $\varphi = \pi/2$: they are continuous at the boundary and are dephased with respect to the ones peaked at $\varphi = \pi$. Both kinds of solutions have to be intended as ground state solutions, not excited levels: they just obey different boundary conditions. Moreover, some solutions clearly show a behaviour which is similar to those of [64], namely the ones which are peaked at $\varphi = \pi$ and decrease smoothly towards the boundaries. The out-of-phase solutions with larger amplitude (peaked at $\varphi = \frac{\pi}{2}$) join continuously at the boundaries and are dephased with the previous set of solutions. We also point out a similarity between the amount of dephasing and the detuning of the boundary conditions; if these ones deviate from those producing the solutions symmetric with respect to the center of the interval, hence the resulting solution gets a phase. This is mathematically trivial (let us just think about plane waves), but it suggests a way to measure a deviations from specified boundary conditions.

This study we showed in this chapter is based upon heat kernel techniques, and can be seen as a complementary part rather than an alternative to worldline techniques, which are being extensively studied throughout this thesis. In fact, in principles, the problem of a scalar field defined on a ring with a cut could be also studied as a 1-dimensional linear σ-model, mapping the circle onto a segment where the extrema are the two sides of the cut. However, some difficulties can arise when trying to represent the rotation in this new setup, and when building worldlines which satisfy continuity on the boundaries.

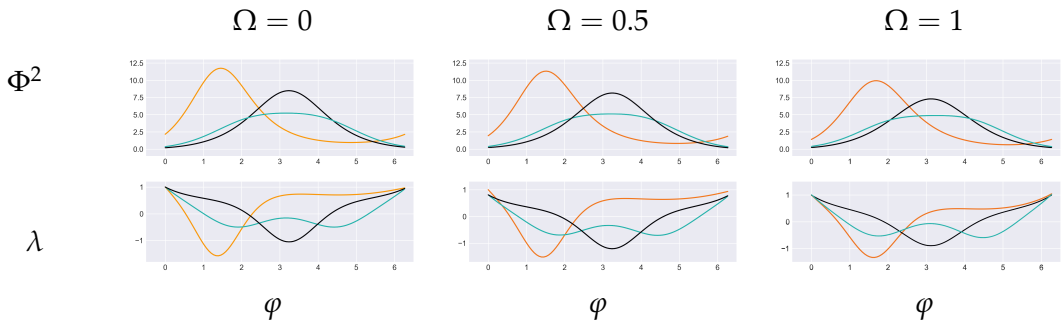

FIGURE 10.1: The figure shows the numerical solutions for Φ^2 and λ for illustrative values of the rotational velocity Ω. We have selected the parameters as follows: $m \times R = 0.3$, $\beta/R = 10$, and $z = 0.1$. The curves correspond to the following solutions: for $\Omega = 0$, orange $\Rightarrow$ ($\bar{\Phi}_{\varphi=0} = 1.121$, $\bar{\Phi}'_{\varphi=0} = 0.95$, $\lambda'_{\varphi=0} = -1.66$), cyan $\Rightarrow (0.001, 0.60, -1.19)$, black $\Rightarrow (0.001, 0.44, -0.76)$; for $\Omega = 0.5$, orange $\Rightarrow (1.011, 0.96, -1.57)$, cyan $\Rightarrow (0.001, 0.60, -1.23)$, black $\Rightarrow (0.001, 0.44, -0.80)$; for $\Omega = 1$, orange $\Rightarrow (1.001, 0.58, -1.37)$, cyan $\Rightarrow (0.001, 0.61, -1.37)$, black $\Rightarrow (0.001, 0.47, -0.92)$.

Chapter 11

Conclusions

In this thesis we have seen how first quantization path integrals can be used to represent and calculate relevant quantities from quantum field theory, such as particle propagators, trace anomalies and effective actions. We have considered both analytical and numerical approaches. After building the general theory for flat spaces, defining then σ-models, we moved to the more general case of curved spaces, where gravity enters as a background. We realized that a lot of subtle points have to be treated carefully, in particular when we consider a non-trivial metric as a source for the space curvature, each perturbative term of the expansion of the path integral gets affected by divergences which bring infinities and ambiguities. Knowing that the result must be finite (and unambiguous), these divergences have to be cancelled properly, and the rule for that is given by three known regularization schemes which are time-slicing, mode regularization and dimensional regularization. In particular we applied the latter to the calculation of the (perturbatively approximated) trace anomaly of a scalar particle living in a maximally symmetric space, adopting a string-inspired BRST quantization of the associated path integral. We also proved the direct equivalence between MR and DR for the particle transition amplitude on a more general space, checking order by order that, although the two techniques give rise to different valued Feynman diagrams, the result doesn't change. We then moved to the numerical part of the thesis: we defined the worldline Monte Carlo (WLMC) method to represent numerically a sample of some of the worldline trajectories which we can imagine the scalar particle travels when a scalar path integral in flat space is considered. In particular we generalized the *YLOOPS* algorithm (one of the most famous ones) to the case of little quadratic term insertion, *i.e.* the *YLOOPS*$^{(\alpha)}$ algorithm. Next, we adapted the WLMC machinery to the case of curved spaces, finding then a new way of treating curved space problems using a numerical technique. We tested this new method using the

YLOOPS$^{(\alpha)}$ algorithm and computing the scalar propagator of a particle moving in a maximally symmetric space, for which the previous analytical (perturbative) solutions can be used as a comparison. This numerical method provides a non-perturbative solution to a problem which has always been treated perturbatively. We then addressed numerically other models, including Casimir configurations and electromagnetic backgrounds. Next, we moved to the more (numerically) complicated problem of Grassmannian path integrals, *i.e.* path integrals involving anticommuting variables. We presented an algorithm originally developed by Creutz and tested its validity on a toy model, the fermionic harmonic oscillator. At this point we have all the ingredients to aim to a numerical treatment of bosonic and spinning non-linear σ-models, an example of which is the Gross-Neveu model. This path integral could be done numerically coupling the WLMC technique in curved space with the Creutz's algorithm, however an actual computation would require more computer power than affordable by us. Finally we ended up with a numerical calculation of the lowest order energies of a system constituted by a scalar field rotating on a one-dimensional ring having a punctual defect on it. We obtained the associated field equations for this model and solved them numerically.

The biggest effort in this work was to find a strategy which was as general as possible to numerically represent and solve σ-models embedded in curved space by using non-perturbative methods. We proved the WLMC formalism, born for flat space worldline path integrals, can be profitably used even with curved space. Our technique may find several interesting fields of applications, including strong curvature-problems, instanton calculations and Schwinger's pair creation.

Appendix A

Curvature tensors conventions

In this brief appendix we fix the conventions involving the curvature tensors used in the present thesis. The Riemann curvature tensor is obtained, as usual, by acting on a vector V^ρ with the commutator of covariant derivatives $[\nabla_\mu, \nabla_\nu]$, *i.e.*

$$[\nabla_\mu, \nabla_\nu]V^\rho = R_{\mu\nu}{}^\rho{}_\sigma V^\sigma, \tag{A.1}$$

which, in turn, gives

$$R_{\mu\nu}{}^\rho{}_\sigma = \partial_\mu \Gamma^\rho{}_{\nu\sigma} + \Gamma^\rho{}_{\mu\lambda}\Gamma^\lambda{}_{\nu\sigma} - \partial_\nu \Gamma^\rho{}_{\mu\sigma} - \Gamma^\rho{}_{\nu\lambda}\Gamma^\lambda{}_{\mu\sigma}. \tag{A.2}$$

The Ricci tensor is here defined by contracting the central indices,

$$R_{\mu\nu} = R_{\mu\sigma}{}^\sigma{}_\nu, \tag{A.3}$$

whereas the curvature scalar is given by

$$R = R_\mu{}^\mu, \tag{A.4}$$

which is negative for spheres.

Appendix B

WLMC convergence with tiny mass term

Adding a tiny mass whose role is played by the parameter α implies a relevant improvement for our heat kernel numerical evaluation. We actually point out that this trick is used only at the stage of the worldline generation, namely when we implement the $YLOOPS^{(\alpha)}$ algorithm instead of $YLOOPS^{(0)}$. Hence, only the shape of the worldlines gets affected, leaving the form of the potential untouched. The latter is calculated on spacetime points whose position depends also on the parameter α. The reason for this choice is that the introduction of α helps the point-particle to explore more accurately the region which is closer to the endpoints (the origin in the case the heat kernel reads $I(0,0;\beta)$), which is optimal for localized potentials like those we are treating mostly. This strategy can be seen as a counterforce (partially at least) against the *undersampling* issue, which forces the particle to move away from the region when the localized potential is relevant at large β.

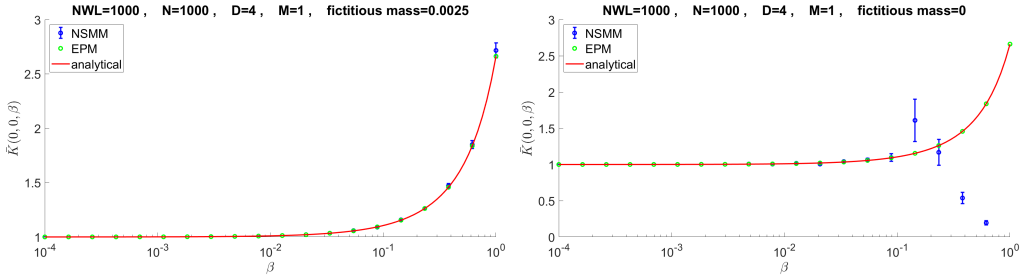

(a) (b)

FIGURE B.1: Two calculations of the heat kernel of a free scalar particle on a 4-sphere with $(N_{WL}, N) = (1000, 1000)$ and $M = 1$. For the left figure, a tiny fictitious mass has been introduced ($\alpha = 0.0025$) in the WL sampling. The right figure is obtained with ($\alpha = 0$), i.e. no fictitious mass term.

In Figures B.1 we show two calculation of the heat kernel on a sphere where the algorithms *YLOOPS*$^{(\alpha)}$ and *YLOOPS*$^{(0)}$ have been used respectively. In the first case we used the value $\alpha = 0.0025$, whereas all other parameters are shared among the two computations ($M = 1$, $D = 4$ and $(N_{WL}, N) = (1000, 1000)$). Figure B.1(b) clearly does not well reproduces the behaviour of the heat kernel, whilst B.1(a) does since we chose $\alpha \neq 0$. Hence, a little change in the value of α is capable of shrinking the worldline cloud around the origin so that it can reproduce the expected behaviour satisfactorily.

We also investigated a possible dependence of α_{min} (the value which minimizes on average the error between NSMM and EPM) with respect to curvature of the MS space. To such a purpose, we considered hyperboloids with sectional curvatures $|M| = 0.01$ and 1.

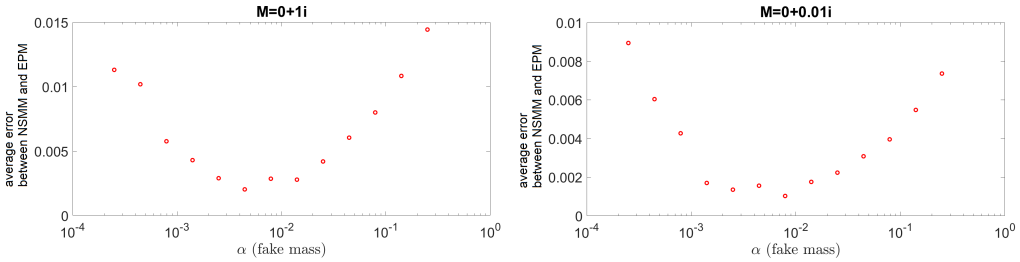

(a) (b)

FIGURE B.2: Comparison between heat kernel calculations of a free scalar particle on the hyperboloid for $|M| = 1,\ 0.01$. Each point denotes a single simulation: on the horizontal axis we have the value of the fictitious mass parameter α adopted, whereas vertically we have reported an arithmetic average of distance between the data of the non-linear sigma model method and the ones of the effective potential method (assumed as a benchmark). The α-value which minimizes the error does not qualitatively depend on the curvature of the space.

In Figure B.2 we see the numerical dependence of the average error between NSMM and EPM on α for $|M| = 1$ and 0.01. The two parabolas allow to detect an optimal value α_{min} which minimizes such error for the two curvatures and what we notice is that this value is substantially independent of $|M|$ over two orders of magnitude (intermediate values of $|M|$ exhibit similar results). To see the minimized average error directly at work, let us consider Figure B.2(a) and extrapolate the minimum via a quadratic fitting (still on log-scale), obtaining $\alpha_{min} = 10^{\bar{\alpha}}$. Then we take two logarithmically equally space points around α_{min}, that is $\alpha_- = 10^{\bar{\alpha}-\Delta}$ and $\alpha_+ = 10^{\bar{\alpha}+\Delta}$, with $\Delta > 0$.

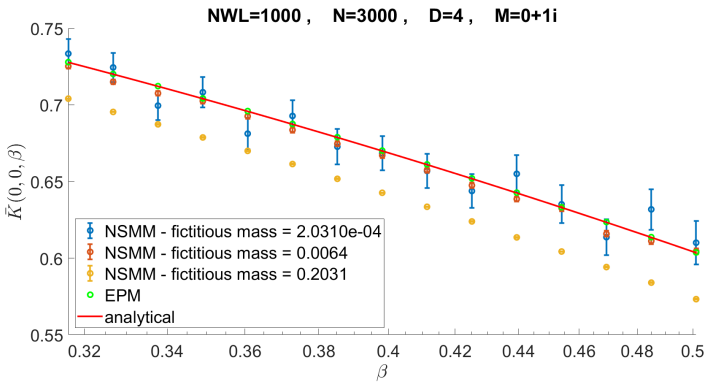

FIGURE B.3: Calculations of the heat kernel for the free scalar particle on a hyperboloid with $D = 4$ and $|M| = 1$, for a window of β-values. The plot shows the comparison of the calculation when different values of α are implemented, in particular $\alpha_{min} = 0.0064$, $\alpha_- = 0.0002$ and $\alpha_+ = 0.2031$.

In Figure B.3 we fixed $\Delta = 1.5$ (arbitrary) and $\bar{\alpha} = 2.1923$ (from the fitting), and computed a portion of the heat kernel for the point-particle on the hyperboloid. As expected, the red points (which correspond to α_{min}) are those which better reproduce the behaviour of the heat kernel.

Appendix C

MATLAB code for WLMC in curved space

In Figure C.1 we show an example of the MATLAB code we used to compute the heat kernel of the free scalar particle on a sphere with EPM and NSMM method.

- lines 1-15. Initialization of the main variables including: number of points per WL, number of WLs, α-parameter, number of Euclidean spacetime dimensions, sectional radius of the sphere, total propertime β-range of values, variables to memorize the results, WL endpoints.
- lines 52-166. Creation of flat and curved space coefficients for the $YLOOPS^{(0)}$ and $YLOOPS^{(\alpha)}$ algorithms respectively. Construction of the worldlines. Computation of the flat and curved space potentials. Computation of the heat kernels for flat and curved spaces with associated errors.
- lines 167-176. Construction of the analytical curve for the heat kernel.
- lines 177-188. Figure production.
- lines 190-223. Declaration of the functions used in the script.

```
N=3000;
NWL=1000;
NMC=1;
alpha=0.0025;
D=4;
M=1;
inizio=-4;
fine=0;
passo=20;
bbeta=logspace(inizio,fine,passo);
PROPcurved_no_gGG=zeros(1,length(bbeta),NMC);
PROPcurved_yes_gGG=zeros(1,length(bbeta),NMC);
PROPflat=zeros(1,length(bbeta),NMC);
initialstate=0*ones(1,D);
finalstate=0*ones(1,D);

closedloop=0;
if isequal(initialstate,finalstate)
    closedloop=1;
end
conta=0;
jjj=0;
errori=zeros(length(bbeta),1);
for nmc=1:1:NMC
    jcont=0;
    potenziali=zeros(1,length(bbeta),NMC);
    for beta=bbeta
        erroris=zeros(NWL,1);
        jjj=jjj+1;

        %%%%%%% flat coefficients
        coeffflat=zeros(1,N-1);
        coeffflat(1)=2;
        for i=2:1:N-1
            coeffflat(i)=coeffflat(1)-1/(coeffflat(i-1));
        end
        %%%%%%%

        %%%%%%% curved coefficients
        coeffcurved=zeros(1,N-1);
        coeffcurved(1)=2+alpha;
        for i=2:1:N-1
            coeffcurved(i)=coeffcurved(1)-1/(coeffcurved(i-1));
        end
        %%%%%%

        wcurved_yesG=0;
        wflat=0;
        wpot=0;
        for s=1:1:NWL
            conta=conta+1;
            switch closedloop
                case 0 % open loop
                    xflat=zeros(1,D,N+1);
                    xcurved=zeros(1,D,N+1);
                    om=zeros(D,N-1);
                    for i=1:1:N-1
                        om(:,i)=Metropolis2(D);
                    end
```

```
 60                      xflat(1,:,2)=sqrt(2/N)*sqrt(1/(coeffflat(N-1)))*om(:,1);
 61                      xcurved(1,:,2)=sqrt(2/N)*sqrt(1/(coeffcurved(N-1)))*om(:,1);
 62                      for i=3:1:N
 63                          xflat(1,:,i)=sqrt(2/N)*sqrt(1/(coeffflat(N-i+1)))*om(:,↙
i-1)'+(1/(coeffflat(N-i+1)))*xflat(1,:,i-1);
 64                          xcurved(1,:,i)=sqrt(2/N)*sqrt(1/(coeffcurved(N-i+1)))*om↙
(:,i-1)'+(1/(coeffcurved(N-i+1)))*xcurved(1,:,i-1);
 65                      end
 66                      xflat(1,:,1)=zeros(1,D,1);
 67                      xflat(1,:,N+1)=zeros(1,D,1);
 68                      xcurved(1,:,1)=zeros(1,D,1);
 69                      xcurved(1,:,N+1)=zeros(1,D,1);
 70                      for qq=1:N+1
 71                          xflat(1,:,qq)=xflat(1,:,qq)+initialstate;
 72                          xcurved(1,:,qq)=xcurved(1,:,qq)+initialstate;
 73                      end
 74                      for qq=2:N+1
 75                          xflat(1,:,qq)=xflat(1,:,qq)+qq/(N+1)*(finalstate-↙
initialstate);
 76                          xcurved(1,:,qq)=xcurved(1,:,qq)+qq/(N+1)*(finalstate-↙
initialstate);
 77                      end
 78                  case 1 % closed loop
 79                      xflat=zeros(1,D,N+1);
 80                      xcurved=zeros(1,D,N+1);
 81                      om=zeros(D,N-1);
 82                      for i=1:1:N-1
 83                          om(:,i)=Metropolis2(D);
 84                      end
 85                      xflat(1,:,2)=sqrt(2/N)*sqrt(1/(coeffflat(N-1)))*om(:,1);
 86                      xcurved(1,:,2)=sqrt(2/N)*sqrt(1/(coeffcurved(N-1)))*om(:,1);
 87                      for i=3:1:N
 88                          xflat(1,:,i)=sqrt(2/N)*sqrt(1/(coeffflat(N-i+1)))*om(:,↙
i-1)'+(1/(coeffflat(N-i+1)))*xflat(1,:,i-1);
 89                          xcurved(1,:,i)=sqrt(2/N)*sqrt(1/(coeffcurved(N-i+1)))*om↙
(:,i-1)'+(1/(coeffcurved(N-i+1)))*xcurved(1,:,i-1);
 90                      end
 91                      xflat(1,:,1)=zeros(1,D,1);
 92                      xflat(1,:,N+1)=zeros(1,D,1);
 93                      xcurved(1,:,1)=zeros(1,D,1);
 94                      xcurved(1,:,N+1)=zeros(1,D,1);
 95                      for qq=1:N+1
 96                          xflat(1,:,qq)=xflat(1,:,qq)+initialstate;
 97                          xcurved(1,:,qq)=xcurved(1,:,qq)+initialstate;
 98                      end
 99              end
100              xflat=xflat*sqrt(beta);
101              xcurved=xcurved*sqrt(beta);
102              fact=1;
103              qcurved=0;
104              qflat=0;
105              pot=0;
106              for qq=2:1:N+1
107                  mezzotutto=(xcurved(1,:,qq)+xcurved(1,:,qq-1))/2;
108                  fact=fact*sqrt((1+func(mezzotutto,M))^(D-1));
109                  mat=zeros(D,D);
110                  for i1=1:1:D
111                      for i2=1:1:D
112                          mat(i1,i2)=(i1==i2)-(mezzotutto(i1))*(mezzotutto(i2))/↙
```

```
(mezzotutto*mezzotutto');
113                     end
114                 end
115                 mat=mat*func(mezzotutto,M);
116                 qcurved=qcurved+((xcurved(1,:,qq)-xcurved(1,:,qq-1))*mat*↙
(xcurved(1,:,qq)-xcurved(1,:,qq-1))');
117             end
118             qcurved=qcurved*(N/2)/beta;
119             for n=2:1:N+1
120                 y_vec=0.5*(xcurved(1,:,n)+xcurved(1,:,n-1));
121                 y_2=(0.5*(xcurved(1,:,n)+xcurved(1,:,n-1)))*(0.5*(xcurved(1,:,n)↙
+xcurved(1,:,n-1)))';
122                 y=sqrt(y_2);
123                 acca=funzione_h(y_vec,M);
124                 f_primo=func_primo(y_vec,M);
125                 funz=func(y_vec,M);
126                 pot=pot-(beta/8/N)*((f_primo*(-4*(D-1)*funz*(1+acca)^2+f_primo*↙
(1*D+acca^2-D*acca^2)*y))/y);
127             end
128             for qqflat=1:1:N
129                 qflat=qflat+beta/2/N*(V(xflat(1,:,qqflat),D,M)+V(xflat(1,:,↙
qqflat+1),D,M));
130             end
131             wcurved_yesG=wcurved_yesG+fact*exp(-qcurved-pot);
132             erroris(s)=fact*exp(-qcurved-pot);
133             wflat=wflat+exp(-qflat);
134             fprintf('build potential - - - %2.2f %% (beta # %i of %i) (MC # %i↙
of %i)\n',100*conta/NWL/length(bbeta)/NMC,jcont,length(bbeta),nmc,NMC);
135         end
136         wcurved_yesG=wcurved_yesG/NWL;
137         PROPcurved_yes_gGG(1,jcont,nmc)=wcurved_yesG*exp(+beta/8*M^2*(D-1)*D);
138         somma=0;
139         for s=1:NWL
140             somma=somma+(erroris(s)-PROPcurved_yes_gGG(1,jcont,nmc))^2;
141         end
142         somma=somma/NWL/(NWL-1);
143         somma=sqrt(somma);
144         errori(jcont)=somma;
145         wflat=wflat/NWL;
146         PROPflat(1,jcont,nmc)=wflat;
147         xflat=xflat/sqrt(beta);
148         xcurved=xcurved/sqrt(beta);
149     end
150 end
151 PROPcurved_no_gGG_real=zeros(1,length(bbeta));
152 PROPcurved_yes_gGG_real=zeros(1,length(bbeta));
153 for nmc=1:1:NMC
154     PROPcurved_yes_gGG_real(1,:)=PROPcurved_yes_gGG_real(1,:)+PROPcurved_yes_gGG↙
(1,:,nmc);
155 end
156 PROPcurved_yes_gGG_real(1,:)=PROPcurved_yes_gGG_real(1,:)/NMC;
157 PROPflat_real=zeros(1,length(bbeta));
158 for nmc=1:1:NMC
159     PROPflat_real(1,:)=PROPflat_real(1,:)+PROPflat(1,:,nmc);
160 end
161 PROPflat_real(1,:)=PROPflat_real(1,:)/NMC;
162 potenziali_real=zeros(1,length(bbeta));
163 for nmc=1:1:NMC
164     potenziali_real(1,:)=potenziali_real(1,:)+potenziali(1,:,nmc);
```

```
end
potenziali_real(1,:)=potenziali_real(1,:)/NMC;
bbetath=logspace(inizio,fine,passo*5);
bbetath2=logspace(inizio,fine,passo);
PROPth=zeros(1,length(bbetath));
PROPth2=zeros(1,length(bbetath2));
for b=1:1:length(bbetath)
    PROPth(b)=exp(D*(D-1)*bbetath(b)*M^2/12+D*(D-1)*(D-3)*(-(bbetath(b)*M^2)↙
^2/720-(bbetath(b)*M^2)^3/factorial(7)*2*(D+2)/9-(bbetath(b)*M^2)^4/factorial(7)*↙
(D^2+20*D+15)/360+(bbetath(b)*M^2)^5/factorial(11)*8*(D+2)*(D^2-12*D-9)/3+(bbetath↙
(b)*M^2)^6/factorial(13)*8*(1623*D^4-716*D^3-65930*D^2-123572*D-60165)/315+(bbetath↙
(b)*M^2)^7/factorial(13)*16*(D+2)*(33*D^4+404*D^3-2510*D^2-6612*D-3915)/315-(bbetath↙
(b)*M^2)^8/factorial(17)*8/45*(12405*D^6-810668*D^5-↙
1953995*D^4+17853784*D^3+71217159*D^2+92279700*D+40157775)));
end
for b=1:1:length(bbetath2)
    PROPth2(b)=exp(D*(D-1)*bbetath2(b)*M^2/12+D*(D-1)*(D-3)*(-(bbetath2(b)*M^2)↙
^2/720-(bbetath2(b)*M^2)^3/factorial(7)*2*(D+2)/9-(bbetath2(b)*M^2)^4/factorial(7)*↙
(D^2+20*D+15)/360+(bbetath2(b)*M^2)^5/factorial(11)*8*(D+2)*(D^2-12*D-9)/3+(bbetath2↙
(b)*M^2)^6/factorial(13)*8*(1623*D^4-716*D^3-65930*D^2-123572*D-60165)/315+(bbetath2↙
(b)*M^2)^7/factorial(13)*16*(D+2)*(33*D^4+404*D^3-2510*D^2-6612*D-3915)/315-↙
(bbetath2(b)*M^2)^8/factorial(17)*8/45*(12405*D^6-810668*D^5-↙
1953995*D^4+17853784*D^3+71217159*D^2+92279700*D+40157775)));
end
figure(31)
hold on
titlename=strcat('NWL=',num2str(NWL),' ,    N=',num2str(N),' ,    D=',num2str↙
(D),' ,    M=',num2str(M),' ,    fictitious mass=',num2str(alpha));
errorbar(bbeta,PROPcurved_yes_gGG_real,errori,'bo','LineWidth',2)
hold on
plot(bbeta,PROPflat_real,'go',bbetath,PROPth,'r-','LineWidth',2)
set(gca,'XScale','log')
legend('NSMM','EPM','analytical','Location','northwest','FontSize',20);
title(titlename);
xlabel('$\beta$','Interpreter','Latex','FontSize',20)
ylabel('$\bar{K}(0,0,\beta)$','Interpreter','Latex','FontSize',20)
set(gca,'FontSize',20)

function [om]=Metropolis2(D)
csi=rand(2,D);
om=zeros(D,1);
for ddd=1:1:D
    om(ddd)=sqrt(-log(csi(1,ddd)))*cos(2*pi*csi(2,ddd));
end
end

function[out]=funzione_h(y,M)
out=-func(y,M)/(1+func(y,M));
end

function[out]=func_primo(y,M)
x=sqrt(y*y');
out=(2*sin(M*x)*cos(M*x)*M*x-2*sin(M*x)*sin(M*x))/(M^2*x^3);
end

function[out]=func(y,MM)
x=sqrt(y*y');
if x==0
    out=0;
```

```
211 else
212     out=(1-2*MM^2*x^2-cos(2*MM*x))/(2*MM^2*x^2);
213 end
214 end
215
216 function[out]=V(y,d,MM)
217 x=sqrt(y*y');
218 if x==0
219     out=d*(1-d)/12*MM^2;
220 else
221     out=d*(1-d)/12*MM^2+(d-1)*(d-3)/48/x^2/(sin(MM*x))^2*(5*MM^2*x^2-3+↙
(MM^2*x^2+3)*cos(2*MM*x));
222 end
223 end
```

FIGURE C.1: MATLAB code for the WLMC in curved space calculation of the heat kernel of a scalar point particle on a sphere.

Appendix D

MATLAB code for Grassmann path integrals

Here we report the MATLAB code we use to compute the fermionic harmonic oscillator propagator using Creutz's algorithm.

```
clc; clearvars; close all;
N=200;   % number of discretized Grassmann integrals (even, >=2)

bmin=0;
bmax=50;
bpace=0.5;
bint=bmin:bpace:bmax;

result=zeros(1,length(bint));    % array to store values of the path integrals

index=0;
for beta=bint
    % computation of the path integral for each beta
    index=index+1;

    % start building the fHO-action (kinetic part)
    S=zeros(N+N/2,3);
    for i=1:1:N
        for j=1:1:3
            if j==1
                S(i,1)=(-1)^(i);
            elseif j==2
                if rem(i,2)==1
                    S(i,2)=i;
                    S(i,3)=i+1;
                else
                    S(i,2)=i-1;
                    S(i,3)=i-2;
                end
            end
        end
    end

    S(2,3)=N;
    S(2,1)=-S(2,1);
    % impose antiperiodic boundary conditions (ABC)

    % start building the fHO-action (interaction part)
    for i=N+1:1:N+N/2
        for j=1:1:3
            if j==1
                S(i,1)=-1;
                S(i,1)=S(i,1)*beta/N;
            elseif j==2
                S(i,2)=(i-N)*2-1;
                S(i,3)=(i-N)*2-2;
            end
        end
    end

    S(N+1,1)=-S(N+1,1);
    S(N+1,3)=N;

    % S is made of 3 columns; each row is a piece of action; the first
    % element is the coefficient the second and third ones are give the
    % number of the field involved

    F=ones(1,N+1);
    % "final" state (right-side): it's the state "fully
```

```
60  % occupied", that the action will provide to empty
61  % ("+1" to include the coefficient)
62
63  acc=1;
64  % variable to accumulate the result
65  aux=zeros(100,N);
66  % auxiliary arrays to store vectors manipulated by the action pieces
67
68  Saux=zeros(3,3,N);
69  % vector of N 3x3-matrices to store, for i=1:N,
70  % the lines of S where the grassmann i appears
71
72  for z=1:1:N
73      k=1;
74      for i=1:1:N+N/2
75          for j=2:1:3
76              % run over grassmanns of S
77              if z==S(i,j)
78                  Saux(k,:,z)=S(i,:);
79                  k=k+1;
80              end
81          end
82      end
83  end
84
85  % I noticed that in each matrix Saux(:,:,i) "similar" lines appear
86  % (similar in the sense that they have the same grassmann fields);
87  % I can goup them: be careful to the last line, where the grouping is
88  % different
89
90  Saux2=zeros(2,3,N);
91  % like Saux but grouped (see comment above)
92
93
94  for k=1:1:N-1
95      Saux2(1,:,k)=Saux(1,:,k);
96      Saux2(2,:,k)=Saux(2,:,k);
97      Saux2(2,1,k)=Saux(2,1,k)+Saux(3,1,k);
98  end
99
100 Saux2(1,:,N)=Saux(1,:,N);
101 Saux2(2,:,N)=Saux(2,:,N);
102 Saux2(1,1,N)=Saux(1,1,N)+Saux(3,1,N);
103
104 % now follow page (4): after each application of (1 \pm ...), apply
105 % "grouping" to the rows obtained
106
107 large=5;
108 A=zeros(1,N+1,N+1,large);
109 % this is a matrix of vectors: each vector is 1x(N+1)
110 % (that is a coefficient and the Fock state)
111 % the matrix is (N+1)x(a "large" number): a row of A is
112 % needed for each grassmann field (passing from a row to
113 % the next one means having applied (1-n_i)(1+S_i) to the
114 % current row). The first row is needed for
115 % the initial state (1,1,1,...1)
116
117 A(:,:,1,1)=F;
118 num=zeros(N+1,1);
```

```
119     num(1,1)=1;
120
121     for z=1:1:N
122         cc=0;
123         for t=1:1:num(z,1)
124             [nout,matout] = algo(A(:,:,z,t),z,N,Saux2);
125             % see "algo" for details
126             for j=1:1:nout
127                 A(:,:,z+1,j+cc)=matout(j,:);
128             end
129             cc=cc+nout;
130         end
131         %fprintf('\nnext\n');
132         %cc
133         if cc==large
134             error('\nWARNING!! EXCEEDING STORAGE MATRIX.\n');
135         end
136         num(z+1,1)=cc;
137         togroup=zeros(cc,N+1);
138         for ss=1:1:cc
139             togroup(ss,:)=A(:,:,z+1,ss);
140         end
141
142         % grouping of A
143         [matouter,counter] = grouping (togroup,N,cc);
144
145         for ss=1:1:counter
146             A(:,:,z+1,ss)=matouter(ss,:);
147         end
148         for ss=counter+1:1:cc
149             A(:,:,z+1,ss)=zeros(1,N+1);
150         end
151     end
152     result(index)=A(1,1,z+1,1);
153     % read the result of the discretized path integral --> the coefficient
154     % of the Fock state in  the last line of A
155     fprintf('\n%3.2f %% computed.\n',100*(beta-bmin)/(bmax-bmin));
156 end
157
158 % build the exact result of the path integral
159 bexact=bmin:0.1*bpace:bmax;
160 resultexact=zeros(1,length(bexact));
161 resultexact(:)=2*cosh(0.25*bexact(:))./exp(0.25*bexact(:));
162
163 function [vecout,info2]=oneapa(i,Ni,vecin)
164 vecout=zeros(Ni,1);
165 if vecin(i)==1
166     info2=0;
167 else
168     vecout=vecin;
169     info2=1;
170 end
171 end
172
173 function [matout,count] = grouping (matin,N,NMAX)
174 % N is the same N of fHO (number of grassmanns);
175 % NMAX is the number of rows to group; each row carries a
176 % coefficient in front
177 matout=zeros(NMAX,N+1);
```

```
178 count=0;
179 matout(1,:)=matin(1,:);
180 count=count+1;
181
182 for k=2:1:NMAX
183     for t=1:1:count
184        info=check(matin(k,:),matout(t,:),N);
185        if info==1
186           matout(t,1)=matout(t,1)+matin(k,1);
187           break
188        end
189     end
190     if info==0
191         matout(count+1,:)=matin(k,:);
192         count=count+1;
193     end
194 end
195 matout(count+1:NMAX,:)=[];
196 end
197
198 function [vecout1,vecout2,info]=doublea(i,j,N,vecin)
199 vecout1=vecin;
200 vecout2=zeros(1,N);
201 if (vecin(i)==1)&&(vecin(j)==1)
202    vecout2=vecin;
203    vecout2(i)=0;
204    vecout2(j)=0;
205    info=1;
206 else
207     info=0;
208
209 end
210 end
211
212 function info=check(riga1,riga2,N)
213 if (riga1(2:1:N+1)-riga2(2:1:N+1)==zeros(1,N))
214     info=1;
215 else
216     info=0;
217 end
218
219 function [nout,matout] = algo (vecin,z,N,Saux2)
220 % "algo" takes a vector (coefficient plus Fock state), index of the field,
221 % N, Saux2 where the pieces of action are stored. I returns the initial
222 % vector modified by the z-piece of Saux2.
223 % matout is the number of Fock's vector produced in matout
224 K=N+1;
225 matout=zeros(K,N+1);
226 matout(1,:)=vecin;
227 t=1;
228 for j=1:1:2
229     % now I want to apply the (1-n_z)(1+S_z); if I do that on a Fock state
230     % where the 2 grassmann are present I write it on matout putting the 2
231     % ones to zero
232     if (vecin(Saux2(j,2,z)+1)==1&&vecin(Saux2(j,3,z)+1)==1)
233         t=t+1;
234         matout(t,:)=vecin;
235         appo=matout(t,:);
236         % Fock vector: used below to take into account anticommution of
```

```
237         % grassmann
238         matout(t,Saux2(j,2,z)+1)=0;
239         matout(t,Saux2(j,3,z)+1)=0;
240         rr=0;
241         % begin of "take into account anticommutation"
242         if Saux2(j,3,z)>Saux2(j,2,z)
243             for rrr=2:1:Saux2(j,3,z)-1
244                 rr=rr+appo(rrr);
245             end
246             for rrr=2:1:Saux2(j,2,z)-1
247                 rr=rr+appo(rrr);
248             end
249             rr=rr+1;
250         else
251             for rrr=2:1:Saux2(j,2,z)-1
252                 rr=rr+appo(rrr);
253             end
254             for rrr=2:1:Saux2(j,3,z)-1
255                 rr=rr+appo(rrr);
256             end
257         end
258         % end of "take into account anticommutation"
259         sg=(-1)^rr;
260         matout(t,1)=vecin(1)*sg*Saux2(j,1,z);
261     end
262 end
263 s=0;
264 for tt=1:1:t
265    if matout(tt,z+1)==1
266       matout(tt,:)=[];
267       s=s+1;
268    end
269 end
270 % I removed Fock states with (1-n_z)
271 if t~=1
272     nout=t-1;
273 else
274     nout=t;
275 end
276 matout(nout+1:K-s,:)=[];
277 % deletion of all unnecessary lines of matout
278
279 % begin of grouping part
280 [matout2,count] = grouping (matout,N,nout);
281 matout=matout2;
282 nout=count;
283 end
```

FIGURE D.1: MATLAB code the evaluation of the fermionic harmonic oscillator propagator using Creutz's algorithm.

Bibliography

[1] S. Laporta and E. Remiddi, Phys. Lett. B **379**, 283-291 (1996) doi:10.1016/0370-2693(96)00439-X [arXiv:hep-ph/9602417 [hep-ph]].

[2] T. Aoyama, M. Hayakawa, T. Kinoshita and M. Nio, Phys. Rev. D **77**, 053012 (2008) doi:10.1103/PhysRevD.77.053012 [arXiv:0712.2607 [hep-ph]].

[3] M. Arzano and G. Calcagni, Phys. Rev. D **93** (2016) no.12, 124065 doi:10.1103/PhysRevD.93.124065 [arXiv:1604.00541 [gr-qc]].

[4] P. Castro-Villareal, Journal of Statistical Mechanics: Theory and Experiment, (2010), vol. 2010, p. 08006

[5] R. P. Feynman, Phys. Rev. 80 (1950) 440, doi:10.1103/PhysRev.80.440.

[6] L. Alvarez-Gaume, Commun. Math. Phys. **90** (1983) 161. doi:10.1007/BF01205500

[7] L. Alvarez-Gaume and E. Witten, Nucl. Phys. B **234** (1984) 269. doi:10.1016/0550-3213(84)90066-X

[8] D. Friedan and P. Windey, Nucl. Phys. B **235** (1984) 395. doi:10.1016/0550-3213(84)90506-6

[9] F. Bastianelli, Nucl. Phys. B **376** (1992) 113 doi:10.1016/0550-3213(92)90070-R [hep-th/9112035].

[10] F. Bastianelli and P. van Nieuwenhuizen, Nucl. Phys. B **389** (1993) 53 doi:10.1016/0550-3213(93)90285-W [hep-th/9208059].

[11] Z. Bern and D. A. Kosower, Phys. Rev. Lett. **66** (1991) 1669. doi:10.1103/PhysRevLett.66.1669

[12] M. J. Strassler, Nucl. Phys. B **385** (1992) 145 doi:10.1016/0550-3213(92)90098-V [hep-ph/9205205].

[13] C. Schubert, Phys. Rept. **355** (2001) 73 doi:10.1016/S0370-1573(01)00013-8 [hep-th/0101036].

[14] J. P. Edwards and C. Schubert, [arXiv:1912.10004 [hep-th]].

[15] F. Bastianelli and P. van Nieuwenhuizen, doi:10.1017/CBO9780511535031

[16] F. Bastianelli and A. Zirotti, Nucl. Phys. B **642** (2002) 372 doi:10.1016/S0550-3213(02)00683-1 [hep-th/0205182].

[17] F. Bastianelli, O. Corradini and A. Zirotti, Phys. Rev. D **67** (2003) 104009 doi:10.1103/PhysRevD.67.104009 [hep-th/0211134].

[18] F. Bastianelli, P. Benincasa and S. Giombi, JHEP **0504** (2005) 010 doi:10.1088/1126-6708/2005/04/010 [hep-th/0503155].

[19] F. Bastianelli and C. Schubert, JHEP **0502** (2005) 069 [gr-qc/0412095].

[20] F. Bastianelli, J. M. Davila and C. Schubert, JHEP **0903** (2009) 086 doi:10.1088/1126-6708/2009/03/086 [arXiv:0812.4849 [hep-th]].

[21] F. Bastianelli and R. Bonezzi, JHEP **1307** (2013) 016 [arXiv:1304.7135 [hep-th]].

[22] R. Bonezzi, A. Meyer and I. Sachs, JHEP **10** (2018), 025 doi:10.1007/JHEP10(2018)025 [arXiv:1807.07989 [hep-th]].

[23] R. Bonezzi, A. Meyer and I. Sachs, [arXiv:2004.06129 [hep-th]].

[24] F. Bastianelli, O. Corradini and E. Latini, JHEP **0811** (2008) 054 doi:10.1088/1126-6708/2008/11/054 [arXiv:0810.0188 [hep-th]].

[25] F. Bastianelli, R. Bonezzi, O. Corradini and E. Latini, JHEP **1212** (2012) 113 doi:10.1007/JHEP12(2012)113 [arXiv:1210.4649 [hep-th]].

[26] F. Bastianelli and N. D. Hari Dass, Phys. Rev. D **64** (2001), 047701 doi:10.1103/PhysRevD.64.047701 [arXiv:hep-th/0104234 [hep-th]].

[27] O. Corradini and M. Muratori, Eur. Phys. J. Plus **133** (2018) no.11, 457 doi:10.1140/epjp/i2018-12293-5 [arXiv:1808.05401 [hep-th]].

[28] A. H. Tavabi, C .B. Boothroyd, E. Yücelen, S. Frabboni, G. C. Gazzadi, R. Dunin-Borkowski, and G. Pozzi, doi.org/10.1038/s41598-019-43323-2

[29] F. Bastianelli, K. Schalm and P. van Nieuwenhuizen, Phys. Rev. D **58** (1998), 044002 doi:10.1103/PhysRevD.58.044002 [arXiv:hep-th/9801105 [hep-th]].

[30] F. Bastianelli, O. Corradini and P. van Nieuwenhuizen, Phys. Lett. B **494** (2000), 161-167 doi:10.1016/S0370-2693(00)01180-1 [arXiv:hep-th/0008045 [hep-th]].

[31] F. Bastianelli, G. Cuoghi and L. Nocetti, Class. Quant. Grav. **18** (2001), 793-806 doi:10.1088/0264-9381/18/5/303 [arXiv:hep-th/0007222 [hep-th]].

[32] D. Friedan, Phys. Rev. Lett. **45** (1980), 1057 doi:10.1103/PhysRevLett.45.1057

[33] F. Bastianelli and O. Corradini, Phys. Rev. D **60** (1999), 044014 doi:10.1103/PhysRevD.60.044014 [arXiv:hep-th/9810119 [hep-th]].

[34] O. Corradini, L. Crispo and M. Muratori, EPJ C **82** (2022), 73 doi:10.1140/epjc/s10052-022-10026-4 [arXiv:2109.11804 [hep-th]].

[35] G. Mogull, J. Plefka and J. Steinhoff, JHEP **02** (2021), 048 [arXiv:2010.02865 [hep-th]].

[36] G. U. Jakobsen, G. Mogull, J. Plefka and J. Steinhoff, [arXiv:2106.10256 [hep-th]].

[37] N. Ahmadiniaz, F. M. Balli, O. Corradini, J. M. Dávila and C. Schubert, Nucl. Phys. B **950** (2020), 114877 [arXiv:1908.03425 [hep-th]].

[38] H. Gies and K. Langfeld, Nucl. Phys. B **613** (2001) 353 doi:10.1016/S0550-3213(01)00377-7 [hep-ph/0102185].

[39] T. Nieuwenhuis and J. Tjon, Phys. Rev. Lett. **77** (1996), 814-817 doi:10.1103/PhysRevLett.77.814 [arXiv:hep-ph/9606403 [hep-ph]].

[40] K.K. Sabelfeld et al., De Gruyter (1995)

[41] H. Gies, K. Langfeld and L. Moyaerts, JHEP **0306** (2003) 018 doi:10.1088/1126-6708/2003/06/018 [hep-th/0303264].

[42] H. Gies and K. Klingmuller, J. Phys. A **39** (2006), 6415-6422 doi:10.1088/0305-4470/39/21/S36 [arXiv:hep-th/0511092 [hep-th]].

[43] H. Gies and K. Klingmuller, Phys. Rev. D **72** (2005) 065001 doi:10.1103/PhysRevD.72.065001 [hep-ph/0505099].

[44] H. Gies, J. Sanchez-Guillen and R. A. Vazquez, JHEP **0508** (2005) 067 doi:10.1088/1126-6708/2005/08/067 [hep-th/0505275].

[45] G. Dunne, H. Gies, K. Klingmuller and K. Langfeld, JHEP **0908** (2009) 010 doi:10.1088/1126-6708/2009/08/010 [arXiv:0903.4421 [hep-th]].

[46] J. P. Edwards, U. Gerber, C. Schubert, M. A. Trejo, T. Tsiftsi and A. Weber, Annals Phys. **411** (2019) 167966 doi:10.1016/j.aop.2019.167966 [arXiv:1903.00536 [quant-ph]].

[47] O. Corradini and M. Muratori, JHEP **11** (2020), 169 doi:10.1007/JHEP11(2020)169 [arXiv:2006.02911 [hep-th]].

[48] G. E. P. Box, M. E. Muller, The Annals of Mathematical Statistics (1958), Vol. 29, No. 2 pp. 610-611

[49] F. Bastianelli, O. Corradini and L. Iacconi, JHEP **1805** (2018) 010 doi:10.1007/JHEP05(2018)010 [arXiv:1802.05989 [hep-th]].

[50] J. Guven, Phys. Rev. D **37** (1988) 2182. doi:10.1103/PhysRevD.37.2182

[51] F. Bastianelli, O. Corradini and E. Vassura, JHEP **04** (2017), 050 doi:10.1007/JHEP04(2017)050 [arXiv:1702.04247 [hep-th]].

[52] G. Miele and P. Vitale, Nucl. Phys. B **494** (1997), 365-387 doi:10.1016/S0550-3213(97)00155-7 [arXiv:hep-th/9612168 [hep-th]].

[53] M. Bordag, D. Hennig and D. Robaschik, J. Phys. A **25**, 4483 (1992)

[54] A.S. Eddington, Cambridge University Press, p. 93 (1924)

[55] A. Ahmad, N. Ahmadiniaz, O. Corradini, S. P. Kim, C. Schubert, NPB 919, 4-29 (2017), arXiv: 1612.02944 [hep-th]

[56] M. Creutz, Nucl. Phys. B Proc. Suppl. **73** (1999), 819-821 doi:10.1016/S0920-5632(99)85213-X [arXiv:hep-lat/9809024 [hep-lat]].

[57] T. Inagaki, T. Muta and S. D. Odintsov, Prog. Theor. Phys. Suppl. **127** (1997) 93 doi:10.1143/PTPS.127.93 [hep-th/9711084].

[58] D. Nickel, Phys. Rev. Lett. **103** (2009) 072301 doi:10.1103/PhysRevLett.103.072301 [arXiv:0902.1778 [hep-ph]].

[59] U. Muller, C. Schubert and A. M. E. van de Ven, Gen. Rel. Grav. **31** (1999) 1759 doi:10.1023/A:1026718301634 [gr-qc/9712092].

[60] O. Corradini, A. Flachi, G. Marmorini, M. Muratori and V. Vitagliano, J. Phys. A **54** (2021) no.40, 405401 doi:10.1088/1751-8121/ac1ee7 [arXiv:2106.03289 [hep-th]].

[61] C. Ryu, M. Andersen, P. Cladé, Natarian, Vasant, K. Helmerson, W. Phillips, Phys. Rev. Lett. **99** (2007) doi:10.1103/physrevlett.99.260401.

[62] K. C. Wright, R. B. Blakestad, C. J. Lobb, W. Phys. Rev. A **88** (2013) doi:10.1103/physreva.88.063633.

[63] S. Beattie, S. Moulder, R. J. Fletcher, Z. Hadzibabic, Phys. Rev. Lett. **110** (2013) doi:10.1103/physrevlett.110.025301.

[64] M. Cominotti, D. Rossini, M. Rizzi, F. Hekking, and A. Minguzzi, Phys. Rev. Lett. **113**, (2014) doi:10.1103/PhysRevLett.113.025301.